UNIVERSITÉ CATHOLIQUE DE LOUVAIN
Louvain Drug Research Institute
Advanced Drug Delivery and Biomaterials

ANTICANCER DRUG-LOADED PHOTOPOLYMERIZABLE HYDROGEL FOR THE TREATMENT OF GLIOBLASTOMA

Mengnan Zhao

Director: Prof. Véronique Préat

2019

ACKNOWLEDGEMENTS

Four years PhD is a long journey. I wish to express my sincere appreciation to those who have contributed to this thesis and supported me in one way or the other during this amazing journey.

Firstly, I would like to express my sincere gratitude to my advisor Prof. Véronique Préat for the continuous support of my PhD research, for her patience, motivation, and immense knowledge. Her guidance helped me in all the time of research and writing of this thesis. I could not have imagined having a better advisor and mentor for my PhD study.

Besides my advisor, I would like to thank to my PhD committee members: Prof. Olivier Feron, Prof. Bernard Gallez, and Prof. Pierre Sonveaux, for their insightful comments and encouragement, which incented me to widen my research from various perspectives. Thank also to Prof. Raymond Schiffelers, Prof. Katrien Remaut and Dr. Florence Lefranc for having accepted to be the jury of my PhD thesis and for the interesting discussion that we had during the private defense.

My sincere thanks also go to Dr. John Bianco, Dr. Fabienne Danhier, Prof. Anne des Rieux and Dr. Jankovski Aleksandar for the nice discussion in every Beware meeting. Without the precious support it would not be possible to conduct this research. I want to thank Dr. Nicolas Joudiou for the time and patience that he dedicated to the works regarding MRI in this project. I would like to acknowledge Demian for contributing to the review as well. Very special thanks to China scholarship council for giving me the opportunity and financially supporting me to carry out my PhD research.

I would also like to take this opportunity to thank to Bernard, Kevin, Murielle, Neha and Gaëlle for their time and patience. Thanks to our cancer team and all the labmates from ADDB for their kindness and help. Finally, I would like to acknowledge my family and my boyfriend for the supports during the hard times, this PhD thesis is also the result of your trust and encouragements.

LIST OF ABBREVIATIONS

ABC	ATP-binding cassette
ATRA	All-trans retinoic acid
BBB	Blood brain barrier
BBTB	Blood brain-tumor barrier
BCNU	Carmustine
BCRP	Breast cancer resistance protein
BER	Base excision repair
BG	Benzylguanine
CDI	Coefficient of drug interaction
CED	Convection-enhanced delivery
CNS	Central nervous system
CSC	Cancer stem cell
CSF	Cerebrospinal fluid
DEXA	Dexamethasone
DOX	Doxorubicin
DTX	Docetaxel
ECM	Extracellular matrix
ECs	Endothelial cells
EGFR	Epidermal growth factor receptor
EPR	Enhanced permeation and retention
FDA	Food and drug administration
GBM	Glioblastoma multiforme
GEM	Gemcitabine
GemC12	Lauroyl-gemcitabine
GSC	Glioma stem cell
IB	Imipramine blue
IDH	Isocitrate dehydrogenase 1/2
LNCs	Lipid nanocapsules
MDR	Multidrug resistance
MGMT	O6-alkylguanine-DNA alkyltransferase
MMP-2	Matrix metalloproteinase-2
MRP	Multidrug resistance-associated protein
MTD	Maximum tolerated dose
MTIC	5-(3-methyltriazen-1-yl) imidazole-4-carboxamide
N3-meA	N3-methyladenine
N7-meG	N7-methylguanine
NPs	Nanoparticles
NSAID	Non-steroidal anti-inflammatory drugs
O6-meG	O6-methylguanine
OS	Overall survival

PEG-DMA	Polyethylene glycol dimethacrylate
PFS	Progression-free survival
P-gp	P-glycoprotein
PLGA	poly (lactic-co-glycolic acid)
PTX	Paclitaxel
RES	Resveratrol
RME	Receptor mediated endocytosis
RT	Radiotherapy
siRNA	Small interfering RNAs
TAM	Tumor associated macrophages
Tf	Transferrin
TJs	Tight junctions
TME	Tumor microenvironment
TMZ	Temozolomide
TTFields	Tumor-treating fields
VEGF	Vascular endothelial growth factor

CHAPTER I

INTRODUCTION

Mengnan Zhao, Demian van Straten, Marike L.D. Broekman, Véronique Préat, Raymond M. Schiffelers
Adapted from "*Nanocarrier-based drug combination therapy for Glioblastoma*" in Theranostics (In revision)

TABLE OF CONTENTS

I. INTRODUCTION

Glioblastoma multiforme (GBM) is the most challenging grade IV malignant glioma with almost unavoidable recurrence in all patients after rigorous treatments [1]. In 60% of cases, GBM initiates de novo, and the other 40% cases develop through lower-grade brain tumors [2]. Currently, despite the studies underway for GBM, no curative treatment options exist and the 5-year survival of GBM-diagnosed patients remains lower than 6% [3]. Upon diagnosis, the current standard of care involves maximal surgical resection, followed by radiotherapy and concurrent temozolomide (TMZ), with 6 maintenance cycles of TMZ with each cycle for 5 days [4]. Unfortunately, complete surgical resection is probably unachievable because GBM is highly invasive and infiltrative to the functional region of the brain that controls senses, actions and speech [5]. Although the development of surgery imaging techniques provides more possibilities to obtain more extensive surgical resection, there is always the fine balance among aggressive removal of tumor tissue, the remaining brain function and the life quality of patients [1]. A median survival of 12.1 months can be obtained through focal irradiation of 2 Gy per fraction administered 5 days per week for 6 weeks with a total dose of 60 Gy. Even by adding complementary TMZ chemotherapy, only slight improvement with a median survival time of 14.6 months was achieved compared with resection alone [4]. However, cognitive impairment, DNA lesions and other systemic effects are severe side effects of radiation [6]. Angiogenesis also offered a promising tumor target because cutting off the blood supply could starve tumor cells. By targeting vascular endothelial growth factor (VEGF), the anti-angiogenic drug bevacizumab was approved by the U.S. Food and Drug Administration (FDA) to treat recurrent GBM that has progressed after prior therapy. The addition of bevacizumab to concomitant chemo-radiotherapy for newly diagnosed GBM showed prolonged progression-free survival (PFS) but failed to show an overall survival (OS) benefit in phase III trials (NCT00884741 and NCT00943826) [7, 8]. Optune®, a device that creates low-intensity and alternating tumor-treating fields (TTFields), also obtained approval from the FDA as treatment together with TMZ for newly diagnosed GBM in 2015. The median PFS and OS were significantly increased (7.1 and 20.5 months, respectively) in the TTFields plus TMZ group compared with those (4.0 and 15.6 months, respectively) in the TMZ-alone group (NCT00916409) [9]. However, despite these multidisciplinary therapies, most patients will still develop tumor recurrence within 1 to 2 years of diagnosis. Patients may then undergo repeated resection, different chemotherapies, bevacizumab therapy or additional radiotherapy. Unfortunately, there is limited evidence showing that those treatments can increase the survival time. Thus, regarding the unmet medical needs for GBM patients, the fight over GBM is far from over (Figure 1).

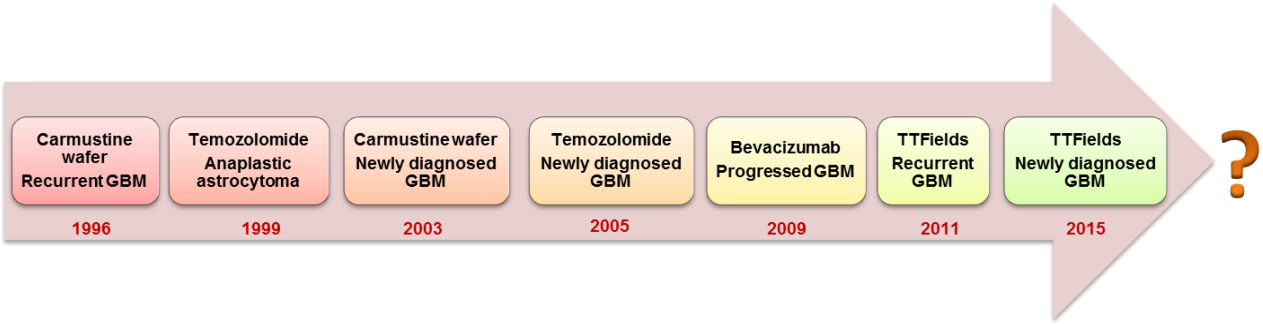

Figure 1: Evolution of FDA-approved GBM treatment approaches (Adapted from [5])

Chemotherapy has always been a standard care for cancer patients. Although a few chemotherapeutic drugs have been tested as treatment strategies for GBM, their clinical efficacy are inadequate and unsatisfactory [10]. The general concerns associated with chemotherapeutic drug administration include complicated tumor heterogeneity, the blood brain barrier, glioma stem cells, DNA damage repair, and drug efflux pumps. Therefore, two or more conventional anti-cancer drugs working in cooperation could be promising to overcome those hurdles and achieve a beneficial therapeutic effect. With growing investigation of the tumor microenvironment, and biological and molecular pathways, increasingly more potential drug combination therapies are emerging currently. Indeed, several chemotherapeutic drug combinations have been applied in the past decade in clinical practice to treat GBM and other central nervous system (CNS) tumors (See Table 4). However, drug combinations are associated with poor drug distribution at the desired tumor site. Different approaches have been raised to defeat unfavorable drug distribution in the brain [11]. Among these approaches, nanotechnology-based drug delivery is a promising strategy to enhance chemotherapy efficiency. Various nanocarriers have been investigated for drug delivery in CNS tumors, such as polymeric nanoparticles (NPs), liposomes, and lipid nanocapsules (LNCs). The nanocarrier-based drug combination could enhance the solubility of hydrophobic drugs, induce long circulation times and sustained drug release, improving therapeutic efficacy and safety [12, 13]. Therapeutic drugs can be administered locally or systemically, with the potential benefit of the enhanced permeation and retention (EPR) effect. Depending on the drugs, delivery can be mediated with both compounds within nanocarriers or with one drug being administered as a free drug. Additionally, drugs can be delivered in two different nanocarriers or co-encapsulated in one nanocarrier. These approaches allow multiple chances to achieve a maximum synergistic effect. To increase the bioavailability and desired therapeutic dose of anticancer drugs, nanoformulations could be investigated for future evaluation in GBM patients for the unmet and urgent clinical needs.

In this review, we will explain major issues in GBM treatment (Figure 2), discuss the advantages of drug combinations with or without nanocarriers and nanomedicine-based tumor targeting

strategies, review current preclinical combinations among low-molecular-weight chemotherapeutic drugs or with high-molecular-weight drugs and drug combination therapies in the clinic. The aim of this review was to highlight the importance of drug combinations, the use of nanocarriers and give comprehensive understanding of different drug combination strategies for GBM therapy.

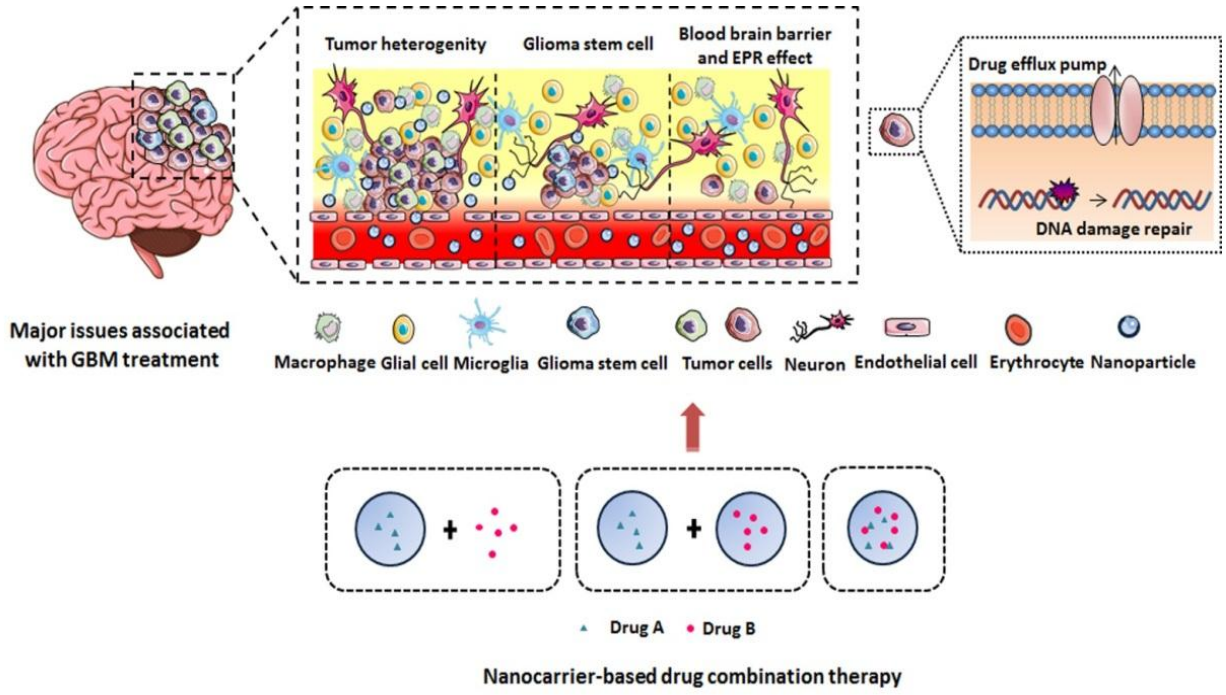

Figure 2: Major issues associated with GBM treatment and nanocarrier-based drug combination therapy

II. RATIONALE OF THE DRUG COMBINATION FOR GBM TREATMENT

Since the approval of the local carmustine wafer by the FDA in 1996, chemotherapy is a standard treatment for GBM until now. However, the treatment benefits are limited because of some major issues associated with GBM treatment including complicated tumor heterogeneity, the blood brain barrier, glioma stem cells, DNA damage repair, and drug efflux pumps (Table 1) [14, 15].

II.1 COMPLEX TUMOR HETEROGENEITY

In the 2016 WHO classification of gliomas, isocitrate dehydrogenase 1/2 (*IDH*) mutations, complete deletion of the short arm of chromosome 1 and long arm of chromosome 19 (*1p/19q* codeletion), *C11orf95–RELA* fusions and *H3F3A* or *HIST1H3B/C K27M* mutations are the requisite diagnostic biomarkers of gliomas. *MGMT*-promoter methylation is a prediction biomarker related to alkylating chemotherapy in patients. Other predictive biomarkers for targeted therapies, such as *BRAF* and epidermal growth factor receptor (*EGFR*) mutations, are also emerging. This glioma classification based on characteristic genetic alterations and epigenetic profiles of gliomas can be used to improve the prediction of patient outcomes and guide individualized treatment [16]. The diagnosis and determination of therapeutic options based on molecular analysis of a single biopsy specimen have profound clinical implications for therapeutic treatment strategies until more is known about molecular pathways and driver mutations in GBM [17]. Despite the major advances in the molecular profiling of GBM, treatments have generally been performed based on molecular biomarkers present in a single tumor specimen. However, an increasing number of studies have unraveled the layers of tumor complexities, with molecular heterogeneity also present within individual tumor specimens. The investigations in genomic research provide us with a broad range of opinions regarding the heterogeneity of GBM [18, 19], which might be determined by the tumor cell origin or subsequent genetic and epigenetic conversions, producing different types of tumor-initiating cells [20]. These tumor-initiating cells grow and establish genetically diverse cell clones. Throughout this clonal development, tumor cell descendants obtain heterogeneous genetic conversions and generate various cell clones. In one study, 430 cells from five primary GBMs were profiled using single-cell RNA sequencing and showed inherently variable gene expression in diverse transcriptional programs associated with oncogenic signaling, hypoxia, proliferation and the complement/immune response [21]. The invasive properties of tumor cells will also produce clonal crosses and deeper brain parenchyma

invasion [22]. Because single agents may kill some subpopulations but may be less efficient to other cells, drug combinations with different mechanisms of action may result in additive or synergistic antitumor effects.

II.2 GLIOMA STEM CELLS

Cancer stem cells (CSC) are well known for their self-renewal, differentiation and propagation abilities. GBM is the most malignant primary brain tumor and contains self-renewing, tumorigenic stem cells that contribute to tumor initiation and therapeutic resistance; thus, the term glioma stem cells (GSCs) was adopted by several studies to describe CSCs found in GBM [23]. Stem cell-like properties allow GSCs to differentiate into highly proliferating progenitor-like tumor cells or other differentiated tumor cells. GSCs can be more resistant to radio- and chemotherapy than non GSC tumor cells both *in vitro* and *in vivo*. Consequently, the populations of glioma stem cells remain alive after initial treatment and reinitiate tumor recurrence [15]. GSCs also have the additional ability of DNA damage repair and angiogenesis promotion [24]. CD133, also known as prominin-1, is a surface glycoprotein on neural stem cells that is highly expressed on cells with higher rates of self-renewal, proliferation and differentiation abilities. Other biomarkers, such as L1CAM, SOX2, CXCR4, Integrin α-6, and CD36, have been investigated in GBM, but their roles in GSCs are not well defined [23]. GSCs can initiate and maintain the primary tumor. Nevertheless, there is another subpopulation of cells that initiates tumor recurrence through repopulating tumors by clonal evolution, called recurrence-initiating, stem-like cancer cells. Such cells are more aggressive than primary tumor-derived GSCs and need to be investigated separately [20]. Due to the resistance to common treatments, primary tumor-maintaining ability and tumor recurrence initiating ability, cancer stem cells could be a valuable target in the pursuit of finding further efficient therapeutic strategies for GBM. Thus, the co-administration of anti-neoplastic drugs and anti-GCS drugs could have synergistic effects for GBM.

II.3 DNA DAMAGE REPAIR

The standard therapy TMZ is an orally administered alkylating agent that can be transported across the BBB and has remarkable distribution at the tumor site. TMZ is spontaneously hydrolyzed at physiological pH to its active metabolite 5-(3-methyltriazen-1-yl) imidazole-4-carboxamide (MTIC), which adds methyl adducts to DNA. The generated O6-methylguanine (O6-meG), N3-methyladenine (N3-meA) and N7-methylguanine (N7-meG) can promote DNA strand damage followed by cell death by interfering with the cell cycle [25]. However, these TMZ-induced

cytotoxic effects can be neutralized by various DNA repair mechanisms, re-enforcing the structural integrity of the methylated DNA bases before causing extensive tumor cell death (Figure 3). The DNA repair protein O6-alkylguanine-DNA alkyltransferase (MGMT) can transfer the methyl group to a cysteine residue, thus rebuilding the structural integrity of DNA bases [26]. Although O6-meG only accounts for a small percentage of the TMZ-induced base lesions (5%-10%), it is considered the most cytotoxic site because it severely interferes with DNA replication [27]. Moreover, the DNA base excision repair (BER) system consists of several DNA repair proteins that can remove damaged DNA bases, especially for N3-meA and N7-meG, which account for most of the base lesions caused by TMZ chemotherapy (~90%) [28]. The prolonged survival of patients with radiotherapy and TMZ chemotherapy is greater in patients whose tumors exhibit methylation of the MGMT promoter than in unmethylated *MGMT* promoter-presenting patients [29]. This study spotlighted the requirements for different treatment strategies in GBM patients based on the *MGMT* methylation status. Patients without *MGMT*-methylation might benefit from combining TMZ with therapeutics that show MGMT inhibition or other independent anti-cancer properties.

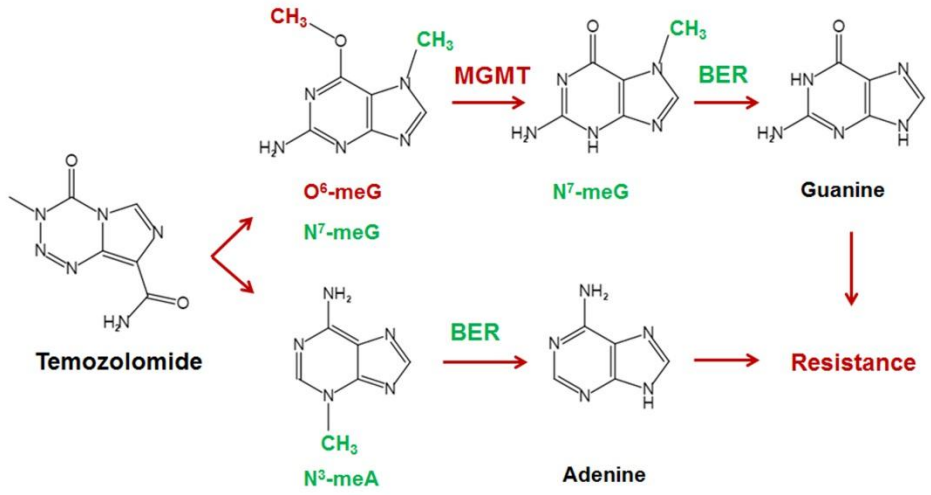

Figure 3: Common TMZ-induced DNA lesions appear on guanine and adenine. O6-methylguanine adducts can be repaired by MGMT, resulting in TMZ resistance. The less toxic N7-methylguanine and N3-methyladenine adducts are readily repaired by the BER system. Adapted from [30] and [31].

II.4 BLOOD BRAIN BARRIER

A particularly formidable challenge of developing therapeutics for brain tumors is the blood brain barrier (BBB), which comprises brain microvascular endothelial cells (ECs), pericytes, astrocytes, tight junctions (TJs), neurons, and the basal membrane [32]. The tight junctions prevent the passive penetration of hydrophilic molecules from the blood circulation to the brain. Several specialized transport systems mediate the entry of essential substances such as nucleosides, glucose, amino acids, hormones and receptor-mediated endocytosis by specific proteins (e.g., transferrin and

lactoferrin). However, conventional chemotherapy for GBM requires the penetration of drugs from the blood to the brain tumor site. Only certain drugs that are highly small lipophilic chemotherapeutic agents with a molecular weight less than 400 Da and 8 hydrogen bonds can passively pass through the BBB [33]. Nevertheless, the functions and organization of the BBB can be modified in GBM conditions (Figure 4). The transformation of lower grade tumors to higher grade tumors causes tumor invasion to healthy brain tissues and the formation of the blood brain-tumor barrier (BBTB). High-grade gliomas are characterized by disrupted and heterogeneous BBTB [34]. The metabolic demands of high-grade glioma create hypoxic areas that trigger increased expression of VEGF and angiogenesis. The highly invasive potential of glioma cells prompts the widespread proliferation of tumor cells outside the disrupted BBTB to areas of normal brain, where the function of the BBTB remains intact. The tricky task in GBM treatment is reaching the residual tumor cells infiltrating to brain parenchyma where the BBTB is intact or less compromised, leading to an insufficient therapeutic effect through passive drug diffusion [35]. The disruption of the BBB or BBTB allows extravasation of therapeutics. To further enhance brain drug delivery, binding active endogenous molecules to receptor on the luminal surface of brain capillary endothelial cells on BBTB can trigger the endocytosis of therapeutic agents.

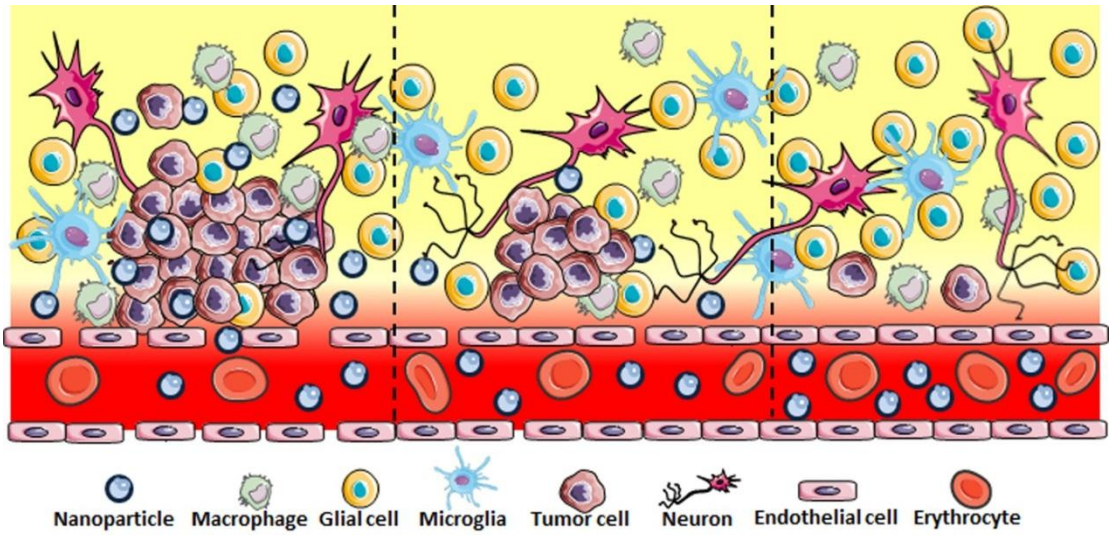

Figure 4: Schematic representation of the heterogeneous blood brain barrier disruption in GBM. Significant BBB breakdown seen in the bulk tumor region (left panel) allows nanoparticle extravasation. Regions with infiltrating GBM cells show less or no breakdown of the BBB (middle and right) preventing NPs or other therapeutics to reach these cells.

II.5 EFFLUX PUMP

Multidrug resistance (MDR) presents another major barrier for chemotherapeutic drugs to get access to brain tumor cells effectively. Among the different mechanisms of MDR, ATP-binding cassette (ABC) transporter-mediated exocytosis was mostly noticed. Proteins such as multidrug resistance-associated protein (MRP), P-glycoprotein (P-gp) and breast cancer resistance protein (BCRP) are responsible for the uptake and efflux of various substances in and out of tumor cells thereby preventing drug accumulation [15]. Among them, P-gp has been mostly considered the cause of anti-cancer drug resistance. P-gp is an energy-dependent drug efflux pump comprising 1,280 amino acids encoded by the human *MDR1* gene [36]. *MDR1* P-gp presents in the brain capillaries of BBB, as well as in many other tissues such as the kidney, intestines and liver. Many drugs exhibit significantly improved brain penetration when drug efflux transporters are absent in gene knockout mice. For example, the knockdown of *MDR1* in GBM cells results in enhanced TMZ-mediated cell death, illustrating a role of *MDR1* for TMZ resistance [37]. Therefore, combination therapy with efflux transporter inhibitors could be an attractive strategy to boost drug administration into the brains without disrupting the integrity of the endothelial layer and tight junctions in BBB.

In conclusion, the right combination of anti-cancer drugs could enhance efficacy compared with the mono-therapy approach because it targets those issues in a synergistic or an additive manner. However, the efficiency of many chemotherapeutic agents is also limited by their dose-related toxicities. Keeping an increasing dose of a specific anticancer drug to increase the therapeutic effect will inevitably lead to significant toxicity to the organs sensitive to this drug. Many GBM chemotherapeutic drugs have demonstrated off-target toxicity. For example, radiotherapy plus TMZ was associated with a slightly higher rate of adverse events than radiotherapy alone, such as lymphopenia, thrombocytopenia and neutropenia [38]. Another FDA-approved drug, bevacizumab, is frequently associated with hypertension, leukopenia, non-central nervous system hemorrhage and thromboembolic events [39]. Thus, combining drugs with non-overlapping toxicities and reducing the dose of a single drug may be a better choice.

Table 1: Rationale of nanocarrier-based drug combinations against GBM

Issues with single drug treatment	Advantages of combination therapy	Advantages of nanocarrier-based drug delivery	Issues with free drug combinations	Advantages of nanocarrier-based combination therapy
• Tumor heterogeneity • Glioma stem cells • DNA damage repair • Efflux pump • Dose-limiting toxicity	• Combination of drugs with different mechanisms of action • Combination with anti-GSC drug • Combination with efflux-pump inhibitor • Combination with MGMT inhibitor • Combination of drugs with non-overlapping toxicity	• Drug encapsulation and solubilization • Drug protection • Increase of cellular uptake of NPs via endocytosis • Targeted delivery • Controlled/sustained release kinetics	• Different BBB permeability • Different drug stabilities • Different drug half lives • Different pharmacokinetics	• Combination of drug with different properties (solubility, BBB permeability, pharmacokinetics) • Ensure the synergistic drug ratio • Control the pharmacokinetics of different drugs • Ensure the colocalization of drugs into tumor site

III. PRINCIPLES OF DRUG COMBINATION

The fundamental principles of combination chemotherapy was first discussed by Frei et al. in the 1960s [40]. These principles remained constant over the decades: Chemotherapeutic drugs should 1) prove to be effective as a single drug, 2) have no-overlapping toxicities to be administered at the maximal dose of each drug; and 3) have different mechanisms of action to overcome drug resistance [10]. With those principles, drug combinations are supposed to be better than one drug. The drug combination effect can be classified and defined as synergism, addition or antagonism. Synergism or antagonism means the combination effect is greater or lesser than the additive effect of individual drug, respectively. Although already classified, many publications have shown different approaches to defining the combination effect and have caused confusion regarding the comparison of different research findings. Next, we propose a short introduction of the current methodology regarding the understanding of combination effects.

III.1 COEFFICIENT OF DRUG INTERACTION

The coefficient of drug interaction (CDI) is a simple and widely used index to measure combination effects. CDI is calculated as CDI=AB/ (A×B). Here, AB is the cell viability of the drug combination group to the control group, while A or B is the cell viability of the single drug group to the control group. For instance, the cell viability of drug A, drug B and drug combination AB is 40%, 50% and 20% respectively, the CDI could be calculated as 0.2/(0.4*0.5)=1. When the CDI value is less, more than or equal to 1, the drug combination is synergistic, antagonistic or additive respectively; a CDI value less than 0.7 indicates that the drugs are significantly synergistic [41-45].

III.2 ISOBOLOGRAM

Classical analysis using the isobologram, which is a graphical method developed 60 years ago by Loewe [46], also provides an approach to measure drug combination effects statistically (Figure 5). Based on the single-drug effect (EC_{50} as example), an additive line will be constructed. The concentrations of the two drugs used in combination to provide the same effect, indicated by points, are placed in the same plot. If the point of the combination dose pair to reach a 50% effect is located left to the additive line, there is a synergistic effect. By contrast, the points located to the right of the additive line indicates an antagonistic effect [47]. However, a linear additive isobole only refers to constant potency. In the situation of variable potency, a nonlinear

additive isobole was constructed by Grabovsky et al., especially when the drug is a partial agonist [48].

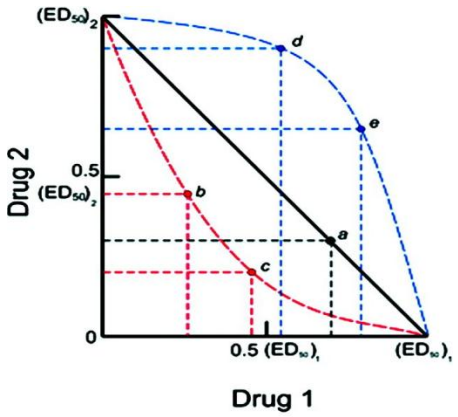

Figure 5: Classic ED50 isobologram for two drugs with actual doses on the x- and y-axis. If the combination data points fall on the hypotenuse (e.g., point a), an additive effect is indicated. If the combination data points fall on the lower left (e.g., points b and c) or on the upper right (e.g., points d and e), synergism or antagonism is indicated, respectively [49].

III.3 CHOU-TALALAY METHOD

The most well-known median-effect-based method was described by Chou and Talalay to analyze the drug combination effect. They introduced a scientific term "combination index" (CI) to quantitatively describe synergism (CI < 1), addition (CI = 1), and antagonism (CI > 1) effects [50]. The results can be achieved using the Compusyn software according to the mass-action law (Figure 6). This method provides strict quantitative standards to establish drug combination therapy by research institutions, drug inspection bureaus and pharmaceutical factories.

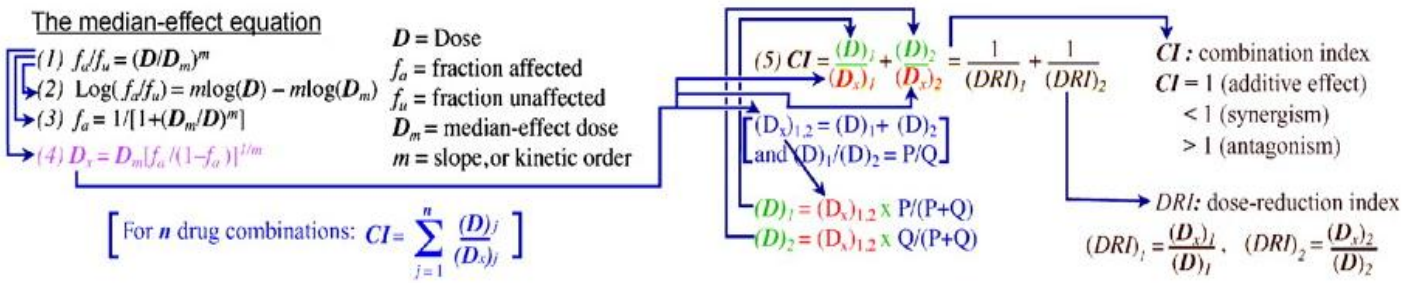

Figure 6: Algorithms for computerized simulation of synergism, addition and antagonism of the effect of multiple drugs in the Chou-Talalay method [50].

III.4 *IN VIVO* DETERMINATION OF THE COMBINATION EFFECT

In the aforementioned part, we reviewed the *in vitro* principles and methods to calculate the synergistic ratio of combination therapy. In one publication from Chou [50], determination of the combination effect *in vitro* and *in vivo* was based on the CI equation (Figure 5). The main practical issues to evaluate the combination effect of drugs in animals are the variability of animals, smaller population size and the approach is costly and time consuming. Robert Clark equations have also been used to calculate the *in vivo* synergism based on the median survival (Figure 7) [51].

Nature of interaction	Formula
Antagonistic	(AB/C) < (A/C) x (B/C)
Additive	(AB/C) = (A/C) x (B/C)
Synergistic	(AB/C) > (A/C) x (B/C)

Figure 7: Calculation of *in vivo* synergism by Robert Clark Equations. A = median survival of treatment 1, B = median survival of treatment 2, AB = median survival of combination groups and C = median survival of no treatment.

Prior to clinical trials, the basis and rationale involving explorative details should be obtained from preclinical studies (*in vitro* and in animals) and are not supposed to be performed in human subjects.

IV.NANOCARRIER-BASED DRUG COMBINATION FOR GBM TREATMENT

Theoretically, combination therapy with anticancer agents that are demonstrated to be effective as single-drug therapy in the clinic should provide better therapeutic effects without additional toxicity. Nevertheless, drug administration to GBM is highly difficult and must overcome many challenges. The major reason of the limited success is the incapability of the drugs to cross the BBB and penetrate inside the tumor tissue. Here, we will discuss the conventional strategies to enhance drug delivery to brain tumors and the rationales of nanocarrier-based combination therapy to treat GBM.

IV.1 LOCAL DELIVERY

Local intracranial delivery is the administration of therapeutic agents directly into the brain or tumor site. This approach not only overcomes BBB-associated delivery issues but also prevents systemic compound clearance and/or degradation and reduces systemic side effects. Thus, intracranial delivery allows higher local drug concentrations using lower doses, increasing the therapeutic index overall [52]. Local drug delivery to and further distribution in the brain is mediated by simple diffusion or positive pressure bulk flow.

Diffusion-mediated intracranial drug delivery is often based on the injection of chemotherapeutic compounds into the brain or tumor resection cavity through a reservoir catheter system. This system allows the continuous release of drugs in the brain tissue surrounding the catheter-tip by concentration gradient-based drug diffusion. It can be used repeatedly to deliver chemotherapeutics, radioactive compounds, antibodies, viruses or cells without the drawbacks of systemic administration [53]. For example, the Ommaya reservoir is a capsule connected to a catheter located in the lateral ventricle. The capsule is embedded under the scalp and is easily accessible for cerebrospinal fluid (CSF) aspiration or drug delivery directly into the ventricular CSF and relies on the flow of CSF to distribute the drugs throughout the brain [54].

Drugs can also be administered to the brain continuously with a positive pressure bulk flow via convection-enhanced delivery (CED). The positive pressure drives convective local transport of therapeutic concentrations of anti-tumor drugs into the interstitial tumor space. This technique achieved higher drug concentrations in the targeted tumor tissue compared with diffusion-limited delivery [55]. A significant reduction in the tumor size was reported through CED with the chemotherapeutic drug carboplatin in a patient with recurrent GBM [56]. A prospective phase Ib dose-escalation study of topotecan, administered by CED, reported progression-free and overall

survival rates of 23 weeks and 60 weeks, respectively, in patients with recurrent malignant glioma, findings that are favorable compared with those in historical control groups [57]. There are some important considerations to ensure the therapeutic efficacy of CED, such as tumor composition, catheter properties and placement, infusion rate and pharmaceutical formulation. Additionally, common side effects, such as edema, infection and backflow along the catheter, have resulted in the limited application of CED to treat GBM [55].

Rather than maintaining a direct, open connection from the brain to the outside, locally implanted (biodegradable) drug delivery depots have gained increasing interest. Currently, the only FDA-approved biodegradable implant is the Gliadel® wafer for newly diagnosed malignant and recurrent GBM. This polymeric implant comprises 1, 3-bis- (p-carboxyphenoxy) propane and sebacic acid and is loaded with the alkylating agent carmustine. The wafers provide sustained carmustine release over 2-3 weeks [58]. However, the success of Gliadel® wafers is restricted by the limited penetration of carmustine into the brain tumor tissue. Moreover, the use of the wafers has been associated with several adverse events, including intracranial infections, wafer migration, cerebral edema, CSF leakage and seizures. Thus, the application of Gliadel® has been disappointing [59].

Nevertheless, the concept of local delivery by implanting drug-releasing depots in the tumor resection cavity remains intriguing for the treatment of GBM. Films, foams and gels have been investigated for their use in local drug delivery; particularly, hydrogels have gained much attention in recent years. Hydrogels are hydrophilic polymer-based 3D networks that can contain large amounts of water. In general, hydrogels are biocompatible, biodegradable, mechanically comparable to soft tissue and can be made injectable, making them attractive for intracranial implantation. They provide a versatile drug delivery system because they can be loaded with small-molecule drugs, biomacromolecules (such as DNA or protein), nano- and microparticles or cells. Moreover, the gels can be engineered to tune the release of their contents in a timeframe ranging from hours up to several months [60]. An extra level of control over the release of small-molecule drugs can be gained by formulating them in a nanoformulation. This also increases the variety in compounds suitable for hydrogel delivery.

Preclinical studies have shown promising results delivering chemotherapeutics intracranially using nanoparticle-loaded hydrogels [52]. A hydrogel based on gemcitabine-loaded LNCs significantly delayed tumor recurrence and prolonged survival in a GBM resection mouse model [61]. Similarly, paclitaxel-loaded NPs (PTX-NPs) delivered via an injectable hydrogel led to increased long-term survival (>150 days) compared with only PTX-NPs without gel (72 days) or gel with empty NPs (63.5 days) [62]. Submicron PLGA nanofibers containing PTX were deposited in an orthotopic

tumor model using M80 and H80 hydrogels. The hydrogel formulations proved therapeutically effective and enhanced drug penetration into the surrounding tissue [63]. PLGA microspheres loaded with camptothecin were intracranially delivered using a commercially available thermoreversible Mebiol gel. The combination of tumor resection and microsphere/gel platform significantly improved survival compared with either modality alone [64].

Besides providing the means for sustained drug release, hydrogels can also accommodate multiple drugs simultaneously (possibly in the form of nanoformulations), thereby enabling possible synergistic therapeutic regimens. A hydrogel loaded with erlotinib, an EGFR inhibitor together with doxorubicin (DOX) -liposomes allowed a time-staggered exposure of the compounds leading to an increased efficacy *in vitro* [65]. Similarly, combining PTX and gemcitabine in the same hydrogel delivery platform improved their efficacy synergistically on several GBM cell lines [66].

Alternatively, hydrogels can harbor both therapeutic and imaging agents to form a theranostic platform. Depending on its design, such systems could allow non-invasive monitoring of gel degradation, gel or drug release and distribution, immune reactions, edema formation and possibly therapeutic efficacy. A thermosensitive biodegradable hydrogel was loaded with PTX and cobalt ferrite imaging NPs to create a theranostic combination. The platform showed sustained release of both cargos and provided therapeutic activity as well as convenient imaging of the tumor for three weeks in a solid tumor mouse model [67]. Lin et al. describe a nanocomposite system of an MRI-traceable gel loaded with PTX and epirubicin that allowed local treatment of residual tumor and simultaneous monitoring of gel degradation in a GBM resection model [68].

Taken together, local delivery was shown to be an effective approach to improve chemotherapy-based treatment for GBM by increasing the local dose of chemotherapeutics and simultaneously reducing systemic side effects. Catheter systems are effective but invasive and cope with (practical) complications. Polymeric implants and hydrogels show great promise but need additional development and optimization before they can be translated to clinical practice [52].

IV.2 SYSTEMIC DELIVERY

Systemic drug delivery to GBM is highly challenging. Due to the physicochemical characteristics of chemotherapeutic drugs and the presence of the BBB, only few drugs can reach the tumor site with a therapeutic dose. TMZ is almost completely absorbed from the gut and penetrates the blood-brain barrier. Other systemically administered drugs, such as the intravenous administration of bevacizumab and oral administration of everolimus and sorafenib, are also in clinical use. Various approaches, such as chemical modification of chemotherapeutic drugs, BBB alteration and efflux transporter inhibition, are being investigated to enhance the systemic delivery

of potential anti-GBM drugs. Drugs can be modified to a more lipophilic form by adding lipid groups to the polar ends of therapeutic molecules. A log P (octanol-water) value ranging from 1.5 to 2.5 of lipophilic analogs has better brain permeability [69]. However, this may also lead to nonspecific uptake of the drug molecule by other tissues through the blood circulation. Several methods have also been investigated to induce BBB alteration, such as hyperosmotic agents, bioactive molecules, surfactants and ultrasound or electromagnetic waves. However, such approaches are often associated with risks such as possible tumor diffusion to the periphery, exposure of the brain to neurotoxins and limited specificity [70]. Because the ABC efflux gene families are increasingly recognized as important determinants of drug distribution to the CNS, inhibition of those efflux transporters seems to be an appealing technique to increase drug penetration into the brain without compromising the integrity of the tight junctions and endothelial layers. However, this approach will also increase the BBB permeability of potential neurotoxic compounds. In fact, many of the efflux pumps could not be fully inhibited the due to various reasons, including multifactorial multidrug resistance and unstable tumor cells [71]. Thus, further investigations of various systemic delivery approaches through enhancing BBB permeability are still required to achieve a significant therapeutic effect for GBM treatment.

IV.3 NANOCARRIER-BASED DRUG DELIVERY STRATEGIES

In recent years, preclinical and clinical research has shown that various factors may compromise the efficacy of (combinations of) therapeutics, which may lead to disappointing clinical outcomes (Table 1). Nanoformulations can overcome many of these hurdles and mask unfavorable characteristics of the active compound and/or improve its efficacy.

Depending on the system, nanoformulations are able to load hydrophilic and hydrophobic drugs, ensure sustained drug release and enhance the half-life of the drug in the circulation. Additionally, improving compound solubility and reducing systemic toxicity are two major goals in designing such formulations. Several FDA approved nanoformulations (e.g. Abraxane®, Doxil®, DaunoXome®) reduce toxicity of the parent compound and thereby improve its therapeutic index. For example, the encapsulation in liposomes prevent the anthracycline drugs DOX and daunorubicin in Doxil®, DaunoXome®, respectively from entering cardiac tissue. Many existing and novel chemotherapeutic drugs have poor water solubility and need to be solubilized with toxic solvents. For instance, Taxol® is a formulation of the poorly soluble Paclitaxel (PTX) that uses Cremophor EL, a polyoxyethylated castor oil, mixed with ethanol to make PTX suitable for intravenous injection. These solvents are associated with numerous side effects, which led to the development of Abraxane® [72]. This albumin-bound formulation of PTX avoids the toxicities

typically associated with Cremophor EL and improves PTX solubility. Compound stability is another important limiting factor. For example, small interfering RNAs (siRNA) show great therapeutic promise but have disappointing clinical relevance due to stability and delivery issues. The only currently FDA approved siRNA therapeutic is Patisiran®, which is based on a lipid nanoparticle formulation that improves siRNA stability. This is essential to reach its destination in the hepatocytes and exert activity.

Two decades have passed since the first nanoparticle-based cancer treatment was approved by the FDA, with an increasing number of clinical trials now ongoing, including many in GBM. It is estimated that due to the BBB, 100% of large molecules and 98% of small molecules fail to sufficiently reach the brain to achieve therapeutic levels [73]. NPs encapsulating these molecules can be tailored to enable specific transport of their payload to the brain or facilitate penetration through the BBB, thereby enabling encapsulated drugs for previously unreachable tumors such as GBM [70].

A variety of systems based on polymers (micelles, dendrimers), inorganic materials (iron, silica, gold) and/or lipids (liposomes, solid lipid nanocarriers) have been investigated for drug delivery to the brain. The therapeutic drugs can be loaded in these particles by encapsulation, covalent linking or surface adsorption [70]. Depending on the design of the drug delivery system, the drugs are either passively or actively targeted to the tumor to exert their effect.

IV.3.1 Passive targeting and EPR effect

Passive tumor targeting is based on the observation that certain sized particles tend to accumulate in tumor tissue much more than they do in normal tissues. This is known as the EPR effect, which was first described by Matsumura and Maeda in 1986 [74].

EPR is based on aberrant pathophysiological characteristics of tumors, mainly the presence of abnormal vasculature and a lack of proper lymphatic drainage. Tumor tissues have a high demand for oxygen and nutrients to support their excessive growth, which leads to increased and uncontrolled formation of blood vessels. As a result, tumor vasculature has abnormally wide fenestrations that lead to increased extravasation of particles with sizes up to several hundreds of nanometers [75]. Additionally, tumor tissues lack effective lymphatic drainage resulting in reduced clearance of the extravasated particles. Together, these phenomena allow for a relatively effective and selective accumulation of NPs in certain solid tumors [76].

However, within the last couple of years, more and more researchers have realized that the EPR effect is highly heterogeneous both intra- and intertumorally, varies during tumor development and does not always hold up in clinical settings (Figure 8).

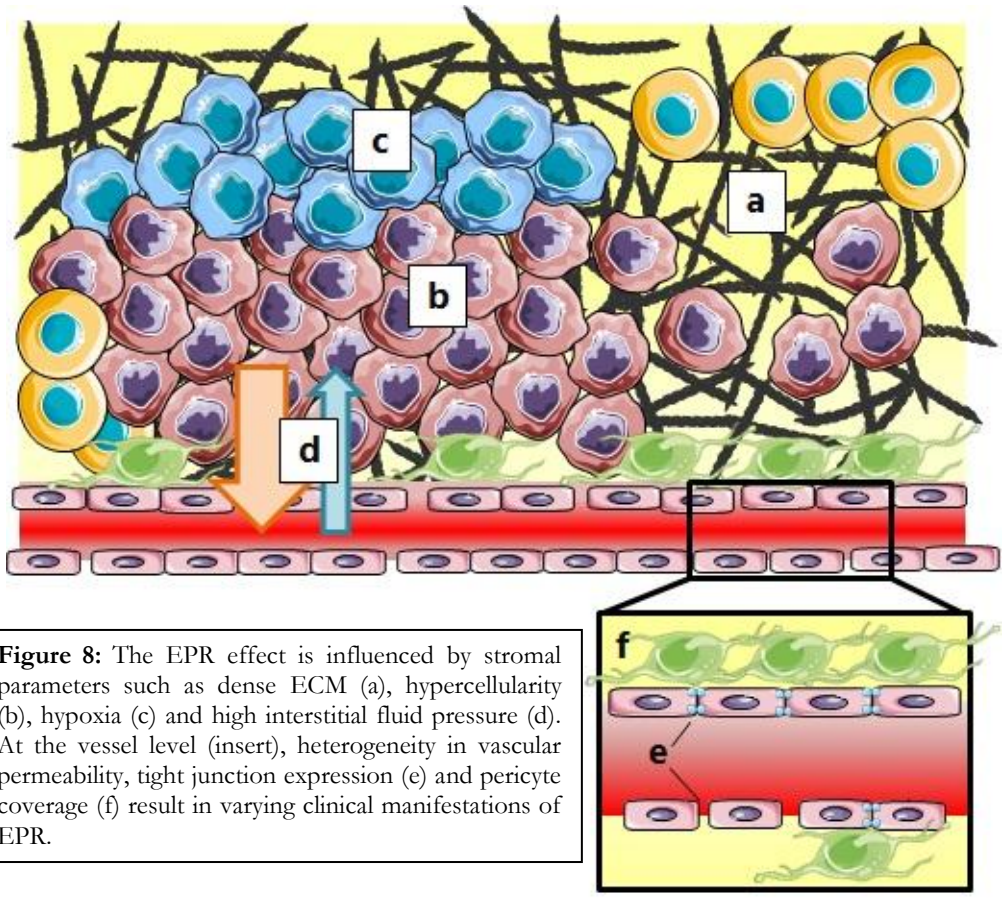

Figure 8: The EPR effect is influenced by stromal parameters such as dense ECM (a), hypercellularity (b), hypoxia (c) and high interstitial fluid pressure (d). At the vessel level (insert), heterogeneity in vascular permeability, tight junction expression (e) and pericyte coverage (f) result in varying clinical manifestations of EPR.

Moreover, the magnitude of the EPR effect as seen in rodent models fails to translate to the clinics. Human tumors are drastically different from preclinical tumor models in many critical aspects, such as: (i) heterogeneity or lack of fenestrations in the tumor endothelium, (ii) presence of acidic and hypoxic areas (iii) lower or heterogeneous pericyte and basement membrane coverage, (iv) and high interstitial fluid pressure induced by dense extracellular matrix (ECM), explaining the difficulty in translating the EPR effect from bench to bedside [77].

Interestingly, GBM is characterized by robust endothelial proliferation resulting in tortuous, disorganized and highly permeable vasculature [78, 79]. Such excessive neovascularization also affects BBB integrity which can be visualized by MRI. Contrast agents such as gadolinium normally do not cross the BBB, but in pathology conditions such as GBM and hypervascularization, causes physical disruptions of the BBB that allow leakage of gadolinium into the tumor tissue, making the tumor visible on T1 weighted MRI. Gadolinium enhanced area forms the golden standard in GBM diagnosis and provide guidance for surgical resection. Thus, theoretically, intravenously administered nanocarriers could exploit this phenomenon in GBM. Yet, it is evidently not true in the clinics.

First of all, when comparing different imaging modalities, it becomes clear that T1-weighted MRI alone does not visualize the entire tumor. Beyond the contrast-enhancing region, essentially all GBM show non-enhancing edema on T2-weighted or fluid attenuation inversion recovery imaging [80]. These areas have impaired fluid regulation yet do not accumulate contrast agent, suggesting that the BBB is intact. Additionally, the impaired fluid regulation leads to high interstitial fluid pressure which compromises transvascular transport of molecules. The invasive tumor- and tumor associated stromal cells in this peritumoral brain zone drive 90% of all recurrences [81, 82]. These cells are also not or barely reached by passively targeted drugs or NPs due to their location behind an intact BBB. This should be considered when designing new therapies and drug delivery systems as the EPR effect may be insufficient to target these cells [34, 79, 81]. Secondly, other key pathological features of GBM are hypoxic areas surrounded by hypercellular rings of actively migrating tumor cells, which are called pseudopalisading tumor cells that are pro-angiogenic, therapy resistant and show decreased proliferation [83, 84]. The hypoxia areas are distant from vasculature, preventing nanocarriers from reaching its target [85].

Due to the differences in EPR effect between and within tumors, approaches to still take advantage of it can vary. In certain situations, one might benefit from tumor vasculature normalization [86], while in others, increasing vascular leakiness or opening up the BBB will improve treatment. This will have to be determined per case and might be patient or tumor specific [87]. On the other hand, it is also affected by the properties of the nanoparticle [88].

The extent of EPR in a tumor could be tested prior to treatment using imaging modalities. In a preclinical study, the relative blood volume was found to correlate with the tumor accumulation of HPMA-based polymeric drug carriers. With the help of contrast-enhanced ultrasound imaging, this vascular parameter proved useful in predicting EPR-mediated tumor accumulation of NPs and could possibly be used to preselect patients [89]. Seo et al. investigated how the size of NPs would affect their tumor distribution in an intracranial rat GBM model. ^{64}Cu-labeled long-circulating particles of different size were systemically administered and tracked via MRI and PET. It was demonstrated that the uptake of 20 nm NPs is significantly greater than 110 nm NPs, 7 hours after systemic injection. It also showed that PET/MRI co-registration of brain images may contribute to the monitoring of disease progression and determining what drug delivery approach is feasible [90].

The high heterogeneity of EPR can be addressed by indirect EPR imaging, utilizing companion diagnostics or developing theranostic systems as well. Indirect EPR imaging can non-invasively visualize and quantify the key EPR-determining parameters of the tumor vasculature, while

theranostics or companion diagnostics can give insight in nanoparticle distribution and tumor response.

IV.3.2 Active targeting

When passive targeting fails, active targeting of NPs can facilitate their transport over the BBB which is needed to be suitable for GBM treatment. With polymeric NPs this is often achieved by modifying their surface with surfactants or (BBB- or glioma specific) ligands. For example, DOX loaded poly butyl-cyanoacrylate NPs were more effective when coated with the surfactant P80 and increased the survival time of GBM tumor-bearing rats compared to the non-coated group as P80 facilitates BBB crossing [91]. Conjugation of the BBB ligand transferrin to PTX loaded PLGA NPs showed significant enhancement of cellular uptake and cytotoxicity on C6 rat glioma cell line, in comparison with the non-conjugated PLGA NPs, by taking advantage of receptor mediated endocytosis (RME) [92]. Similarly, targeting polymeric micelles with cyclic RGD, a ligand with selective affinity for the αvβ3 and αvβ5 integrin that is overexpressed on tumor vasculature and tumor cells, vastly enhanced micelle uptake in tumor in an orthotopic mouse GBM model. Compared to a specific targeted micelles, RGD-micelles loaded with oxiplatin significantly reduced tumor growth [93]. Polymeric NPs are readily modifiable and can be tailored to be suited for brain delivery.

Lipid NPs, liposomes in particular, are also widely investigated in the drug delivery field. Liposomes can encapsulate hydrophilic compounds in the aqueous compartment and hydrophobic compounds in the bilayer making it a versatile delivery vehicle. Positively charged liposomes have been shown to penetrate the BBB by electrostatic interaction with polyanions on the BBB, which leads to adsorptive-mediated endocytosis [94]. Covering the surface of these particles (or NPs in general) with PEG neutralizes surface charge but thereby ensures prolonged circulation and increases the EPR effect. Radiotherapy supplemented with PEGylated liposomal DOX (Caelyx®) resulted in a significantly higher intratumoral concentration of DOX than normal brain tissue in GBM patients [95]. Alternatively, the liposomal surface can be decorated with targeting ligands to facilitate BBB transport via RME and promote tumor specific uptake. Transferrin-conjugated liposomes increased brain delivery of 5-fluorouracil by 13 times compared to non-conjugated liposomes [96]. In another study, interleukin-13 grafted liposomes significantly enhanced the cytotoxicity and tumor accumulation of DOX in comparison with the free drug on a subcutaneous mouse glioma model [97]. Lipid nanocarriers are also able to load both hydrophilic and hydrophobic molecules in an aqueous core by formation of reversed micelles [98]. They have been shown to accumulate in glioma cells within minutes of incubation through

clathrin/caveolae-independent pathways [99]. Similar to liposomes, LNCs may also be coated with PEG or grafted with ligands to ensure efficient brain drug delivery [100]. One LNC component, the non-ionic surfactant HS15, was indicated as a key element in producing a P-gp suppressing effect which could aid retaining the delivered therapeutic in the brain [101].

Inorganic NPs such as those made out of gold or silica have been investigated for brain drug delivery. Their properties allow them to be used for radio-sensitization, therapy, imaging and biomedical sensoring [102-104]. Especially the magnetic and optical features of metallic NPs prove valuable in GBM treatment as it can be used to monitor delivery non-invasively. A transactivator of transcription peptide-targeted gold nanoparticle was able to efficiently cross the blood brain barrier in an intracranial GBM mouse model. Conjugating BBB-impermeable DOX to these particles facilitated its uptake in the brain and improved anti-tumor efficacy [105]. Another study describes an organic-inorganic hybrid NP consisting of PLGA and gold, which was loaded with docetaxel (DTX) and targeted using angiopep-2 and tested in a xenograft GBM mouse model. Targeting the NPs improved the efficacy of DTX due to improved delivery, while the gold allowed X-ray imaging of the accumulated NPs. Moreover, thermal therapy could be applied by exposing the gold NPs to an 808 nm laser, which further increased therapeutic efficacy through local heating [106].

Overall, NPs show great potential in preclinical studies. They often improve accumulation of therapeutic compounds via passive targeting, while active targeting might be employed to increase this accumulation in hard to reach tumors such as GBM. Imaging (whether direct or indirect) can give an indication of the potential of certain tumors to be treated with nanoparticle formulations, thereby preselecting patients and possibly improving treatment success. Otherwise, NP design can reinforce this by including materials that can be imaged, creating theranostic platforms to guide and monitor treatment.

IV.3.3 Tumor associated macrophages and nanoparticle based therapy

Many cancers are preceded by infections or (chronic) inflammation and it is increasingly clear that the immune system plays a central role not only in cancer development but also in tumor progression [107]. In GBM, the tumor immune microenvironment heavily influences progression, invasion, metabolic reprogramming and therapy resistance, mostly orchestrated by the presence of immune cells [108]. Peripheral monocytes are attracted by tumor-secreted factors, infiltrate the brain, differentiate to macrophages and together with the residential microglia develop a class of cells called tumor-associated microglia/macrophages (TAM) [109]. They can represent up to 50% of the GBM mass and high TAM density has been correlated with glioma grade [110] and poor prognosis [111]. GBM cells produce and secrete chemo attractants and signaling molecules to

create an environment that drives TAM towards a predominantly immunosuppressive and tumor supportive, rather than an immune-stimulatory and anti-tumor phenotype [112]. Immunosuppressive TAM promotes tissue remodeling and angiogenesis, thereby driving GBM progression [109]. Key regulators of tissue remodeling include the ECM degrading metalloproteases, prominently MMP-2, -9 and -14, that are found to be upregulated in many cancer tissues [113]. GBM cells lack sufficient MMP-14 needed to activate MMP-2 [109] and therefore stimulate TAM to upregulate MMP-14 expression [114]. This, in turn, drives tissue remodeling, angiogenesis and facilitates tumor invasion [115]. Additionally, TAM further drive angiogenesis via the secretion of pro-angiogenic factors such as VEGF and CXC-chemokine ligand 2, paving the way for hypervascularity as seen in GBM [116].

The tumor immune microenvironment can impact drug distribution via important EPR mechanisms. First, the inflammatory response observed in GBM results in increased vascular permeability. In turn, this will not only allow for extravasation of immune cells, but also of therapeutics including NPs. Furthermore, ECM remodeling can influence NP transport through the interstitial space [117]. Second, in addition to modulation of the physical tumor environment (e.g. ECM and vasculature), TAM can also directly contribute to drug retention. Macrophages protect the body by specializing in phagocytosing pathogens, cellular debris and foreign materials. It can be expected that the bulk of NPs that are taken up by the tumor ends up in these cells [118]. Indeed, most NPs end up in TAM, even when they only represent 1% of tumor mass [119].

Elegant studies by Miller et al. show that NPs predominantly accumulate in tumor-associated immune cells rather than tumor cells. They used fluorescently labeled polymeric NP (~100 nm) together with magnetic NP (~20 nm) in several tumor mouse models to predict NP tumor accumulation and treatment outcome. It appeared that NP distribution was mainly determined by vascularization and permeability at early time points, but at later time points by cellular uptake. Both NPs were mostly taken up by host phagocytes (> 90%). High local TAM counts correlated with increased NP accumulation and as such proved an important component of the EPR effect [120]. Interestingly, the same group showed that NP accumulating TAM can function as a drug depot, which slowly releasing encapsulated therapeutics to surrounding (tumor) cells. Depleting TAM numbers reduced NP accumulation and treatment efficacy, illustrating a role for TAM in tumor drug retention [121].

Furthermore, it was observed that phagocytes, after ingestion of NPs, can move across the vascular wall and carry the NP to the extravascular space. *In vitro* studies show monocyte-mediated transfer of NP over an endothelial monolayer [122]. *In vivo*, TAM with ingested NPs has been observed to cross the BBB and migrate to (distant) tumors. As such, NPs were shuttled between contralateral

CNS tumors via migrating TAM ([123].

Thus, TAM are able to modulate the tumor microenvironment thereby enhancing vascular and interstitial permeability, while their phagocytic nature drives NP uptake and prolongs retention in the tumor. Since TAM is key regulator of several EPR driving mechanisms, it seems natural to investigate ways to take advantage and try to improve drug delivery via these cells.

IV.3.4 Targeting the tumor immune microenvironment to improve nanoparticle delivery

Abnormal tumor vasculature is a double-edged sword for NP delivery. On the one hand it allows extravasation of NPs out of circulation and accumulation in tumor tissues. On the other hand, it results in edema, high IFP and tumor hypo-perfusion, limiting drug delivery. The similarities between inflamed vasculature and tumor vasculature in this regard have led to the hypothesis that targeting tumor inflammation might be beneficial for EPR-based drug delivery, much like the vascular normalization strategies discussed earlier [124]. Indeed, the anti-inflammatory steroid dexamethasone is routinely prescribed to reduce edema and thus IFP in GBM patients [125]. This suggests it might be possible to control inflammation in order to modulate the EPR effect.

Non-steroidal anti-inflammatory drugs (NSAID) are clinically prescribed to treat pain and inflammation. They inhibit COX-1 and COX-2, two enzymes responsible for the production of several pro-inflammatory prostaglandins that are key drivers of inflammation. Moreover, the NSAID aspirin is able to trigger the production of inflammation resolution mediator lipoxin-A4, thereby actively resolving inflammation and reducing vascular permeability [126]. Indeed, COX-inhibitors are able to reduce BBB disruption in neuro-inflammation [127] and prevent protein extravasation in glioma [128]. Moreover, COX-2 inhibition normalized the tumor microenvironment including its vasculature and improved the penetration and accumulation of micelles (22 nm) rather than bigger (100 nm) NPs in a solid tumor mouse model [129].

It is not completely clear whether COX inhibition is fundamental for these observations or that other mechanisms are at play. Interestingly, some NSAIDs are able to inhibit VEGF expression [130] and prevent VEGF-induced vascular permeability [131]. Additionally, both COX-2 [132] and VEGF inhibition (together with angiopoietin-2 inhibition) polarizes TAM towards an anti-tumor phenotype [133, 134]. Skewing the TAM population towards such a phenotype leads to vascular normalization and improved drug distribution in a rat glioma model, thereby improving treatment efficacy [135]. Thus, NSAID treatment might improve drug delivery via direct reduction of vascular permeability while simultaneously polarizing TAM to a vasculature-normalizing, anti-tumor phenotype.

Rather than using local TAM, some have opted for macrophage-mediated NP delivery to the brain. Macrophages were loaded with NPs and administered systemically to an intracranial glioma mouse model. Compared to free NPs, macrophage engulfed NPs were more efficiently reaching the brain due to the ability of macrophages to cross the intact BBB [136]. Whether this is viable to implement in the clinics remains has to be investigated. However, it does suggest that addressing macrophages rather than tumor cells might improve drug delivery to the brain. Indeed, targeting liposomes to the TAM marker CD163 improved their accumulation in the brain of a Parkinson mouse model [137]. Very limited clinical data are available on the combination of drug delivery and tumor microenvironment (TME) modulation. Several studies investigated the use of Aspirin or NSAIDs on the risk of glioma, with conflicting results [138-140]. No positive effect of NSAIDs was seen on patient survival [141] or only in lower grade Glioma [142]. However, these studies do not address topics such as the effect on vascular permeability, TAM polarization status and drug distribution. Also, these parameters are difficult to measure in patients.

Nevertheless, one can imagine a similar role for NSAIDs as seen with bevacizumab, where adding bevacizumab (prior) to chemotherapy can improve patient survival but otherwise has underwhelming effects. It is possible that pretreatment of patients with NSAIDs (or bevacizumab) can help to normalize tumor vasculature (directly or via TAM), and thereby improve the efficacy of chemotherapeutics. Carefully set up trials are necessary to investigate such intricate mechanisms.

The tumor immune microenvironment clearly plays a prominent role in NP-mediated GBM treatment. Current preclinical data warrants further investigation to use the local immune milieu to improve NP mediated drug delivery.

IV.4 RATIONALE OF NANOCARRIER-BASED DRUG COMBINATION

Often a specific ratio of two anticancer agents is required to generate a synergistic anticancer effect, which is difficult to achieve when the drugs are administered in free form. As discussed above, the BBB hinders the penetration of most therapeutic compounds. Thus, not all component drugs of a combination therapy will reach the tumor at the desired ratio at the minimally required concentration and for the most advantageous duration, resulting in sub-optimal efficacy. Due to differing pharmacokinetics, the initial drug ratio is not likely to be maintained until the drugs reach the tumor tissue after systemic administration. This can be resolved when the drugs are co-encapsulated inside a single nanocarrier, which can be designed to balance the pharmacokinetic properties of its contents. The carrier can additionally improve targeting to the tumor site, maintain the drug-to-drug ratio and control drug release within the tumor to reach the ideal therapeutic efficacy.

By properly integrating nanotechnology into combination therapy, the issues with free drug formulations could be addressed and simultaneously leaves room for additional improvements. For instance, implementing imaging agents could non-invasively monitor drug delivery and possibly tumor response. Loading a targeted gold NP with DOX and Gadolinium, improved their delivery across the BBB and their respective functionality as chemotherapeutic and contrast agent in a murine intracranial glioma model [105]. Such theranostic (and diagnostic) nanoplatforms have the potential to become powerful tools as they increase imaging possibilities and allow non-invasive monitoring of treatment and response, which benefits clinicians and patients alike. Many examples in recent years have shown the potential of such platforms for brain cancer in preclinical as well as clinical settings [143-145].

Additionally, NPs can encapsulate or function as radiosensitizers, thereby increasing efficacy of concomitant radiotherapy. Encapsulating novel radiosensitizers in a polymeric NP provided sustained release and improved survival when combined with fractionated radiotherapy in an orthotopic glioma rat model [146]. Correspondingly, incorporating radiosensitizing metronidazoles in a targeted TMZ-loaded NP prolonged survival compared to free TMZ+Radiotherapy (RT) or NP-TMZ+RT in an intracranial glioma mouse model, showing the potential of adding sensitizers to a treatment regimen [147]. Otherwise, NPs can be radiosensitizing by itself [103]. Especially gold- [148, 149] and silver- [150-152] based NPs have shown to enhance radiosensitivity in glioma cells besides being functional drug carriers and imaging modalities.

The possibility to encapsulate multiple agents in a single carrier makes NPs interesting platforms for combination therapies as both agents will travel and reach their destination together. By tweaking the release kinetics of the individual compounds, it is possible to control drug ratios and achieve desired effects. Moreover, the carriers also provide opportunities to encapsulate additional supportive compounds such as imaging agents or radiosensitizers.

V. EXAMPLES OF DRUG COMBINATIONS AGAINST GBM

Combination therapy approaches have been designed and conducted against GBM with innovative combination drug regimens being tested in preclinical and clinical trials. In the following section, we will discuss some of the preclinical examples of nanocarrier-based drug combinations and clinical drug combination therapies. Because different drugs have different mechanisms of action, and will target distinctly different tasks, we will review them separately, discussing two different classifications: combinations of low-molecular-weight chemotherapeutic drugs and combinations between low-molecular-weight and high-molecular-weight drugs (such as proteins, peptides and genes) in preclinical studies.

V.1 NANOCARRIER-BASED COMBINATION DELIVERY OF LOW-MOLECULAR-WEIGHT DRUGS IN PRECLINICAL STUDIES

The development of nanomedicine could magnify the therapeutic results of small-molecular-weight chemotherapeutic drugs through different ways, such as improving cellular uptake, sustained drug release, overcoming the BBB, and targeting the drug to the tumor site. Table 2 lists some non-exhaustive examples from PubMed of the nanomedicine-based combination for different small-molecular-weight chemotherapeutic drugs.

Table 2: Nanocarrier-based combination delivery of low molecular weight drugs in preclinical studies

Nanocarriers	Drugs	Mechanism of action	Cells or animal model	Key findings	References
Liposomes	IB; DOX	Modulate signaling networks upstream of actin polymerization and inhibit ROS production; Topoisomerase inhibitor	RT2 astrocytoma rodent model	IB inhibited invasion of rat and human glioma cells and enhanced chemotherapy with DOX *in vivo*. (Intravenous administration)	[153]
Magnetic NPs	Curcumin; TMZ	Anti-inflammatory, proapoptotic, anti-angiogenic, anti-mitogenic, and immunomodulatory agent, inhibiting gene expression of matrix metalloproteinases; Alkylating agent	2D and spheroid 3D culture of T98G cell line	The dual drug-loaded NPs demonstrated higher cytotoxic effect than single drug-loaded NPs in 2D and 3D cell culture. The combination index revealed synergistic effect.	[154]
Transferrin-conjugated magnetic silica NPs	PTX; DOX	Mitotic inhibitor; Topoisomerase inhibitor	Orthotopic U87MG mice model	The enhanced cellular uptake and cytotoxicity of drug-loaded NPs was achieved with the formulation. The drug combination treatment exhibited the strongest anti-glioma activity compared with the controls. (Intravenous administration)	[155]
Lactoferrin-tethered magnetic nanocapsules	Curcumin; DOX	Anti-inflammatory, proapoptotic, anti-angiogenic, anti-mitogenic, and immunomodulatory agent, inhibiting gene expression of matrix metalloproteinases; Topoisomerase inhibitor	Subcutaneous RG2 mice model	Elevated uptake of nanocapsules in the RG2 cells was obtained. The codelivered chemotherapeutics with magnetic targeting suppressed tumor growth more efficiently than the controls *in vivo*. (Intravenous administration)	[156]
mPEG-PLGA based thermosensitive hydrogels	PTX; TMZ	Mitotic inhibitor; Alkylating agent	U87 and C6 cell lines	The PTX and TMZ were sustained released from the composite gel. The drug coloaded gel possessed much higher tumor cell growth inhibition and apoptosis induction than other	[157]

				formulations.	
mPEG-PCL block copolymeric micelles	Rapamycin (Sirolimus); Curcumin	mTOR inhibitor; Anti-inflammatory, proapoptotic, anti-angiogenic, anti-mitogenic, and immunomodulatory agent, inhibiting gene expression of matrix metalloproteinases;	U373 and T98G cell lines	The drug-loaded micelles showed higher cellular uptake and enhanced mitochondrial membrane potential depolarization than native drugs in cell culture. The drug combination downregulated P13/AKT and serine/threonine kinase proteins and led to programmed cell death.	[158]
DSPE-PEG2000 liposomes	Quercetin; TMZ	Radical-scavenging antioxidant; Alkylating agent	Orthotopic U87 rats model	The drug coloaded liposomes induced higher cellular uptake and higher cytotoxicity in the cell culture. A significant accumulation of drug coloaded liposomes was observed in the brain, with significantly increased plasma drug concentrations and delayed clearance in rat model. (Oral administration)	[159]
Ca-alginate microparticle-based fibers	PTX; TMZ	Mitotic inhibitor; Alkylating agent	C6 cell line	The optimal synergistic ratio of PTX to TMZ was 1:1 (w:w).	[160]
mPEG-PLGA NPs	PTX; TMZ	Mitotic inhibitor; Alkylating agent	Subcutaneous U87 mice model	The optimal synergistic ratios of PTX to TMZ were 1:5 and 1:100 (w:w) n U87 and C6 cells, respectively. The PTX: TMZ (1:5)-loaded NPs significantly inhibited tumor growth in the subcutaneous U87 model. (Intravenous administration)	[161]
mPEG-PCL NPs	RES; TMZ	Targeting proteins involved in cell proliferation and drug transport; Alkylating agent	Subcutaneous U87 mice model	TMZ/RES-coloaded NPs induced higher apoptosis in U87 glioma cells, caused inhibition of phosphor-Akt and upregulation of the downstream apoptotic proteins and a superior tumor-delaying effect in a subcutaneous model. (Intraperitoneal administration)	[162]

Motif B6 peptide, DSPE-PEG2000, poly (β-amino ester) and azobenzene-based nanoparticle	Combretastatin A4; ATRA; DOX	Anti-angiogenesis; Induction of GSCs differentiate to GBM cells; Topoisomerase inhibitor	U87MG and CD133 positive GSCs; Orthotopic U87MG mice model	Combretastatin A4 was first released through NPs. DOX was released after internalization into cells. After endocytosis, the released ATRA induces GSC differentiation and downregulates survival pathways. The synergistic antitumor effect significantly extended the survival time of the GBM mouse model. (Intravenous administration)	[163]
PLGA microsphere	Aspirin; TMZ	Inhibition of the b-catenin/TCF signaling pathway; Alkylating agent	Subcutaneous LN229 mice model	Aspirin/TMZ coloaded microspheres induced more apoptosis and repressed proliferation in LN229 and U87 cells. Intratumor injection of aspirin/TMZ microspheres significantly delayed tumor growth in a subcutaneous LN229 mouse model. (Intratumoral injection)	[164]
LNCs	GemC12; PTX	Inhibition of DNA synthesis	9L and GL261 cell lines	The drug combination showed synergy between PTX and GemC12.	[66]
PLGA wafer	TMZ; BCNU	Alkylating agent	Orthotopic 9L rats model	The rats treated with the BCNU-TMZ wafer had the longest median survival. (Intracranial implantation)	[165]
Transferrin-functionalized nanoparticle	TMZ; JQ1	Alkylating agent; bromodomain inhibitor	Orthotopic U87MG and GL261 mice model	Treatment of tumor-bearing mice with transferrin-NPs loaded with TMZ and JQ1 leads to increased DNA damage and apoptosis, a decrease in the tumor burden and a corresponding increase in survival compared with free-drug dosing. (Intravenous administration)	[166]

Abbreviations: IB, imipramine blue; DOX, doxorubicin; PTX, paclitaxel; TMZ, temozolomide; RES, resveratrol; BCNU, carmustine; GemC12, lauroyl-gemcitabine; ATRA, all-trans retinoic acid; NPs, Nanoparticles.

V.1.1 Polymeric NP-based combination delivery of low-molecular-weight drugs

After Xu et al. encapsulated PTX and TMZ together within mPEG-PLGA nanoparticles and pluronics-based thermosensitive hydrogels, a sustained release of the two drugs was observed and the drug combination inhibited tumor cell growth and induced apoptosis [157]. The best synergistic ratios between PTX and TMZ, which were 1:5 and 1:100 for U87 and C6 cells, respectively, and the intravenously administered drug combination significantly inhibited tumor growth in a U87 subcutaneous model *in vivo* [161]. Some of the small-molecular-weight drugs may improve the therapeutic effect of anti-tumor drugs by making tumor cells sensitive to those drugs. By encapsulation in PLGA microspheres, Shi et al. found that aspirin could sensitize glioma cells to TMZ through inhibition of the b-catenin/TCF signaling pathway [164]. The methoxy poly (ethylene glycol)-poly (ε-caprolactone) block copolymeric micelles loaded with rapamycin and curcumin was shown to downregulate serine/threonine kinase and P13/AKT, enhancing cellular uptake to more than 3.3 times compared to native drug [158]. Not only synthetic polymers but using materials of natural biodegradable polymers to make NPs has provoked great interests. Using Ca-alginate microparticle-based fibers, a decreased initial burst release and a prolonged release were observed and C6 cells were more sensitive to the drug combination [160].

V.1.2 Liposome-based combination delivery of low-molecular-weight drugs

Compared with synthetic nanocarriers, lipid-based nanocarriers have less concern about being toxic for *in vivo* applications; thus, they are widely used in drug combination therapy. Munson et al. investigated the sequential combination strategy of liposome-imipramine blue and liposome-DOX. Imipramine Blue is a NADPH oxidase inhibitor that has anti-invasive potential, while DOX is the topoisomerase inhibitor. The combination of the two drugs resulted in prolonged survival compared with single-drug treatment in an aggressive rodent high-grade astrocytoma model [153]. Hu et al. found that DSPE-PEG polymeric liposomes helped to enhance the cellular uptake of quercetin and TMZ and increased their potency in a TMZ-resistant U87 cell line [159]. Shin et al. conjugated CD133 monoclonal antibody to liposomes to induce increased cytotoxicity of gemcitabine to glioma stem cells *in vitro*. The anti-stem cell ability was increased by the drug combination with bevacizumab in stem cell-xenografted mice [167].

V.1.3 Magnetic NP-based combination delivery of low-molecular-weight drugs

Magnetic NPs are widely utilized for advanced magnetic resonance imaging and guided drug delivery and are currently a blooming research field for combination treatment. Iron oxide-loaded magnetic nanoparticles are MRI imaging contrast agents and drug delivery vehicles. With the magnetic nanoparticles loaded with curcumin and TMZ, the combination index was calculated to be synergistic between two drugs on 2D and spheroid 3D culture of the T98G cell line [154]. The combination loading of curcumin and DOX by lactoferrin-tethered magnetic double emulsion nanocapsules enhanced the tumor accumulation and delayed tumor growth in the subcutaneous RG2 model [156]. In another study, transferrin (Tf) was conjugated as a targeting ligand on magnetic silica PLGA NPs, and U87MG cells treated with DOX-PTX-NPs-Tf resulted in the highest cytotoxicity compared with cells treated with single drug or drug combination without transferrin [155]. The same promising result was observed also in an orthotopic U87MG model. A biodistribution study showed enhanced accumulation of PLGA-based NPs loaded with PTX and SPIO in the brain of GBM-bearing mice with magnetic targeting. When tested for *in vivo* efficacy, the magnetic targeting treatment significantly prolonged the median survival time compared with the control treatments and passive targeting [168].

V.2 NANOCARRIER-BASED COMBINATION DELIVERY OF LOW- AND HIGH-MOLECULAR-WEIGHT DRUGS IN PRECLINICAL STUDIES

Although combination treatments of anti-cancer drugs with different mechanisms of action show promising therapeutic effects, the intrinsic and acquired chemoresistance are the major reasons for the failure of chemotherapy in GBM [169]. High-molecular-weight drugs, including proteins, peptides, antibodies or genes, have been investigated to prevent chemoresistance in cancer treatment by different targeting modes. Therefore, the approaches of the combination between low- and high-molecular-weight drugs are demonstrating increasingly more potential perspectives. The non-exhaustive summary of the recent combination delivery of low- and high-molecular-weight drugs from PubMed are listed in Table 3.

Table 3: Nanocarrier-based combination delivery of low- and high-molecular-weight drugs (proteins, peptides and genes) in preclinical studies

Nanocarriers	Drugs	Mechanism of action	Cells and animal model	Key findings	References
anti-CD133-conjugated liposomes	GEM; Bevacizumab	Inhibition of thymidylate synthetase; Anti-VEGF antibody	Subcutaneous GBM stem cell mice model	Liposomal encapsulation and conjugation of anti-CD133 antibody enhanced the cytotoxicity of GEM in GBM stem cells. The antitumor efficacy of combination therapy with liposome-GEM and bevacizumab in a xenograft model was significantly greater than that of monotherapy. (Intravenous administration)	[167]
RGD-conjugated micelles	MDM2/MDMX antagonists; TMZ	p53 activator; Alkylating agent	Orthotopic and subcutaneous U87MG mice model	The formulation inhibited the proliferation of glioma cells by activating the p53 signaling pathway. The drug coloaded micelles increased the antitumor efficacy against GBM in orthotopic and subcutaneous mouse models. (TMZ: oral administration; Micelles: intravenous administration)	[170]
PLGA NPs	Ft peptide; PTX	Targeting the ECM component and neovasculature; Mitotic inhibitor	Orthotopic U87MG mice model	Ft peptide enabled the internalization of PLGA NPs in U87MG cells and HUVECs and facilitated its deep penetration in 3D glioma spheroids. An accumulation of the Ft-NPs in the glioma foci of intracranial U87 glioma-bearing mice was observed. The median survival of Ft-NP-PTX-treated mice was enhanced by 269% compared with that in untreated mice. (Intravenous administration)	[171]
Poly(amidoamine) dendrimers	Transferrin; Tamoxifen; DOX	Targeting ligand for BBB; MDR inhibitor; Topoisomerase inhibitor	C6 cell line	The carrier was internalized into C6 glioma cells upon crossing the BBB model by the coactions of transferrin receptor-mediated endocytosis and the inhibition effect of TAM to the drug efflux transports. *In vitro* accumulation of DOX in avascular C6 glioma spheroids made the tumor volume effectively reduced.	[172]
mPEG-PCL and HOOC-PEG-PCL-based polymersomes	Lactoferrin; Tetrandrine; DOX	Targeting ligand for BBB; MDR inhibitor; Topoisomerase inhibitor	Orthotopic C6 rats model	The polymersomes could enter the brain and accumulate at the tumor site. The tumor volume of the drug coloaded polymersome-treated group was significantly smaller than that in the other therapeutic groups. (Intravenous administration)	[173]

Magnetic polymeric NPs	BG; TMZ	DNA repair inhibitors; Alkylating agent	Orthotopic GBM6 mice model	Controlled, localized BG release and proper trafficking of BG in human GBM cells was achieved. Drug-loaded NPs reduced MGMT activity. Concurrent treatment with two drugs showed a 3-fold increase in the median overall survival compared with single drug-treated mice. (Convection enhanced delivery)	[174]
Chitosan-LNCs	siRNA; TMZ	Downregulation of Galectin-1 EGFR; Alkylating agent	Orthotopic U87MG mice model	The survival of mice treated with the combination of siRNAs and TMZ was significantly increased compared with animals treated by single siRNAs loaded in chitosan-LNCs. (LNC: convection enhanced delivery; TMZ: intraperitoneal injection)	[175]
Antitransferrin receptor single-chain antibody fragment-conjugated liposomes	P53 DNA; TMZ	Induction of wtp53-mediated silencing of MGMT	Subcutaneous T98G mice model	The liposomes crossed the BBB and efficiently targeted GBM and cancer stem cells. The systemic delivery of liposomes-p53 downregulated MGMT and induced apoptosis in intracranial GBM xenografts. The combination of liposomes-p53 and TMZ enhanced survival in a mouse model of highly TMZ-resistant GBM. (Intravenous administration)	[176]
star-branched copolymers	miRNA inhibitor; DOX	Downregulation of miR-21; Topoisomerase inhibitor	Subcutaneous LN229 mice model	The micelles could mediate lysosome escape of miR-21i and the release of DOX to the nucleus. Codelivery of DOX and miR-21i exhibited better anti-proliferative efficiency than single drug alone. (Intratumoral injection)	[177]
Gold NPs; folate-chitosan nanogels	miR-218 mimics; TMZ	Upregulation of miR-218; Alkylating agents	Subcutaneous U87MG mice model	Using nanogels allowed drugs to be targeted to the tumor site, the intracellular uptake is enhanced to a greater extent, and significant antitumor efficacy is fold increase compared with the free drug administration group without noticeable system cytotoxicity. (Intravenous administration)	[178]
Folate-conjugated PEI-PCL NPs	siRNA; DOX	Downregulation of BCL-2	Orthotopic C6 rats model	Drug-loaded NPs effectively suppressed the anti-apoptotic response and sensitized C6 cells to DOX treatment. The folate-targeted drug codelivery caused downregulation of the anti-apoptotic BCL-2 gene and remarkable cell apoptosis in tumor tissues. An excellent therapeutic effect was achieved using the folate-targeted codelivery strategy in an animal model. (Intratumoral injection)	[179]

receptor-specific peptide-modified liposomes	VEGF siRNA; DTX	Downregulation of VEGF; Mitotic inhibitor	Subcutaneous mice U87MG model	The dual peptide-modified liposomes persisted the binding ability to glioma cells and enhanced the internalization via specific receptor-mediated endocytosis and tissue penetration. The combination of VEGF siRNA and DTX showed superiority in anti-tumor efficacy after both intratumor and system application against tumors in a mouse model. (Intratumoral injection)	[180]
PEI NPs and PLGA-based fibers	MMP-2 expression RNAi; PTX	Downregulation of matrix metallopeptidase; Mitotic inhibitor	Orthotopic U87MG mice model	Potent inhibition effects on MMP-2 mRNA and protein expression, *in vitro* cell angiogenesis and invasion were demonstrated both with PEI/DNA NPs alone and NPs embedded in microfibers. Local treatment with gene/drug dual delivery microfiber imposed significant tumor regression compared with single-drug delivery microfibers and commercial drug treatment in an intracranial xenograft tumor model. (Intracranial implantation)	[181]
Transferrin-conjugated dendrimer	DNA; T7 peptide; DOX	Expression of TNF-related apoptosis-inducing ligand; Targeting ligand for BBB; Topoisomerase inhibitor	Orthotopic U87MG mice model	The T7-modified codelivery system showed higher efficiency in cellular uptake and gene expression than the unmodified system in U87MG cells and accumulated in tumors more efficiently *in vivo*. The combination treatment resulted in synergistic growth inhibition in U87MG cells and displayed more anti-glioma activity than control groups *in vivo*. (Intravenous administration)	[182]
PEI	DNA; DEXA	Glioma and hypoxia dual-specific plasmids; glucocorticoid agonist	Orthotopic and subcutaneous U87MG mice model	The plasmid showed higher gene expression under hypoxia in a GBM-specific manner and specifically induced caspase activity and cell death in hypoxic GBM cells. The tumor size was reduced more effectively in the drug delivery system-treated group than in the controls in GBM models. (Intratumoral injection)	[183]
Amphiphilic peptides (R3V6)	siRNA; BCNU	Downregulation of VEGF; Alkylating agent	C6 cell line	R3V6 delivered both VEGF-siRNA and BCNU efficiently into GBM cells, resulting in remarkable VEGF expression.	[184]

PEG-PLA micelle and RGD-PEG-PEI	DNA; PTX	Expression of TNF-related apoptosis-inducing ligand; Mitotic inhibitor	Orthotopic U87 mouse model	The median survival of the intracranial GBM-bearing model mice treated with the drug codelivery system is significantly longer than that of solely treated mice. (Intravenous administration)	[185]
lipid-polymer hybrid NPs	oligonucleotide; Pemetrexed	miR-21 antisense	U87MG cell line	Sustained release of pemetrexed up to 10 hours was obtained. Encapsulation of pemetrexed remarkably increased cellular uptake. Codelivery of anti-miR-21 significantly improved the accumulation of NPs in the nucleus of U87MG cells.	[186]

Abbreviations: DOX, doxorubicin; PTX, paclitaxel; TMZ, temozolomide; BCNU, carmustine; GEM, gemcitabine; DTX, docetaxel; DEXA, dexamethasone; BG, O(6)-benzylguanine; MMP-2, matrix metalloproteinase-2.

V.2.1 BBB-targeted drug combination therapy

The BBB and multidrug resistance are the main causes of the low prognosis of GBM patients [187]. A few endogenous cellular transporter ligands, such as transferrin and lactoferrin, have been widely studied in brain-targeting drug delivery systems. The receptors of those ligands are overexpressed on both the brain capillary endothelium and many malignant cells [188, 189]. Several studies reported that drug-loaded carriers could transport their content across the BBB via those targeting groups [190, 191]. Two dual-targeting agent-loaded drug delivery systems, transferrin- and tamoxifen-conjugated pH-sensitive dendrimers loaded with DOX, were developed by Li et al. This system demonstrated both BBB and glioma-targeting and MDR inhibition ability [192]. Using a similar idea, Pang et al. developed lactoferrin-conjugated biodegradable polymersomes loaded with DOX and tetrandrine. The *in vivo* study illustrated the polymersomes could accumulate at the brain tumor site [193].

V.2.2 GBM pathway-targeted drug combination therapy

Next to BBB and efflux pump-related drug resistance, cancer cells may develop several other pathways to escape apoptosis induced by chemotherapeutic agents. Several genes have been found to be responsible for the development of chemoresistance in GBM, such as the overexpression of EGFR, oncogenic miR21, tumor suppressor gene p53, anti-apoptotic protein BCL-2, MGMT, and matrix metalloproteinase-2.

Because TMZ is the first-line treatment in brain cancer, most of the studies were focused on overcoming TMZ resistance. For example, studies have suggested that the resistance to TMZ can be hindered by subsiding MGMT activity with DNA repair inhibitors such as O6-benzylguanine [194]. However, although the co-administration of O6-BG enhanced TMZ cytotoxicity, the systemic delivery of O6-BG with TMZ in human patients resulted in serious dose-dependent toxicities with myelosuppression [195]. Stephen et al. developed superparamagnetic iron oxide NPs to use convection-enhanced delivery of O6-BG to the GBM. The NPs consist of a magnetic core coated with a biocompatible chitosan-PEG copolymer. Concomitant therapy of O6-BG-loaded NPs and TMZ showed a 3-time increase in the median survival compared with the non O6-BG-treated and untreated groups [196].

The tumor suppressor gene p53 is frequently mutationally inactivated, and aberrant p53 expression is presented in GBM patients, making it a potential therapeutic target [197]. Overexpression of

wtp53 has been shown to increase the sensitivity of cancer cells to TMZ *in vitro* and *in vivo* in preclinical studies [198]. Because p53-based treatment for GBM is limited by the lack of BBB permeability, Kim et al. systemically administered p53 via tumor-targeting liposome nanocomplexes that could cross the BBB and downregulate MGMT, leading to enhanced survival with the combination of TMZ in a TMZ-resistant GBM mouse model [176]. The p53 signaling pathway can also be impaired due to functional inhibition by its negative regulators MDM2 and MDMX [199]. MDM2 and MDMX bind together to impede p53 transactivation. They are frequently overexpressed in tumors retaining wild-type p53, including gliomas [200, 201]. Chen et al. developed an RGD peptide-conjugated PEG-co-poly (lactic acid) polymeric micelle loaded with an antagonistic stapled peptide of both MDM2 and MDMX. The RGD peptide could recognize αvβ3 integrin expressed on tumor neovasculature and glioma cells. *In vitro* studies showed that this system effectively activated the p53 signaling pathway, and the combination with TMZ increased the anti-tumor efficacy against GBM in subcutaneous and intracranial U87MG glioma models [170].

Short-nucleotide, double-stranded siRNAs can affect gene expression post-transcriptionally by modifying the translation of target mRNA and is involved in a few biological processes [202]. One target for GBM treatment is BCL-2, which is an anti-apoptotic protein predominantly found in the outer membrane of mitochondria, preventing the release of apoptogenic factors such as apoptosis-inducing factor and cytochrome c [203]. Cheng et al. built a folate-targeted co-delivery system loaded with BCL-2 siRNA and DOX, which effectively inhibited the anti-apoptotic response and sensitized C6 cells to DOX treatment, demonstrating the synergistic effect of the DOX and BCL-siRNA combination in accelerating glioma C6 cell apoptosis [179].

MMP-2 has been found to be frequently overexpressed in glioma cell lines, and its activation has been reported to enhance tumor invasion and angiogenesis [204, 205]. Lei et al. co-loaded MMP-2 siRNA and PTX in PLGA-based submicron implants to attain the sustained release of both drugs. It was demonstrated that the siRNA/PTX dual-loaded microfibers could show significant tumor prevention compared with single drug-loaded microfibers and the commercial Taxol-treated group [181].

VEGF-targeted therapies have been developed to inhibit new blood vessel growth and starve tumors of necessary oxygen and nutrients [206-208]. In a study by Yi et al., BCNU and vascular VEGF siRNA were co-loaded to treat C6 GBM cells based on a nontoxic peptide-based carrier. The peptide is amphiphilic and forms micelles in aqueous solution. Peptide micelles-BCNU showed higher transfection efficiency into cells than BCNU only. Finally, it was proven that, in C6 cells, VEGF expression was significantly decreased by transfection of VEGF-siRNA/micelles or

VEGF siRNA/micelles-BCNU complexes [184]. Thus, the combination between chemotherapeutic drugs and gene or peptide therapy provides great potential in the treatment against malignant GBMs.

V.3 RECENT CLINICAL TRIALS OF DRUG COMBINATIONS FOR GBM TREATMENT

Several drug combination strategies have been studied to reach multiple goals of treating GBM patients in the clinics. In this section, non-exhaustive clinical trials of drug combinations for GBM treatment are summarized in Table 4 (Source: ClinicalTrials.gov). The combination possibility of bevacizumab and different anti-tumor agents has been investigated in several clinical trials. In those with published results in PubMed, a phase II clinical trial using bevacizumab and the topoisomerase inhibitor irinotecan showed a 6-month progression-free survival rate approximately 50.3% compared with 42.6% with bevacizumab alone in recurrent GBM [209]. Another target in the clinics is TMZ resistance. A phase II clinical trial showing the combination of TMZ and an MGMT inhibitor can rebuild drug sensitivity in TMZ-resistant anaplastic glioma [210]. However, even with the promising anti-tumor efficacy in preclinical studies, negative results were obtained frequently in some of these clinical trials. For example, a phase I/II trial to determine the efficacy of vorinostat + erlotinib versus vorinostat + erlotinib + TMZ in patients with recurrent GBM multiforme was terminated because of unanticipated toxicities (NCT01110876). With the combination of the histone deacetylase inhibitor vorinostat and proteasome inhibitor bortezomib to treat recurrent GBM, no patient had progression-free at 6 months with only one patient showed a partial response according to the Macdonald criteria [211]. Currently, some promising nanotechnology-based therapeutics are in clinical trials. For example, a Phase II clinical trial is currently looking into the effects of the combination of oral TMZ and intravenously administered SGT-53, a complex of cationic liposome encapsulating a normal human wild-type p53 DNA sequence in a plasmid backbone, in patients with confirmed GBM who have proven tumor recurrence or progression (NCT02340156). Although we hope that these trials will lead to promising new therapies for GBM, additional studies are still required to identify the potential nanotechnology drug delivery systems that may ultimately have a significant impact on GBM patients compared with the naked drugs.

Table 4: Recent clinical trials of drug combination for GBM treatment

Drugs	Mechanism of action	Condition	Phase/Status	Clinical trial ID
Bevacizumab; Irinotecan	Anti-VEGF antibody; Topoisomerase I inhibitor	Recurrent Gliomas	phase II/Completed in 2013	NCT00921167
O6-Benzylguanine; Temozolomide	O6-alkylguanine-DNA alkyltransferase inhibitor; Alkylating agent	Temozolomide-Resistant Malignant Glioma	phase II/Completed in 2008	NCT00613093
Vorinostat; Bortezomib	Histone deacetylase inhibitor; Proteasome inhibitor	Recurrent GBM	phase II/Completed in 2010	NCT00641706
Imatinib; Hydroxyurea	Tyrosine kinase inhibitor; ribonucleoside diphosphate reductase inhibitor	Recurrent/Progressive Grade II Low-Grade Glioma	phase II/Completed in 2012	NCT00615927
Cediranib; Lomustine	Tyrosine kinase; Alkylating agent	Recurrent GBM	Phase III/Completed in 2016	NCT00777153
Erlotinib; Vorinostat; Temozolomide	Tyrosine kinase inhibitor; Histone deacetylase inhibitor; Alkylating agent	Recurrent GBM	Phase II/Terminated in 2014 (Unanticipated Toxicities)	NCT01110876
Sorafenib; Temsirolimus	Tyrosine kinase inhibitor; mTOR inhibitor	Recurrent GBM	Phase I/II/Completed in 2013	NCT00329719
Bevacizumab; Sorafenib	Anti-VEGF antibody; Tyrosine protein kinases	Recurrent GBM	Phase II/Completed in 2014	NCT00621686
Bevacizumab; Temsirolimus	Anti-VEGF antibody; mTOR inhibitor	Recurrent GBM	Phase II/Completed in 2010	NCT00800917
Erlotinib; Sirolimus	Tyrosine kinase inhibitor; mTOR inhibitor	Recurrent GBM	Phase II/Completed in 2009	NCT00672243
Vorinostat; Bortezomib	Deacetylase inhibitor; Proteasome inhibitor	Recurrent GBM	Phase II/ Completed in 2010	NCT00641706
Bevacizumab; Erlotinib	Anti-VEGF antibody; Tyrosine kinase inhibitor;	Recurrent GBM	Phase II/ Completed in 2010	NCT00671970
Temozolomide;	Alkylating agent;	Recurrent GBM	Phase II/ Recruiting	NCT02340156

SGT-53	Liposome-p53 DNA			
Glasdegib; Temozolomide	Inhibits SHH pathway interfering with cancer stem cells and endothelial migration; Alkylating agent	Newly Diagnosed GBM	Phase IB/II/ Recruiting	NCT03466450
Bortezomib; Temozolomide	Deplete the MGMT enzyme; Alkylating agent	Recurrent GBM With Unmethylated MGMT Promoter	Phase IB/II/ Recruiting	NCT03643549
Bevacizumab; Capecitabine	Anti-VEGF antibody; Target myeloid-derived suppressor cells	Recurrent GBM	Phase I/ Recruiting	NCT02669173

VI. PERSPECTIVES BEFORE MOVING TO THE CLINICS

Although the combination therapy for GBM has already been investigated in many clinical trials, the following key points are required to be considered before reaching clinical trials.

VI.1 DRUG TO DRUG RATIOS

In clinical combination chemotherapy, each single agent is usually administered at its maximum tolerated dose (MTD). The key idea within this strategy is that maximal anti-cancer efficiency could be obtained at each drug's MTD. Indeed, for most anti-cancer drugs, the therapeutic window is typically narrow with a sigmoidal dose-inhibition of tumor cell survival [10]. However, this principle for chemotherapeutic drug combinations might not always be optimal because it was confirmed that anti-cancer drug combinations can act synergistically, additionally or antagonistically against tumor cell growth depending on the ratios of the single drug in combination [212]. For example, Mayer et al. evaluated three different chemotherapeutic combinations with distinct molecular mechanisms (cytarabine/daunorubicin, irinotecan/floxuridine and cisplatin/daunorubicin) to determine ratio-dependent synergistic effect for each of the two drugs. In all cases, a synergistic effect was obtained at a certain drug to drug molar ratio *in vitro*; however, with other ratios, the drugs were shown to be additive or even antagonistic [213]. In most cases, the discrepancy of the combination effects will not be that much. For example, the arsenic trioxide and silibinin showed additive or synergistic effects with different drug ratios in the U87MG cell line, with a CI value ranging from 0.739 to 1.005 [214]. However, in the case that the combination ratio at MTD is actually an antagonistic effect rather than a synergistic effect, the therapeutic benefits of the drug combination will be useless or even cause adverse effects for cancer treatment. The *in vitro* combination effect of two drugs must be well studied; thus, the drug combination at the synergistic ratio could be treated as a "new drug" for *in vivo* use.

VI.2 LOCAL SYNERGISTIC CONCENTRATION

Although we can control the ratio of two drugs to make them act synergistically *in vitro*, it is still not sufficient to obtain a synergistic therapeutic effect ratio *in vivo*. One of the key points of *in vivo* combination administration is to control drugs at certain ratios even after systemic administration because of the differences in the distribution, metabolism and excretion for each single drug. Specifically, when talking about GBM, there is a huge discrepancy in the BBB permeability of each drug. For example, PTX, the first chemotherapeutic mitotic inhibitor that received FDA approval for cancer therapy, exhibited limited brain uptake due to poor BBB-permeability. This prevents its

use in CNS indications even though it shows promising results *in vitro*. Nanotechnology can change the pharmacokinetics of the payloads by modifying the circulation time, tissue distribution and metabolism of the drug. However, whether the combination drug candidates could reach the tumor in a synergistic ratio remains critical. Not only the comprehensive understanding of PB/ PK/PD of the single drug in blood circulation crucial but also knowledge about brain local bioavailability is necessary to design an effective synergistic drug combination for GBM treatment. To reach this synergistic ratio of combination drugs is highly challenging. In some cases, techniques such as using radio- or fluorescence-labeled drug could be a useful tool for scientists to understand drug concentrations and distribution inside the brain. Nanomedicine-based local drug delivery could be another promising way to overcome the challenges of reaching synergistic drug ratios that are difficult to achieve by systemic delivery. Combinations of agents could be encapsulated in the same or different carriers at their synergistic ratio and administered directly into the tumor resection cavity to obtain better therapeutic efficacy.

VI.3 TIMING OF DRUG COMBINATION ADMINISTRATION

The timing and order in which drugs are administered can have significant effects on the treatment outcome. Particularly, the complex tumor microenvironment, which includes an abnormal tumor vasculature, hypercellularity, elevated interstitial fluid pressure, growth-induced solid stress and a stromal ECM, can greatly impair drug distribution within the tumor [215].

To reduce the negative impact that these factors pose to therapy, it is possible to improve drug distribution and efficacy by administering the drugs in a specific order, thereby "priming" the microenvironment. As described in the EPR section, vascular normalization using anti-angiogenic therapeutics can improve the treatment outcome. Patients who were treated with the antiangiogenic drug cediranib together with radio-chemotherapy had improved PFS and OS when they showed improved tumor perfusion because of the vasculature normalization induced by the anti-angiogenic kinase inhibitor given first [216]. Whether the improved survival is due to increased efficacy of the secondary treatment, the additional effect of the anti-angiogenic therapy or both remains unclear [217]. Additionally, several clinical studies observed that bevacuzimab only provided survival benefits in combination with radiochemotherapy [218]. This suggests that the anti-angiogenic drug alone was not primarily responsible for the therapeutic effect and was more important in a supportive role to improve drug distribution with possible additional effects on interstitial fluid pressure and hypoxia, two factors that influence both drug distribution and patient survival [218].

The strongest evidence for the beneficial effect of vascular normalization, appears to exist for

smaller drugs. The normalization also reduces vessel leakiness, possibly preventing extravasation of larger molecules. This was shown when, after vascular normalization in a mouse breast tumor model, Abraxane (~130 nm) prolonged the tumor doubling times, while Doxil (~100 nm) did not [86]. Therefore, it is therefore important to realize the effect of a certain compound when a follow-up treatment is intended.

Another approach addresses the movement of (nano-) particles in the tumor interstitial space. Inducing cellular apoptosis can open up this space, thereby improving tumor penetration and transfection by siRNA NPs [219]. Similar results were achieved by attacking structural ECM molecules. Pretreating mice with Losartan, a drug against hypertension that additionally acts as an anti-fibrotic agent, reduced collagen I levels and improved the distribution and efficacy of an oncolytic virus and Doxil (both ~100 nm) in several tumor models [117].

In addition to changing the microenvironment, the timing of treatments can also affect the way tumor cells respond to certain insults. Knocking down EGFR signaling in triple-negative breast cancer cells markedly increased their sensitivity to subsequent DOX treatment. EGFR knockdown led to a change in apoptotic signaling that made the cells more susceptible to DNA damage. Reverse order or simultaneous administration had no such effect and could even be inhibitory, emphasizing the importance of timing [220]. Intelligent designs of NPs [221, 222] or more elaborate drug delivery system [65] can facilitate such sequential drug exposures and might improve the therapeutic efficacy of compound combinations that failed in clinical trials for GBM. Evidently, only co-administering therapeutics might not be sufficient to achieve the intended synergistic effects. Timing can play a large role in successful treatment. Drug delivery systems can enable such time-staggered treatment regimens.

VII. CONCLUSIONS

GBM is a complicated cancer that involves various sophisticated molecular pathways, gene mutations, and tumor microenvironments. Despite plentiful investigations, an unmet medical need persists for the treatment of invasive GBM. We have abstracted the drug combination therapy with or without nanocarriers and the current strategies for nanomedicine-based drug combinations. With increasing knowledge of GBM molecular pathways, increasingly more intelligent drug combination strategies will be developed and nanocarriers for synergistic drug combinations will be designed to target different pathways and the tumor microenvironment. The next perspective before moving to the clinics is to comprehensively understand the synergistic ratio of drug candidates *in vivo*, the effective local dose in the brain tumor site and timing of administration, thus minimizing overlapping toxicity and achieving the desired therapeutic effect. With the broad knowledge and efforts of researchers, nanocarrier-based combination therapies are expanding the way for success in the battle for GBM treatment.

VIII. REFERENCES

1. Young RM, Jamshidi A, Davis G, Sherman JH. Current trends in the surgical management and treatment of adult glioblastoma. Annals of translational medicine. 2015; 3.
2. Anjum K, Shagufta BI, Abbas SQ, Patel S, Khan I, Shah SAA, et al. Current status and future therapeutic perspectives of glioblastoma multiforme (GBM) therapy: A review. Biomedicine and Pharmacotherapy. 2017; 92: 681-9.
3. Shergalis A, Bankhead A, Luesakul U, Muangsin N, Neamati N. Current Challenges and Opportunities in Treating Glioblastoma. Pharmacological Reviews. 2018; 70: 412-45.
4. Stupp R, Mason WP, van den Bent MJ, Weller M, Fisher B, Taphoorn MJ, et al. Radiotherapy plus concomitant and adjuvant temozolomide for glioblastoma. New England Journal of Medicine. 2005; 352: 987-96.
5. Davis ME. Glioblastoma: Overview of Disease and Treatment. Clinical Journal of Oncology Nursing. 2016; 20: S2-S8.
6. Ozdemir-Kaynak E, Qutub AA, Yesil-Celiktas O. Advances in Glioblastoma Multiforme Treatment: New Models for Nanoparticle Therapy. Frontiers in Physiology. 2018; 9.
7. Chinot OL, Wick W, Mason W, Henriksson R, Saran F, Nishikawa R, et al. Bevacizumab plus radiotherapy–temozolomide for newly diagnosed glioblastoma. New England Journal of Medicine. 2014; 370: 709-22.
8. Gilbert MR, Dignam JJ, Armstrong TS, Wefel JS, Blumenthal DT, Vogelbaum MA, et al. A randomized trial of bevacizumab for newly diagnosed glioblastoma. New England Journal of Medicine. 2014; 370: 699-708.
9. Stupp R, Taillibert S, Kanner AA, Kesari S, Steinberg DM, Toms SA, et al. Maintenance therapy with tumor-treating fields plus temozolomide vs temozolomide alone for glioblastoma: a randomized clinical trial. JAMA. 2015; 314: 2535-43.
10. Zhang RX, Wong HL, Xue HY, Eoh JY, Wu XY. Nanomedicine of synergistic drug combinations for cancer therapy–Strategies and perspectives. Journal of Controlled Release. 2016; 240: 489-503.
11. Alam MI, Beg S, Samad A, Baboota S, Kohli K, Ali J, et al. Strategy for effective brain drug delivery. European Journal of Pharmaceutical Sciences. 2010; 40: 385-403.
12. Davis ME, Chen Z, Shin DM. Nanoparticle therapeutics: an emerging treatment modality for cancer. Nanoscience And Technology: A Collection of Reviews from Nature Journals: World Scientific; 2010. p. 239-50.
13. Peer D, Karp JM, Hong S, Farokhzad OC, Margalit R, Langer R. Nanocarriers as an emerging platform for cancer therapy. Nature nanotechnology. 2007; 2: 751.
14. Ganipineni LP, Danhier F, Préat V. Drug delivery challenges and future of chemotherapeutic nanomedicine for glioblastoma treatment. Journal of Controlled Release. 2018; 281: 42-57.
15. Haar CP, Hebbar P, Wallace GC, Das A, Vandergrift WA, Smith JA, et al. Drug resistance in glioblastoma: a mini review. Neurochemical Research. 2012; 37: 1192-200.
16. Reifenberger G, Wirsching H-G, Knobbe-Thomsen CB, Weller M. Advances in the molecular genetics of gliomas—implications for classification and therapy. Nature reviews Clinical oncology. 2017; 14: 434.
17. Parker NR, Khong P, Parkinson JF, Howell VM, Wheeler HR. Molecular Heterogeneity in Glioblastoma: Potential Clinical Implications. Frontiers in Oncology. 2015; 5.
18. Parsons DW, Jones S, Zhang X, Lin JC-H, Leary RJ, Angenendt P, et al. An integrated genomic analysis of human glioblastoma multiforme. Science. 2008.
19. Network CGAR. Comprehensive genomic characterization defines human glioblastoma genes and core pathways. Nature. 2008; 455: 1061.
20. Osuka S, Van Meir EG. Overcoming therapeutic resistance in glioblastoma: the way forward. The Journal of clinical investigation. 2017; 127: 415-26.

21. Patel AP, Tirosh I, Trombetta JJ, Shalek AK, Gillespie SM, Wakimoto H, et al. Single-cell RNA-seq highlights intratumoral heterogeneity in primary glioblastoma. Science. 2014; 344: 1396-401.
22. Osswald M, Jung E, Sahm F, Solecki G, Venkataramani V, Blaes J, et al. Brain tumour cells interconnect to a functional and resistant network. Nature. 2015; 528: 93.
23. Safa AR, Saadatzadeh MR, Cohen-Gadol AA, Pollok KE, Bijangi-Vishehsaraei K. Glioblastoma stem cells (GSCs) epigenetic plasticity and interconversion between differentiated non-GSCs and GSCs. Genes & Diseases. 2015; 2: 152-63.
24. Bao S, Wu Q, Sathornsumetee S, Hao Y, Li Z, Hjelmeland AB, et al. Stem cell–like glioma cells promote tumor angiogenesis through vascular endothelial growth factor. Cancer Research. 2006; 66: 7843-8.
25. Johannessen T-CA, Bjerkvig R. Molecular mechanisms of temozolomide resistance in glioblastoma multiforme. Expert review of anticancer therapy. 2012; 12: 635-42.
26. Fan CH, Liu WL, Cao H, Wen C, Chen L, Jiang G. O6-methylguanine DNA methyltransferase as a promising target for the treatment of temozolomide-resistant gliomas. Cell Death & Disease. 2013; 4: e876.
27. Johannessen T-CA, Bjerkvig R, Tysnes BB. DNA repair and cancer stem-like cells–potential partners in glioma drug resistance? Cancer Treatment Reviews. 2008; 34: 558-67.
28. Lee SY. Temozolomide resistance in glioblastoma multiforme. Genes & Diseases. 2016; 3: 198-210.
29. Hegi ME, Diserens A-C, Gorlia T, Hamou M-F, De Tribolet N, Weller M, et al. MGMT gene silencing and benefit from temozolomide in glioblastoma. New England Journal of Medicine. 2005; 352: 997-1003.
30. Zhang J, FG Stevens M, D Bradshaw T. Temozolomide: mechanisms of action, repair and resistance. Current Molecular Pharmacology. 2012; 5: 102-14.
31. Wightman SM. The Overexpression of Basigin-3 in Glioblastoma. 2016.
32. Dong X. Current Strategies for Brain Drug Delivery. Theranostics. 2018; 8: 1481-93.
33. Pardridge WM. Drug transport across the blood–brain barrier. Journal of Cerebral Blood Flow and Metabolism. 2012; 32: 1959-72.
34. van Tellingen O, Yetkin-Arik B, de Gooijer MC, Wesseling P, Wurdinger T, de Vries HE. Overcoming the blood–brain tumor barrier for effective glioblastoma treatment. Drug Resistance Updates. 2015; 19: 1-12.
35. Wolburg H, Noell S, Fallier-Becker P, Mack AF, Wolburg-Buchholz K. The disturbed blood–brain barrier in human glioblastoma. Molecular Aspects of Medicine. 2012; 33: 579-89.
36. Li Y, Yuan H, Yang K, Xu W, Tang W, Li X. The structure and functions of P-glycoprotein. Current Medicinal Chemistry. 2010; 17: 786-800.
37. Munoz JL, Walker ND, Scotto KW, Rameshwar P. Temozolomide competes for P-glycoprotein and contributes to chemoresistance in glioblastoma cells. Cancer Letters. 2015; 367: 69-75.
38. Perry JR, Laperriere N, O'callaghan CJ, Brandes AA, Menten J, Phillips C, et al. Short-course radiation plus temozolomide in elderly patients with glioblastoma. New England Journal of Medicine. 2017; 376: 1027-37.
39. Diaz RJ, Ali S, Qadir MG, De La Fuente MI, Ivan ME, Komotar RJ. The role of bevacizumab in the treatment of glioblastoma. Journal of Neuro-Oncology. 2017; 133: 455-67.
40. Mayer LD, Janoff AS. Optimizing combination chemotherapy by controlling drug ratios. Molecular interventions. 2007; 7: 216.
41. Huang W, Zhou Q, Yuan X, Ge Z-m, Ran F-x, Yang H-y, et al. Proteasome inhibitor YSY01A enhances cisplatin cytotoxicity in cisplatin-resistant human ovarian cancer cells. Journal of Cancer. 2016; 7: 1133.

42. Xu S-P, Sun G-P, Shen Y-X, Wei W, Peng W-R, Wang H. Antiproliferation and apoptosis induction of paeonol in HepG2 cells. World Journal of Gastroenterology: WJG. 2007; 13: 250.
43. Jin J-l, Gong J, Yin T-j, Lu Y-j, Xia J-j, Xie Y-y, et al. PTD4-apoptin protein and dacarbazine show a synergistic antitumor effect on B16-F1 melanoma in vitro and in vivo. European Journal of Pharmacology. 2011; 654: 17-25.
44. Kong R, Sun B, Jiang H, Pan S, Chen H, Wang S, et al. Downregulation of nuclear factor-κB p65 subunit by small interfering RNA synergizes with gemcitabine to inhibit the growth of pancreatic cancer. Cancer Letters. 2010; 291: 90-8.
45. Li X, Lin Z, Zhang B, Guo L, Liu S, Li H, et al. β-elemene sensitizes hepatocellular carcinoma cells to oxaliplatin by preventing oxaliplatin-induced degradation of copper transporter 1. Scientific Reports. 2016; 6: 21010.
46. Loewe S. The problem of synergism and antagonism of combined drugs. Arzneimittel-Forschung. 1953; 3: 285-90.
47. Tallarida RJ. Quantitative methods for assessing drug synergism. Genes & Cancer. 2011; 2: 1003-8.
48. Grabovsky Y, Tallarida RJ. Isobolographic analysis for combinations of a full and partial agonist: curved isoboles. Journal of Pharmacology and Experimental Therapeutics. 2004; 310: 981-6.
49. Chou T-C. Theoretical basis, experimental design, and computerized simulation of synergism and antagonism in drug combination studies. Pharmacological Reviews. 2006; 58: 621-81.
50. Chou T-C. Drug combination studies and their synergy quantification using the Chou-Talalay method. Cancer Research. 2010: 0008-5472. CAN-09-1947.
51. Van Woensel M, Mathivet T, Wauthoz N, Rosière R, Garg AD, Agostinis P, et al. Sensitization of glioblastoma tumor micro-environment to chemo-and immunotherapy by Galectin-1 intranasal knock-down strategy. Scientific reports. 2017; 7: 1217.
52. Bastiancich C, Danhier P, Préat V, Danhier F. Anticancer drug-loaded hydrogels as drug delivery systems for the local treatment of glioblastoma. Journal of Controlled Release. 2016; 243: 29-42.
53. Chaichana KL, Pinheiro L, Brem H. Delivery of local therapeutics to the brain: working toward advancing treatment for malignant gliomas. Therapeutic Delivery. 2015; 6: 353-69.
54. Ommaya AK. Subcutaneous reservoir and pump for sterile access to ventricular cerebrospinal fluid. The Lancet. 1963; 2: 983-4.
55. Vogelbaum MA, Aghi MK. Convection-enhanced delivery for the treatment of glioblastoma. Neuro-Oncology. 2015; 17: ii3-ii8.
56. Barua NU, Hopkins K, Woolley M, O'Sullivan S, Harrison R, Edwards RJ, et al. A novel implantable catheter system with transcutaneous port for intermittent convection-enhanced delivery of carboplatin for recurrent glioblastoma. Drug Delivery. 2016; 23: 167-73.
57. Bruce JN, Fine RL, Canoll P, Yun J, Kennedy BC, Rosenfeld SS, et al. Regression of recurrent malignant gliomas with convection-enhanced delivery of topotecan. Neurosurgery. 2011; 69: 1272-80.
58. Perry J, Chambers A, Spithoff K, Laperriere N. Gliadel wafers in the treatment of malignant glioma: a systematic review. Current oncology. 2007; 14: 189.
59. De Bonis P, Anile C, Pompucci A, Fiorentino A, Balducci M, Chiesa S, et al. Safety and efficacy of Gliadel wafers for newly diagnosed and recurrent glioblastoma; 2012.
60. Buwalda SJ, Vermonden T, Hennink WE. Hydrogels for Therapeutic Delivery: Current Developments and Future Directions. Biomacromolecules. 2017; 18: 316-30.
61. Bastiancich C, Bianco J, Vanvarenberg K, Ucakar B, Joudiou N, Gallez B, et al. Injectable nanomedicine hydrogel for local chemotherapy of glioblastoma after surgical resection. Journal of Controlled Release. 2017; 264: 45-54.

62. Zhao M, Danhier F, Bastiancich C, Joudiou N, Ganipineni LP, Tsakiris N, et al. Post-resection treatment of glioblastoma with an injectable nanomedicine-loaded photopolymerizable hydrogel induces long-term survival. International Journal of Pharmaceutics. 2018; 548: 522-9.
63. Ranganath SH, Fu Y, Arifin DY, Kee I, Zheng L, Lee HS, et al. The use of submicron/nanoscale PLGA implants to deliver paclitaxel with enhanced pharmacokinetics and therapeutic efficacy in intracranial glioblastoma in mice. Biomaterials. 2010; 31: 5199-207.
64. Ozeki T, Kaneko D, Hashizawa K, Imai Y, Tagami T, Okada H. Improvement of survival in C6 rat glioma model by a sustained drug release from localized PLGA microspheres in a thermoreversible hydrogel. International Journal of Pharmaceutics. 2012; 427: 299-304.
65. Majumder P, Baxa U, Walsh STR, Schneider JP. Design of a Multicompartment Hydrogel that Facilitates Time-Resolved Delivery of Combination Therapy and Synergized Killing of Glioblastoma. Angewandte Chemie International Ed In English. 2018; 57: 15040-4.
66. Bastiancich C, Bozzato E, Luyten U, Danhier F, Bastiat G, Préat V. Drug combination using an injectable nanomedicine hydrogel for glioblastoma treatment. International Journal of Pharmaceutics. 2019; 559: 220-7.
67. Kim JI, Lee BS, Chun C, Cho JK, Kim SY, Song SC. Long-term theranostic hydrogel system for solid tumors. Biomaterials. 2012; 33: 2251-9.
68. Lin FW, Chen PY, Wei KC, Huang CY, Wang CK, Yang HW. Rapid In Situ MRI Traceable Gel-forming Dual-drug Delivery for Synergistic Therapy of Brain Tumor. Theranostics. 2017; 7: 2524-36.
69. Lu C-T, Zhao Y-Z, Wong HL, Cai J, Peng L, Tian X-Q. Current approaches to enhance CNS delivery of drugs across the brain barriers. International journal of nanomedicine. 2014; 9: 2241.
70. Karim R, Palazzo C, Evrard B, Piel G. Nanocarriers for the treatment of glioblastoma multiforme: current state-of-the-art. Journal of Controlled Release. 2016; 227: 23-37.
71. Van Tellingen O, Yetkin-Arik B, De Gooijer M, Wesseling P, Wurdinger T, De Vries H. Overcoming the blood–brain tumor barrier for effective glioblastoma treatment. Drug Resistance Updates. 2015; 19: 1-12.
72. Gelderblom H, Verweij J, Nooter K, Sparreboom A. Cremophor EL: the drawbacks and advantages of vehicle selection for drug formulation. European Journal of Cancer. 2001; 37: 1590-8.
73. Pardridge WM. The blood-brain barrier: bottleneck in brain drug development. NeuroRx. 2005; 2: 3-14.
74. Matsumura Y, Maeda H. A New Concept for Macromolecular Therapeutics in Cancer Chemotherapy: Mechanism of Tumoritropic Accumulation of Proteins and the Antitumor Agent Smancs. Cancer Research. 1986; 46: 6387-92.
75. Moghimi SM, Hunter AC, Murray JC. Long-circulating and target-specific nanoparticles: theory to practice. Pharmacological Reviews. 2001; 53: 283-318.
76. Fang J, Nakamura H, Maeda H. The EPR effect: Unique features of tumor blood vessels for drug delivery, factors involved, and limitations and augmentation of the effect. Advanced Drug Delivery Reviews. 2011; 63: 136-51.
77. Danhier F. To exploit the tumor microenvironment: Since the EPR effect fails in the clinic, what is the future of nanomedicine? Journal of Controlled Release. 2016; 244: 108-21.
78. Jain RK, di Tomaso E, Duda DG, Loeffler JS, Sorensen AG, Batchelor TT. Angiogenesis in brain tumours. Nature Reviews: Neuroscience. 2007; 8: 610-22.
79. D'Alessio A, Proietti G, Sica G, Scicchitano BM. Pathological and Molecular Features of Glioblastoma and Its Peritumoral Tissue. Cancers. 2019; 11.

80. Sarkaria JN, Hu LS, Parney IF, Pafundi DH, Brinkmann DH, Laack NN, et al. Is the blood-brain barrier really disrupted in all glioblastomas? A critical assessment of existing clinical data. Neuro-Oncology. 2018; 20: 184-91.
81. Lemée J-M, Clavreul A, Menei P. Intratumoral heterogeneity in glioblastoma: don't forget the peritumoral brain zone. Neuro-Oncology. 2015; 17: 1322-32.
82. Lemee JM, Clavreul A, Aubry M, Com E, de Tayrac M, Eliat PA, et al. Characterizing the peritumoral brain zone in glioblastoma: a multidisciplinary analysis. Journal of Neuro-Oncology. 2015; 122: 53-61.
83. Rong Y, Durden DL, Van Meir EG, Brat DJ. 'Pseudopalisading' necrosis in glioblastoma: a familiar morphologic feature that links vascular pathology, hypoxia, and angiogenesis. Journal of Neuropathology and Experimental Neurology. 2006; 65: 529-39.
84. Huang WJ, Chen WW, Zhang X. Glioblastoma multiforme: Effect of hypoxia and hypoxia inducible factors on therapeutic approaches. Oncology Letters. 2016; 12: 2283-8.
85. Haar CP, Hebbar P, Wallace GCt, Das A, Vandergrift WA, 3rd, Smith JA, et al. Drug resistance in glioblastoma: a mini review. Neurochemical Research. 2012; 37: 1192-200.
86. Chauhan VP, Stylianopoulos T, Martin JD, Popovic Z, Chen O, Kamoun WS, et al. Normalization of tumour blood vessels improves the delivery of nanomedicines in a size-dependent manner. Nature Nanotechnology. 2012; 7: 383-8.
87. Golombek SK, May J-N, Theek B, Appold L, Drude N, Kiessling F, et al. Tumor targeting via EPR: Strategies to enhance patient responses. Advanced drug delivery reviews. 2018.
88. Maeda H. The link between infection and cancer: tumor vasculature, free radicals, and drug delivery to tumors via the EPR effect. Cancer Science. 2013; 104: 779-89.
89. Theek B, Gremse F, Kunjachan S, Fokong S, Pola R, Pechar M, et al. Characterizing EPR-mediated passive drug targeting using contrast-enhanced functional ultrasound imaging. Journal of controlled release : official journal of the Controlled Release Society. 2014; 182: 83-9.
90. Seo JW, Ang J, Mahakian LM, Tam S, Fite B, Ingham ES, et al. Self-assembled 20-nm (64)Cu-micelles enhance accumulation in rat glioblastoma. Journal of controlled release : official journal of the Controlled Release Society. 2015; 220: 51-60.
91. Steiniger SC, Kreuter J, Khalansky AS, Skidan IN, Bobruskin AI, Smirnova ZS, et al. Chemotherapy of glioblastoma in rats using doxorubicin ‐loaded nanoparticles. International Journal of Cancer. 2004; 109: 759-67.
92. Shah N, Chaudhari K, Dantuluri P, Murthy R, Das S. Paclitaxel-loaded PLGA nanoparticles surface modified with transferrin and Pluronic® P85, an in vitro cell line and in vivo biodistribution studies on rat model. Journal of Drug Targeting. 2009; 17: 533-42.
93. Miura Y, Takenaka T, Toh K, Wu S, Nishihara H, Kano MR, et al. Cyclic RGD-linked polymeric micelles for targeted delivery of platinum anticancer drugs to glioblastoma through the blood-brain tumor barrier. ACS Nano. 2013; 7: 8583-92.
94. Vieira DB, Gamarra LF. Getting into the brain: liposome-based strategies for effective drug delivery across the blood-brain barrier. International journal of nanomedicine. 2016; 11: 5381-414.
95. Koukourakis M, Koukouraki S, Fezoulidis I, Kelekis N, Kyrias G, Archimandritis S, et al. High intratumoural accumulation of stealth® liposomal doxorubicin (Caelyx®) in glioblastomas and in metastatic brain tumours. British Journal of Cancer. 2000; 83: 1281.
96. Soni V, Kohli DV, Jain SK. Transferrin coupled liposomes as drug delivery carriers for brain targeting of 5-florouracil. Journal of Drug Targeting. 2005; 13: 245-50.
97. Madhankumar A, Slagle-Webb B, Mintz A, Sheehan JM, Connor JR. Interleukin-13 receptor–targeted nanovesicles are a potential therapy for glioblastoma multiforme. Molecular Cancer Therapeutics. 2006; 5: 3162-9.

98. Anton N, Mojzisova H, Porcher E, Benoit JP, Saulnier P. Reverse micelle-loaded lipid nano-emulsions: new technology for nano-encapsulation of hydrophilic materials. International Journal of Pharmaceutics. 2010; 398: 204-9.
99. Paillard A, Hindré F, Vignes-Colombeix C, Benoit J-P, Garcion E. The importance of endo-lysosomal escape with lipid nanocapsules for drug subcellular bioavailability. Biomaterials. 2010; 31: 7542-54.
100. Aparicio-Blanco J, Torres-Suarez AI. Glioblastoma Multiforme and Lipid Nanocapsules: A Review. Journal of Biomedical Nanotechnology. 2015; 11: 1283-311.
101. Garcion E, Lamprecht A, Heurtault B, Paillard A, Aubert-Pouessel A, Denizot B, et al. A new generation of anticancer, drug-loaded, colloidal vectors reverses multidrug resistance in glioma and reduces tumor progression in rats. Molecular Cancer Therapeutics. 2006; 5: 1710-22.
102. Ma Pa, Xiao H, Li C, Dai Y, Cheng Z, Hou Z, et al. Inorganic nanocarriers for platinum drug delivery. Materials Today. 2015; 18: 554-64.
103. Liu Y, Zhang P, Li F, Jin X, Li J, Chen W, et al. Metal-based NanoEnhancers for Future Radiotherapy: Radiosensitizing and Synergistic Effects on Tumor Cells. Theranostics. 2018; 8: 1824-49.
104. Pinel S, Thomas N, Boura C, Barberi-Heyob M. Approaches to physical stimulation of metallic nanoparticles for glioblastoma treatment. Advanced Drug Delivery Reviews. 2019; 138: 344-57.
105. Cheng Y, Dai Q, Morshed RA, Fan X, Wegscheid ML, Wainwright DA, et al. Blood-brain barrier permeable gold nanoparticles: an efficient delivery platform for enhanced malignant glioma therapy and imaging. Small. 2014; 10: 5137-50.
106. Hao Y, Zhang B, Zheng C, Ji R, Ren X, Guo F, et al. The tumor-targeting core-shell structured DTX-loaded PLGA@Au nanoparticles for chemo-photothermal therapy and X-ray imaging. Journal of Controlled Release. 2015; 220: 545-55.
107. Coussens LM, Werb Z. Inflammation and cancer. Nature. 2002; 420: 860-7.
108. Charles NA, Holland EC, Gilbertson R, Glass R, Kettenmann H. The brain tumor microenvironment. Glia. 2011; 59: 1169-80.
109. Broekman ML, Maas SLN, Abels ER, Mempel TR, Krichevsky AM, Breakefield XO. Multidimensional communication in the microenvirons of glioblastoma. Nature Reviews: Neurology. 2018; 14: 482-95.
110. Prosniak M, Harshyne LA, Andrews DW, Kenyon LC, Bedelbaeva K, Apanasovich TV, et al. Glioma grade is associated with the accumulation and activity of cells bearing M2 monocyte markers. Clinical Cancer Research. 2013; 19: 3776-86.
111. Sorensen MD, Dahlrot RH, Boldt HB, Hansen S, Kristensen BW. Tumour-associated microglia/macrophages predict poor prognosis in high-grade gliomas and correlate with an aggressive tumour subtype. Neuropathology and Applied Neurobiology. 2018; 44: 185-206.
112. Zhang J, Sarkar S, Cua R, Zhou Y, Hader W, Yong VW. A dialog between glioma and microglia that promotes tumor invasiveness through the CCL2/CCR2/interleukin-6 axis. Carcinogenesis. 2012; 33: 312-9.
113. Kessenbrock K, Plaks V, Werb Z. Matrix metalloproteinases: regulators of the tumor microenvironment. Cell. 2010; 141: 52-67.
114. Szulzewsky F, Pelz A, Feng X, Synowitz M, Markovic D, Langmann T, et al. Glioma-associated microglia/macrophages display an expression profile different from M1 and M2 polarization and highly express Gpnmb and Spp1. PloS One. 2015; 10: e0116644.
115. Du R, Petritsch C, Lu K, Liu P, Haller A, Ganss R, et al. Matrix metalloproteinase-2 regulates vascular patterning and growth affecting tumor cell survival and invasion in GBM. Neuro-Oncology. 2008; 10: 254-64.

116. Brandenburg S, Muller A, Turkowski K, Radev YT, Rot S, Schmidt C, et al. Resident microglia rather than peripheral macrophages promote vascularization in brain tumors and are source of alternative pro-angiogenic factors. Acta Neuropathologica. 2016; 131: 365-78.
117. Diop-Frimpong B, Chauhan VP, Krane S, Boucher Y, Jain RK. Losartan inhibits collagen I synthesis and improves the distribution and efficacy of nanotherapeutics in tumors. Proceedings of the National Academy of Sciences of the United States of America. 2011; 108: 2909-14.
118. Gustafson HH, Holt-Casper D, Grainger DW, Ghandehari H. Nanoparticle Uptake: The Phagocyte Problem. Nano Today. 2015; 10: 487-510.
119. Roode LE, Brighton H, Bo T, Perry JL, Parrott MC, Kersey F, et al. Subtumoral analysis of PRINT nanoparticle distribution reveals targeting variation based on cellular and particle properties. Nanomedicine: Nanotechnology, Biology, and Medicine. 2016; 12: 1053-62.
120. Miller MA, Gadde S, Pfirschke C, Engblom C, Sprachman MM, Kohler RH, et al. Predicting therapeutic nanomedicine efficacy using a companion magnetic resonance imaging nanoparticle. Science Translational Medicine. 2015; 7: 314ra183.
121. Miller MA, Zheng YR, Gadde S, Pfirschke C, Zope H, Engblom C, et al. Tumour-associated macrophages act as a slow-release reservoir of nano-therapeutic Pt(IV) pro-drug. Nature Communications. 2015; 6: 8692.
122. Moore TL, Hauser D, Gruber T, Rothen-Rutishauser B, Lattuada M, Petri-Fink A, et al. Cellular Shuttles: Monocytes/Macrophages Exhibit Transendothelial Transport of Nanoparticles under Physiological Flow. ACS Appl Mater Interfaces. 2017; 9: 18501-11.
123. Alizadeh D, Zhang L, Hwang J, Schluep T, Badie B. Tumor-associated macrophages are predominant carriers of cyclodextrin-based nanoparticles into gliomas. Nanomedicine: Nanotechnology, Biology, and Medicine. 2010; 6: 382-90.
124. Gkretsi V, Zacharia LC, Stylianopoulos T. Targeting Inflammation to Improve Tumor Drug Delivery. Trends Cancer. 2017; 3: 621-30.
125. Dietrich J, Rao K, Pastorino S, Kesari S. Corticosteroids in brain cancer patients: benefits and pitfalls. Expert Review of Clinical Pharmacology. 2011; 4: 233-42.
126. Freire MO, Van Dyke TE. Natural resolution of inflammation. Periodontology 2000. 2013; 63: 149-64.
127. Candelario-Jalil E, Taheri S, Yang Y, Sood R, Grossetete M, Estrada EY, et al. Cyclooxygenase inhibition limits blood-brain barrier disruption following intracerebral injection of tumor necrosis factor-alpha in the rat. Journal of Pharmacology and Experimental Therapeutics. 2007; 323: 488-98.
128. Reichman HR, Farrell CL, Del Maestro RF. Effects of steroids and nonsteroid anti-inflammatory agents on vascular permeability in a rat glioma model. Journal of Neurosurgery. 1986; 65: 233-7.
129. Zhang B, Hu Y, Pang Z. Modulating the Tumor Microenvironment to Enhance Tumor Nanomedicine Delivery. Frontiers in Pharmacology. 2017; 8: 952-.
130. Wei D, Wang L, He Y, Xiong HQ, Abbruzzese JL, Xie K. Celecoxib inhibits vascular endothelial growth factor expression in and reduces angiogenesis and metastasis of human pancreatic cancer via suppression of Sp1 transcription factor activity. Cancer Research. 2004; 64: 2030-8.
131. Pakneshan P, Birsner AE, Adini I, Becker CM, D'Amato RJ. Differential suppression of vascular permeability and corneal angiogenesis by nonsteroidal anti-inflammatory drugs. Investigative Ophthalmology and Visual Science. 2008; 49: 3909-13.
132. Dubey P, Shrivastava R, Tripathi C, Jain NK, Tewari BN, Lone MU, et al. Cyclooxygenase-2 inhibition attenuates hypoxic cancer cells induced m2-polarization of macrophages. Cellular and Molecular Biology (Noisy-Le-Grand, France). 2014; 60: 10-5.
133. Peterson TE, Kirkpatrick ND, Huang Y, Farrar CT, Marijt KA, Kloepper J, et al. Dual inhibition of Ang-2 and VEGF receptors normalizes tumor vasculature and prolongs

survival in glioblastoma by altering macrophages. Proceedings of the National Academy of Sciences of the United States of America. 2016; 113: 4470-5.
134. Kloepper J, Riedemann L, Amoozgar Z, Seano G, Susek K, Yu V, et al. Ang-2/VEGF bispecific antibody reprograms macrophages and resident microglia to anti-tumor phenotype and prolongs glioblastoma survival. Proceedings of the National Academy of Sciences of the United States of America. 2016; 113: 4476-81.
135. Qin T, Wang C, Chen X, Duan C, Zhang X, Zhang J, et al. Dopamine induces growth inhibition and vascular normalization through reprogramming M2-polarized macrophages in rat C6 glioma. Toxicology and Applied Pharmacology. 2015; 286: 112-23.
136. Pang L, Qin J, Han L, Zhao W, Liang J, Xie Z, et al. Exploiting macrophages as targeted carrier to guide nanoparticles into glioma. Oncotarget. 2016; 7: 37081-91.
137. Tentillier N, Etzerodt A, Olesen MN, Rizalar FS, Jacobsen J, Bender D, et al. Anti-Inflammatory Modulation of Microglia via CD163-Targeted Glucocorticoids Protects Dopaminergic Neurons in the 6-OHDA Parkinson's Disease Model. Journal of Neuroscience. 2016; 36: 9375-90.
138. Sivak-Sears NR, Schwartzbaum JA, Miike R, Moghadassi M, Wrensch M. Case-control study of use of nonsteroidal antiinflammatory drugs and glioblastoma multiforme. American Journal of Epidemiology. 2004; 159: 1131-9.
139. Daugherty SE, Moore SC, Pfeiffer RM, Inskip PD, Park Y, Hollenbeck A, et al. Nonsteroidal anti-inflammatory drugs and glioma in the NIH-AARP Diet and Health Study cohort. Cancer Prevention Research (Philadelphia, Pa). 2011; 4: 2027-34.
140. Amirian ES, Ostrom QT, Armstrong GN, Lai RK, Gu X, Jacobs DI, et al. Aspirin, NSAIDs, and Glioma Risk: Original Data from the Glioma International Case-Control Study and a Meta-analysis. Cancer Epidemiology, Biomarkers and Prevention. 2019; 28: 555-62.
141. Bruhns RP, James WS, Torabi M, Borgstrom M, Roussas A, Lemole M. Survival as a Function of Nonsteroidal Anti-inflammatory Drug Use in Patients with Glioblastoma. Cureus. 2018; 10: e3277.
142. Seliger C, Schaertl J, Gerken M, Luber C, Proescholdt M, Riemenschneider MJ, et al. Use of statins or NSAIDs and survival of patients with high-grade glioma. PloS One. 2018; 13: e0207858.
143. Koo YE, Reddy GR, Bhojani M, Schneider R, Philbert MA, Rehemtulla A, et al. Brain cancer diagnosis and therapy with nanoplatforms. Adv Drug Deliv Rev. 2006; 58: 1556-77.
144. Meyers JD, Doane T, Burda C, Basilion JP. Nanoparticles for imaging and treating brain cancer. Nanomedicine (Lond). 2013; 8: 123-43.
145. Gobbo OL, Sjaastad K, Radomski MW, Volkov Y, Prina-Mello A. Magnetic Nanoparticles in Cancer Theranostics. Theranostics. 2015; 5: 1249-63.
146. King AR, Corso CD, Chen EM, Song E, Bongiorni P, Chen Z, et al. Local DNA Repair Inhibition for Sustained Radiosensitization of High-Grade Gliomas. Molecular Cancer Therapeutics. 2017; 16: 1456-69.
147. Zong Z, Hua L, Wang Z, Xu H, Ye C, Pan B, et al. Self-assembled angiopep-2 modified lipid-poly (hypoxic radiosensitized polyprodrug) nanoparticles delivery TMZ for glioma synergistic TMZ and RT therapy. Drug Delivery. 2019; 26: 34-44.
148. Joh DY, Sun L, Stangl M, Al Zaki A, Murty S, Santoiemma PP, et al. Selective targeting of brain tumors with gold nanoparticle-induced radiosensitization. PloS One. 2013; 8: e62425.
149. Sun L, Joh DY, Al-Zaki A, Stangl M, Murty S, Davis JJ, et al. Theranostic Application of Mixed Gold and Superparamagnetic Iron Oxide Nanoparticle Micelles in Glioblastoma Multiforme. Journal of Biomedical Nanotechnology. 2016; 12: 347-56.
150. Liu P, Jin H, Guo Z, Ma J, Zhao J, Li D, et al. Silver nanoparticles outperform gold nanoparticles in radiosensitizing U251 cells in vitro and in an intracranial mouse model of glioma. International Journal of Nanomedicine. 2016; 11: 5003-14.

151. Liu Z, Tan H, Zhang X, Chen F, Zhou Z, Hu X, et al. Enhancement of radiotherapy efficacy by silver nanoparticles in hypoxic glioma cells. Artificial Cells, Nanomedicine, and Biotechnology. 2018; 46: S922-S30.
152. Zhang X, Liu Z, Lou Z, Chen F, Chang S, Miao Y, et al. Radiosensitivity enhancement of Fe3O4@Ag nanoparticles on human glioblastoma cells. Artificial Cells, Nanomedicine, and Biotechnology. 2018; 46: 975-84.
153. Munson JM, Fried L, Rowson SA, Bonner MY, Karumbaiah L, Diaz B, et al. Anti-invasive adjuvant therapy with imipramine blue enhances chemotherapeutic efficacy against glioma. Science Translational Medicine. 2012; 4: 127ra36.
154. Dilnawaz F, Sahoo SK. Enhanced accumulation of curcumin and temozolomide loaded magnetic nanoparticles executes profound cytotoxic effect in glioblastoma spheroid model. European Journal of Pharmaceutics and Biopharmaceutics. 2013; 85: 452-62.
155. Cui Y, Xu Q, Chow PK-H, Wang D, Wang C-H. Transferrin-conjugated magnetic silica PLGA nanoparticles loaded with doxorubicin and paclitaxel for brain glioma treatment. Biomaterials. 2013; 34: 8511-20.
156. Fang JH, Lai YH, Chiu TL, Chen YY, Hu SH, Chen SY. Magnetic Core–Shell Nanocapsules with Dual‐Targeting Capabilities and Co‐Delivery of Multiple Drugs to Treat Brain Gliomas. Advanced healthcare materials. 2014; 3: 1250-60.
157. Xu Y, Shen M, Sun Y, Gao P, Duan Y. Polymer Nanocomposites Based Thermo-Sensitive Gel for Paclitaxel and Temozolomide Co-Delivery to Glioblastoma Cells. Journal of Nanoscience and Nanotechnology. 2015; 15: 9777-87.
158. Mohanty AK, Mohanta GP. Micelle-assisted combination therapies for effective glioblastoma treatment: an in-vitro assessment. Anti-Cancer Drugs. 2015; 26: 312-22.
159. Hu J, Wang J, Wang G, Yao Z, Dang X. Pharmacokinetics and antitumor efficacy of DSPE-PEG2000 polymeric liposomes loaded with quercetin and temozolomide: Analysis of their effectiveness in enhancing the chemosensitization of drug-resistant glioma cells. International Journal of Molecular Medicine. 2016; 37: 690-702.
160. Ni S, Fan X, Wang J, Qi H, Li X. Biodegradable Implants Efficiently Deliver Combination of Paclitaxel and Temozolomide to Glioma C6 Cancer Cells In Vitro. Annals of Biomedical Engineering. 2014; 42: 214-21.
161. Xu Y, Shen M, Li Y, Sun Y, Teng Y, Wang Y, et al. The synergic antitumor effects of paclitaxel and temozolomide co-loaded in mPEG-PLGA nanoparticles on glioblastoma cells. Oncotarget. 2016; 7: 20890-901.
162. Xu H, Jia F, Singh PK, Ruan S, Zhang H, Li X. Synergistic anti-glioma effect of a coloaded nano-drug delivery system. International Journal of Nanomedicine. 2017; 12: 29-40.
163. Lu Z, Li Y, Shi Y, Li Y, Xiao Z, Zhang X. Traceable nanoparticles with spatiotemporally controlled release ability for synergistic glioblastoma multiforme treatment. Advanced Functional Materials. 2017; 27: 1703967.
164. Shi Z-D, Qian X-M, Liu C-Y, Han L, Zhang K-L, Chen L-Y, et al. Aspirin-/TMZ-coloaded Microspheres Exert Synergistic Antiglioma Efficacy via Inhibition of β-catenin Transactivation. CNS Neuroscience & Therapeutics. 2013; 19: 98-108.
165. Shapira-Furman T, Serra R, Gorelick N, Doglioli M, Tagliaferri V, Cecia A, et al. Biodegradable wafers releasing Temozolomide and Carmustine for the treatment of brain cancer. Journal of Controlled Release. 2019; 295: 93-101.
166. Lam FC, Morton SW, Wyckoff J, Han T-L, Hwang MK, Maffa A, et al. Enhanced efficacy of combined temozolomide and bromodomain inhibitor therapy for gliomas using targeted nanoparticles. Nature communications. 2018; 9: 1991.
167. Shin DH, Lee SJ, Kim JS, Ryu JH, Kim JS. Synergistic Effect of Immunoliposomal Gemcitabine and Bevacizumab in Glioblastoma Stem Cell-Targeted Therapy. Journal of Biomedical Nanotechnology. 2015; 11: 1989-2002.

168. Ganipineni LP, Ucakar B, Joudiou N, Bianco J, Danhier P, Zhao M, et al. Magnetic targeting of paclitaxel-loaded poly(lactic-co-glycolic acid)-based nanoparticles for the treatment of glioblastoma. International journal of nanomedicine. 2018; 13: 4509-21.
169. Sarkaria JN, Kitange GJ, James CD, Plummer R, Calvert H, Weller M, et al. Mechanisms of chemoresistance to alkylating agents in malignant glioma. Clinical cancer research : an official journal of the American Association for Cancer Research. 2008; 14: 2900-8.
170. Chen X, Tai L, Gao J, Qian J, Zhang M, Li B, et al. A stapled peptide antagonist of MDM2 carried by polymeric micelles sensitizes glioblastoma to temozolomide treatment through p53 activation. Journal of Controlled Release. 2015; 218: 29-35.
171. Kang T, Zhu Q, Jiang D, Feng X, Feng J, Jiang T, et al. Synergistic targeting tenascin C and neuropilin-1 for specific penetration of nanoparticles for anti-glioblastoma treatment. Biomaterials. 2016; 101: 60-75.
172. Li Y, He H, Jia X, Lu W-L, Lou J, Wei Y. A dual-targeting nanocarrier based on poly(amidoamine) dendrimers conjugated with transferrin and tamoxifen for treating brain gliomas. Biomaterials. 2012; 33: 3899-908.
173. Pang Z, Feng L, Hua R, Chen J, Gao H, Pan S, et al. Lactoferrin-Conjugated Biodegradable Polymersome Holding Doxorubicin and Tetrandrine for Chemotherapy of Glioma Rats. Molecular Pharmaceutics. 2010; 7: 1995-2005.
174. Stephen ZR, Kievit FM, Veiseh O, Chiarelli PA, Fang C, Wang K, et al. Redox-responsive magnetic nanoparticle for targeted convection-enhanced delivery of O6-benzylguanine to brain tumors. ACS Nano. 2014; 8: 10383-95.
175. Danhier F, Messaoudi K, Lemaire L, Benoit J-P, Lagarce F. Combined anti-Galectin-1 and anti-EGFR siRNA-loaded chitosan-lipid nanocapsules decrease temozolomide resistance in glioblastoma: In vivo evaluation. International Journal of Pharmaceutics. 2015; 481: 154-61.
176. Kim SS, Rait A, Kim E, Pirollo KF, Nishida M, Farkas N, et al. A nanoparticle carrying the p53 gene targets tumors including cancer stem cells, sensitizes glioblastoma to chemotherapy and improves survival. ACS Nano. 2014; 8: 5494-514.
177. Qian X, Long L, Shi Z, Liu C, Qiu M, Sheng J, et al. Star-branched amphiphilic PLA-b-PDMAEMA copolymers for co-delivery of miR-21 inhibitor and doxorubicin to treat glioma. Biomaterials. 2014; 35: 2322-35.
178. Fan L, Yang Q, Tan J, Qiao Y, Wang Q, He J, et al. Dual loading miR-218 mimics and Temozolomide using AuCOOH@FA-CS drug delivery system: promising targeted anti-tumor drug delivery system with sequential release functions. Journal of Experimental & Clinical Cancer Research : CR. 2015; 34: 106.
179. Cheng D, Cao N, Chen J, Yu X, Shuai X. Multifunctional nanocarrier mediated co-delivery of doxorubicin and siRNA for synergistic enhancement of glioma apoptosis in rat. Biomaterials. 2012; 33: 1170-9.
180. Yang ZZ, Li JQ, Wang ZZ, Dong DW, Qi XR. Tumor-targeting dual peptides-modified cationic liposomes for delivery of siRNA and docetaxel to gliomas. Biomaterials. 2014; 35: 5226-39.
181. Lei C, Cui Y, Zheng L, Kah-Hoe Chow P, Wang C-H. Development of a gene/drug dual delivery system for brain tumor therapy: Potent inhibition via RNA interference and synergistic effects. Biomaterials. 2013; 34: 7483-94.
182. Liu S, Guo Y, Huang R, Li J, Huang S, Kuang Y, et al. Gene and doxorubicin co-delivery system for targeting therapy of glioma. Biomaterials. 2012; 33: 4907-16.
183. Kim HA, Park JH, Yi N, Lee M. Delivery of hypoxia and glioma dual-specific suicide gene using dexamethasone conjugated polyethylenimine for glioblastoma-specific gene therapy. Molecular Pharmaceutics. 2014; 11: 938-50.
184. Yi N, Oh B, Kim HA, Lee M. Combined delivery of BCNU and VEGF siRNA using amphiphilic peptides for glioblastoma. Journal of Drug Targeting. 2014; 22: 156-64.

185. Zhan C, Wei X, Qian J, Feng L, Zhu J, Lu W. Co-delivery of TRAIL gene enhances the anti-glioblastoma effect of paclitaxel in vitro and in vivo. Journal of Controlled Release. 2012; 160: 630-6.
186. Küçüktürkmen B, Devrim B, Saka OM, Yilmaz Ş, Arsoy T, Bozkir A. Co-delivery of pemetrexed and miR-21 antisense oligonucleotide by lipid-polymer hybrid nanoparticles and effects on glioblastoma cells. Drug Development and Industrial Pharmacy. 2017; 43: 12-21.
187. Régina A, Demeule M, Laplante A, Jodoin J, Dagenais C, Berthelet F, et al. Multidrug resistance in brain tumors: roles of the blood–brain barrier. Cancer and Metastasis Reviews. 2001; 20: 13-25.
188. Li H, Qian ZM. Transferrin/transferrin receptor ‐mediated drug delivery. Medicinal Research Reviews. 2002; 22: 225-50.
189. Jefferies WA, Brandon MR, Hunt SV, Williams AF, Gatter KC, Mason DY. Transferrin receptor on endothelium of brain capillaries. Nature. 1984; 312: 162.
190. Huang R, Ke W, Liu Y, Jiang C, Pei Y. The use of lactoferrin as a ligand for targeting the polyamidoamine-based gene delivery system to the brain. Biomaterials. 2008; 29: 238-46.
191. Ji B, Maeda J, Higuchi M, Inoue K, Akita H, Harashima H, et al. Pharmacokinetics and brain uptake of lactoferrin in rats. Life Sciences. 2006; 78: 851-5.
192. Li Y, He H, Jia X, Lu WL, Lou J, Wei Y. A dual-targeting nanocarrier based on poly(amidoamine) dendrimers conjugated with transferrin and tamoxifen for treating brain gliomas. Biomaterials. 2012; 33: 3899-908.
193. Pang Z, Feng L, Hua R, Chen J, Gao H, Pan S, et al. Lactoferrin-conjugated biodegradable polymersome holding doxorubicin and tetrandrine for chemotherapy of glioma rats. Mol Pharm. 2010; 7: 1995-2005.
194. Bobola MS, Silber JR, Ellenbogen RG, Geyer JR, Blank A, Goff RD. O6-methylguanine-DNA methyltransferase, O6-benzylguanine, and resistance to clinical alkylators in pediatric primary brain tumor cell lines. Clinical Cancer Research. 2005; 11: 2747-55.
195. Quinn JA, Desjardins A, Weingart J, Brem H, Dolan ME, Delaney SM, et al. Phase I trial of temozolomide plus O6-benzylguanine for patients with recurrent or progressive malignant glioma. Journal of Clinical Oncology. 2005; 23: 7178-87.
196. Stephen ZR, Kievit FM, Veiseh O, Chiarelli PA, Fang C, Wang K, et al. Redox-responsive magnetic nanoparticle for targeted convection-enhanced delivery of O 6-benzylguanine to brain tumors. ACS nano. 2014; 8: 10383-95.
197. Nagpal J, Jamoona A, Gulati ND, Mohan A, Braun A, Murali R, et al. Revisiting the role of p53 in primary and secondary glioblastomas. Anticancer Research. 2006; 26: 4633-9.
198. Bobustuc GC, Baker CH, Limaye A, Jenkins WD, Pearl G, Avgeropoulos NG, et al. Levetiracetam enhances p53-mediated MGMT inhibition and sensitizes glioblastoma cells to temozolomide. Neuro-Oncology. 2010; 12: 917-27.
199. Picksley SM, Lane DP. What the papers say: The p53 ‐mdm2 autoregulatory feedback loop: A paradigm for the regulation of growth control by p53? Bioessays. 1993; 15: 689-90.
200. Momand J, Zambetti GP, Olson DC, George D, Levine AJ. The mdm-2 oncogene product forms a complex with the p53 protein and inhibits p53-mediated transactivation. Cell. 1992; 69: 1237-45.
201. Shadfan M, Lopez-Pajares V, Yuan Z-M. MDM2 and MDMX: Alone and together in regulation of p53. Translational cancer research. 2012; 1: 88-9.
202. Dykxhoorn DM, Novina CD, Sharp PA. Killing the messenger: short RNAs that silence gene expression. Nature reviews Molecular cell biology. 2003; 4: 457.
203. Youle RJ, Strasser A. The BCL-2 protein family: opposing activities that mediate cell death. Nature reviews Molecular cell biology. 2008; 9: 47.
204. Yong VW, Power C, Forsyth P, Edwards DR. Metalloproteinases in biology and pathology of the nervous system. Nature Reviews Neuroscience. 2001; 2: 502.

205. Kodera T, Nakagawa T, Kubota T, Kabuto M, Sato K, Kobayashi H. The expression and activation of matrix metalloproteinase-2 in rat brain after implantation of C6 rat glioma cells. Journal of Neuro-Oncology. 2000; 46: 105-14.
206. Frumovitz M, Sood AK. Vascular endothelial growth factor (VEGF) pathway as a therapeutic target in gynecologic malignancies. Gynecologic Oncology. 2007; 104: 768-78.
207. Plate KH, Breier G, Weich HA, Risau W. Vascular endothelial growth factor is a potential tumour angiogenesis factor in human gliomas in vivo. Nature. 1992; 359: 845.
208. Carmeliet P, Jain RK. Angiogenesis in cancer and other diseases. Nature. 2000; 407: 249.
209. Friedman HS, Prados MD, Wen PY, Mikkelsen T, Schiff D, Abrey LE, et al. Bevacizumab alone and in combination with irinotecan in recurrent glioblastoma. Journal of Clinical Oncology. 2009; 27: 4733-40.
210. Quinn JA, Jiang SX, Reardon DA, Desjardins A, Vredenburgh JJ, Rich JN, et al. Phase II Trial of Temozolomide Plus O(6)-Benzylguanine in Adults With Recurrent, Temozolomide-Resistant Malignant Glioma. Journal of Clinical Oncology. 2009; 27: 1262-7.
211. Giannini C, Yu C, Pajon E, Galanis E, Geoffroy F, Gross H, et al. Phase II trial of vorinostat in combination with bortezomib in recurrent glioblastoma: a north central cancer treatment group study. Neuro-Oncology. 2011; 14: 215-21.
212. Harasym TO, Tardi PG, Johnstone SA, Bally MB, Janoff A, Mayer L. Fixed drug ratio liposome formulations of combination cancer therapeutics. Liposome technology. 2006; 3: 25-48.
213. Mayer LD, Harasym TO, Tardi PG, Harasym NL, Shew CR, Johnstone SA, et al. Ratiometric dosing of anticancer drug combinations: controlling drug ratios after systemic administration regulates therapeutic activity in tumor-bearing mice. Molecular Cancer Therapeutics. 2006; 5: 1854-63.
214. Dizaji MZ, Malehmir M, Ghavamzadeh A, Alimoghaddam K, Ghaffari SH. Synergistic Effects of Arsenic Trioxide and Silibinin on Apoptosis and Invasion in Human Glioblastoma U87MG Cell Line. Neurochemical Research. 2012; 37: 370-80.
215. Khawar IA, Kim JH, Kuh H-J. Improving drug delivery to solid tumors: priming the tumor microenvironment. Journal of Controlled Release. 2015; 201: 78-89.
216. Batchelor TT, Gerstner ER, Emblem KE, Duda DG, Kalpathy-Cramer J, Snuderl M, et al. Improved tumor oxygenation and survival in glioblastoma patients who show increased blood perfusion after cediranib and chemoradiation. Proceedings of the National Academy of Sciences of the United States of America. 2013; 110: 19059-64.
217. Sorensen AG, Emblem KE, Polaskova P, Jennings D, Kim H, Ancukiewicz M, et al. Increased survival of glioblastoma patients who respond to antiangiogenic therapy with elevated blood perfusion. Cancer Research. 2012; 72: 402-7.
218. Jain RK. Normalizing tumor microenvironment to treat cancer: bench to bedside to biomarkers. Journal of Clinical Oncology. 2013; 31: 2205-18.
219. Wong HL, Shen Z, Lu Z, Wientjes MG, Au JL-S. Paclitaxel tumor-priming enhances siRNA delivery and transfection in 3-dimensional tumor cultures. Molecular Pharmaceutics. 2011; 8: 833-40.
220. Lee MJ, Ye AS, Gardino AK, Heijink AM, Sorger PK, MacBeath G, et al. Sequential application of anticancer drugs enhances cell death by rewiring apoptotic signaling networks. Cell. 2012; 149: 780-94.
221. Morton SW, Lee MJ, Deng ZJ, Dreaden EC, Siouve E, Shopsowitz KE, et al. A nanoparticle-based combination chemotherapy delivery system for enhanced tumor killing by dynamic rewiring of signaling pathways. Science Signaling. 2014; 7: ra44.
222. Zhou Z, Kennell C, Jafari M, Lee JY, Ruiz-Torres SJ, Waltz SE, et al. Sequential delivery of erlotinib and doxorubicin for enhanced triple negative Breast cancer treatment using polymeric nanoparticle. International Journal of Pharmaceutics. 2017; 530: 300-7.

CHAPTER II

AIM OF THE THESIS

Glioblastoma multiforme (GBM) is an aggressive and malignant brain tumor. These tumors show chemoresistance, variable histopathology and are diffusely infiltrative to adjacent brain tissue [1]. The current standard therapy includes surgical resection, balanced between the need to remove maximum of the tumor and to limit any resulting impairments, followed by radiotherapy and oral alkylating chemotherapy with temozolomide (TMZ; Temodar®) [2].

However, the incapability of drugs to cross the BBB and penetrate inside the tumor tissue leads to less-than-optimal therapeutic efficacy [3]. Additionally, the complete removal of the primary tumor is not curative as infiltrating tumor cells invariably remain in the surrounding brain parenchyma, resulting in relapse and development of a new tumor [4]. Therefore, innovative methods are highly required to deliver drugs to the tumor site and to reduce its impact on the healthy tissues. Direct drug administration to brain parenchyma with locally implanted systems ensures a direct contact of the drug with tumor cells, a sustained drug release, a limited drug degradation and a reduction of off-target effects in healthy tissues [3].

Due to the cellular and molecular heterogeneity of GBM, multi-drug synergistic approaches to target different tumorigenic pathways are required. Paclitaxel (PTX) is one of several cytoskeletal drugs that target tubulin, which stabilizes the microtubule polymer and protects it from disassembly. Chromosomes are thus unable to achieve a metaphase spindle configuration. This blocks the progression of mitosis and prolonged activation of the mitotic checkpoint triggers apoptosis or reversion to the G0-phase of the cell cycle without cell division [5]. Since PTX has different mechanisms of action, non-overlapping toxicities and distinct mechanisms of resistance compared to TMZ [6], we suppose the combination of PTX and TMZ will generate synergistic anti-GBM efficacy and contribute to improvement of treatment.

The aim of this project is based on the hypothesis that the PTX and TMZ-loaded hydrogel directly injected in the resection cavity after surgery, and able to sustainably release the two agents over time, could result in the inhibition of local recurrences of GBM.

To undertake the aim, a photopolymerizable hydrogel formed of polyethylene glycol dimethacrylate (PEG-DMA) was developed to confirm this assumption. PEG-DMA has the advantage of very rapid polymerization in the presence of a photoinitiator and wavelength rays equal to 400 nm [7]. This mechanism is based on radical reaction initiated by the radical initiator 2, 4, 6-Trimethylbenzoyldiphenyl phosphineoxide (TPO) (Figure 1). Thus, the pre-gel mixture can be injected in the tumor resection cavity, immediately photopolymerized according to the shape of resection cavity.

To enhance the solubility as well as ensure the sustained drug release, PTX will be encapsulated in PLGA nanoparticles (PLGA-NPs). TMZ will be solubilized in water with the help of the solubility

enhancing agent L-histidine. This photopolymerizable hydrogel drug co-delivery system in the tumor resection cavity combines the advantages of nanomedicine and the local delivery of chemotherapeutic agents to prevent GBM recurrences and could fill the wound-healing gap between the GBM resection and the chemo-radiotherapy.

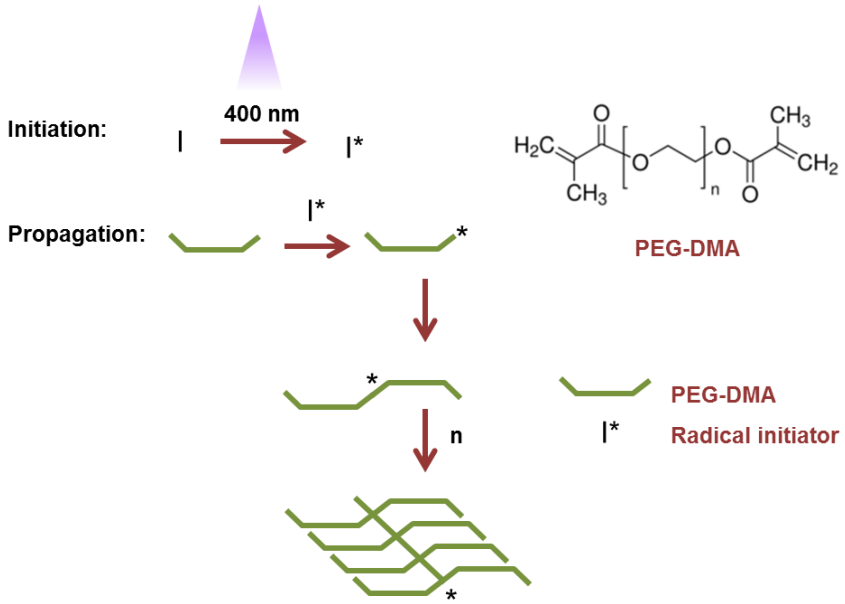

Figure 1: Mechanism of radical polymerization and crosslinking of PEG-DMA

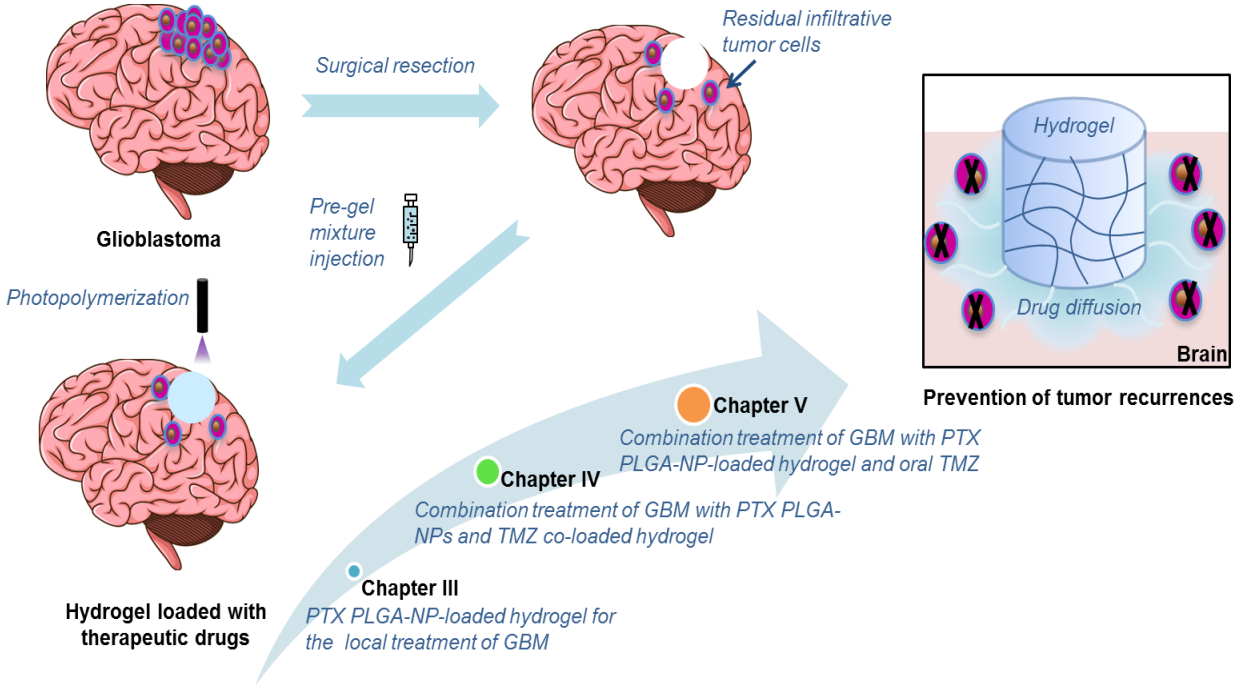

Figure 2: The major objectives of this PhD thesis

REFERENCES

1. Milano MT, Okunieff P, Donatello RS, Mohile NA, Sul J, Walter KA, et al. Patterns and timing of recurrence after temozolomide-based chemoradiation for glioblastoma. International Journal of Radiation Oncology* Biology* Physics. 2010; 78: 1147-55.
2. Stupp R, Mason WP, Van Den Bent MJ, Weller M, Fisher B, Taphoorn MJ, et al. Radiotherapy plus concomitant and adjuvant temozolomide for glioblastoma. New England Journal of Medicine. 2005; 352: 987-96.
3. Bastiancich C, Danhier P, Préat V, Danhier F. Anticancer drug-loaded hydrogels as drug delivery systems for the local treatment of glioblastoma. Journal of Controlled Release. 2016; 243: 29-42.
4. Davis ME. Glioblastoma: overview of disease and treatment. Clinical journal of oncology nursing. 2016; 20: S2.
5. Bharadwaj R, Yu H. The spindle checkpoint, aneuploidy, and cancer. Oncogene. 2004; 23: 2016.
6. Koncar RF, Chu Z, Romick-Rosendale LE, Wells SI, Chan TA, Qi X, et al. PLK1 inhibition enhances temozolomide efficacy in IDH1 mutant gliomas. Oncotarget. 2017; 8: 15827-37.
7. Fourniols T, Randolph LD, Staub A, Vanvarenberg K, Leprince JG, Préat V, et al. Temozolomide-loaded photopolymerizable PEG-DMA-based hydrogel for the treatment of glioblastoma. Journal of Controlled Release. 2015; 210: 95-104.

CHAPTER III

POST-RESECTION TREATMENT OF GLIOBLASTOMA WITH AN INJECTABLE NANOMEDICINE-LOADED PHOTOPOLYMERIZABLE HYDROGEL INDUCES LONG-TERM SURVIVAL

Mengnan Zhao, Fabienne Danhier, Chiara Bastiancich, Nicolas Joudiou, Lakshmi Pallavi Ganipineni, Nikolaos Tsakiris, Bernard Gallez, Aleksandar Jankovski, John Bianco, Véronique Préat

Adapted from International Journal of Pharmaceutics, 2018 5; 548(1):522-529.

TABLE OF CONTENTS

ABSTRACT

Glioblastoma multiforme (GBM) is the most common primary malignant brain tumor. Despite available therapeutic options, the prognosis for patients with GBM remains very poor. We hypothesized that the intra-operative injection of a photopolymerizable hydrogel into the tumor resection cavity could sustain the release of the anti-cancer drug paclitaxel (PTX) encapsulated in poly (lactic-co-glycolic acid) (PLGA) nanoparticles and prevent GBM recurrence. The tumor was resected 13 days after implantation and a pre-gel solution composed of polyethylene glycol dimethacrylate (PEG-DMA) polymer, a photoinitiator and PTX-loaded PLGA nanoparticles (PTX PLGA-NPs) was injected into the tumor resection cavity. A solid gel filling the whole cavity was formed immediately by photopolymerization using a 400 nm light. PTX *in vitro* release study showed a burst release (11%) in the first 8 h and a sustained release of 29% over a week. *In vitro*, U87 MG cells were sensitive to PTX PLGA-NPs with IC_{50} level of approximately 0.010 μg/mL. The hydrogel was well-tolerated when implanted in the brain of healthy mice for 2 and 4 months. Administration of PTX PLGA-NPs-loaded hydrogel into the resection cavity of GBM orthotopic model lead to more than 50% long-term survival mice (150 days) compared to the control groups (mean survival time 52 days). This significant delay of recurrence is very promising for the post-resection treatment of GBM.

I. INTRODUCTION

Glioblastoma multiforme (GBM) is the most aggressive and lethal type of brain tumor. GBM exhibits a high proliferation rate, high tumor cell infiltration into adjacent brain tissue, resistance to conventional treatment and the ability to quickly develop recurrences, which are responsible for its poor prognosis [1]. The current standard therapy includes surgical resection, balanced between the need to remove a maximum of the tumor and to limit any resulting impairments, followed by radiotherapy and oral alkylating chemotherapy with temozolomide (TMZ;Temodar®) [2, 3]. Massive and thorough surgical resection of GBM is frequently not achievable because GBM frequently infiltrates the brain parenchyma beyond the main mass of the tumor, or the brainstem, the diencephalon and neocortical areas that control speech, motor function and sensation [2]. If achievable, the macroscopically complete resection of the primary tumor is not curative since infiltrating tumor cells invariably remain in the surrounding brain parenchyma, leading to later tumor recurrences. As a consequence, approximately 70% of GBM patients experience local recurrence within one year of diagnosis [4]; the 2-year survival rate is only 27%, and the long-term survival rate is less than 5% [5, 6].

The blood brain barrier (BBB), which acts very effectively to protect the brain from harmful molecules, limits the entry of most systemically administered drugs to the brain [7]. To overcome this issue, one of the promising strategies to limit or delay GBM recurrences is the direct administration into tumor resection cavity of a local drug delivery system, via a local delivery system ensuring sustained release of cytotoxic drugs. Indeed, a local drug delivery system will ensure *(i)* a direct contact of the drug with tumor cells, *(ii)* a sustained drug release, *(iii)* a limited drug degradation and *(iv)* a reduction of off-target effects in healthy tissues [7]. The rationale for this approach is that biocompatible materials can be introduced directly into the brain inside the surgical tumor resection cavity. Indeed, after surgical resection, patients have to wait a period of time before starting the radio/chemotherapy regimen because of the duration of the post-surgical wound healing process; thus, residual infiltrative cells will keep proliferating during this time [8]. Consequently, in this time gap, a local drug delivery system could be administered before starting the conventional radio/chemotherapy regimen. In this approach, cytotoxic agents diffuse into the brain parenchyma to kill residual tumor cells around the resection cavity borders, which are responsible for recurrences. The only system applying this strategy approved by FDA is Gliadel®, a polymeric wafer loaded with carmustin. However, Gliadel® showed minimal and controversial advantages. Although a significant survival benefit for patients who received Gliadel® treatment was reported, the short sustained intracerebral release of most drug (1 week) and the local sides effects are involved in the major limitations of Gliadel® wafer [9-11].

Recently, we developed an innovative hydrogel uniquely comprised of photopolymerizable polyethylene glycol dimethacrylate (PEG-DMA) delivering TMZ for the local treatment of GBM [12]. This injectable hydrogel presented mechanical properties compatible with brain implantation. *In vivo*, this system was well tolerated over one week in a healthy mouse brain and reduced tumor growth in a subcutaneous human U87 MG GBM model. However, O6-methylguanine-DNA methyltransferase (MGMT) is involved in the drug resistance mechanism of GBM, which limits the efficacy of TMZ [13]. To bypass this issue, other anti-cancer drugs were investigated for the treatment of GBM, such as lauroyl-gemcitabine ($GemC_{12}$) and doxorubicin [12, 14-16]. Among them, paclitaxel (PTX) could be an alternative as it is an efficient anti-tumor agent that inhibits cell proliferation and induces apoptosis [17]. Also, it kills GBM cells via a MGMT-independent mechanism [18-20]. However, the anti-glioma effect of PTX is very limited when administered systemically as it can't cross the BBB and, in consequence, does not accumulate in the CNS at therapeutic doses [21]. We hypothesized that PTX would be a promising drug for the local delivery before radio- and chemotherapy.

Encapsulation of a bioactive molecule in nanoparticles (NPs) is one of the strategies widely applied to solubilize lipophilic drugs, to protect them from degradation and to obtain a sustained delivery. Poly (lactic-co-glycolic acid) (PLGA) is one the most successful polymers developed to formulate polymeric NPs for the delivery of anti-cancer drugs. PLGA has attracted considerable attention due to the following favorable attributes: *(i)* biodegradability and biocompatibility, *(ii)* FDA/EMA approval for parenteral administration, *(iii)* possibility of sustained drug release and *(iv)* efficient encapsulation of poorly soluble drugs [22]. Additionally, PTX-loaded PLGA-NPs have been previously developed with good encapsulation and loading efficiencies and significant regrowth delays of various *in vivo* tumor models [23-26].

The aim of the present study was to develop an injectable photopolymerizable hydrogel capable of sustaining the release of PTX over a period to fill the gap between surgical resection and the conventional radio/chemotherapy regimen (Figure 1). The hydrogel consists of a PEG-DMA polymer, the Lucirin-TPO® photoinitiator and PTX PLGA-NPs. PLGA NPs are incorporated to slow down the PTX release from the hydrogel. The pre-gel solution is injected into the resection cavity right after surgery and then photopolymerized under blue light (400 nm) irradiation. The PTX release as well as the cytotoxic effect of PTX PLGA-NPs on U87 MG cells were studied, the mid- and long-term tolerability in healthy mouse brain and anti-tumor efficacy after local injection in the resection cavity in an orthotopic U87 MG model were investigated *in vivo*.

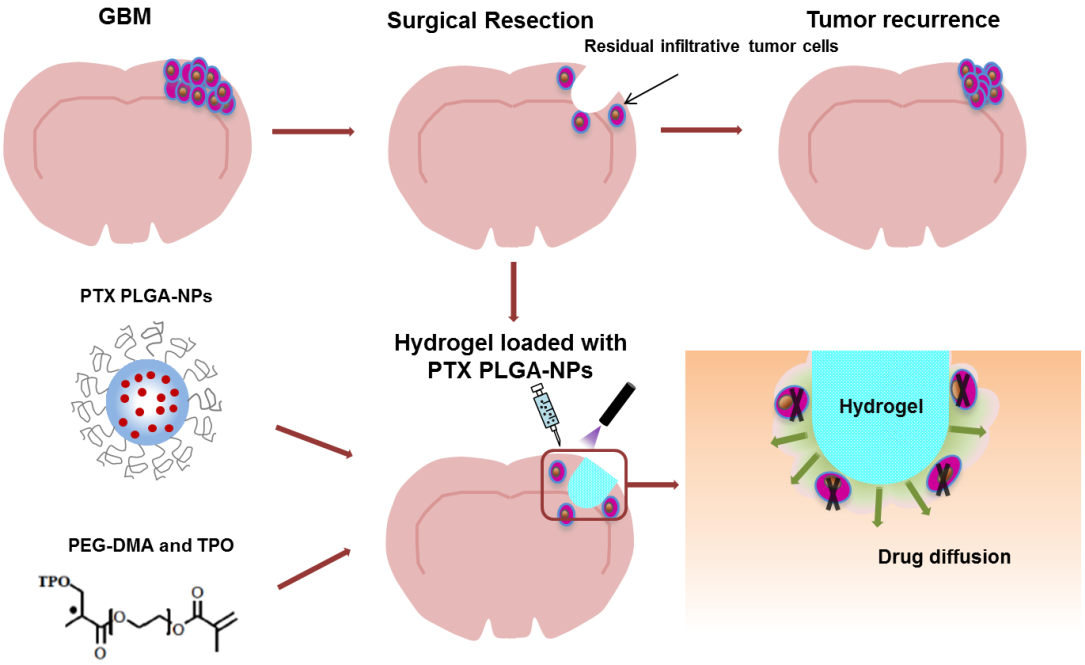

Figure 1: Schematic representation of the main objective of the study.

II. MATERIALS AND METHODS

II.1 HYDROGEL FORMULATION

II.1.1 Formulation of PTX PLGA-NPs

PTX PLGA-NPs were formulated using a modified emulsion-evaporation method as previously reported [27]. Briefly, PLGA (Resomer® RG 502, Mw=7000-17000 g/mol, 56 mg, Sigma-Aldrich, USA), PLGA-PEG (M_W=4600-10040 g/mol, 12 mg), PCL-PEG (M_W=5000-13100 g/mol, 12 mg) (synthesized as previously described [28]) and PTX (6 mg, Chemieliva, China) were dissolved in dichloromethane. This organic solution was then added to an aqueous solution containing 3% (w/v) PVA (M_W=30–70 kDa, Sigma-Aldrich, USA), emulsified using a vortex for 2 min, and then sonicated (4×30 s, 50 W). The mixture was rotary evaporated for 1 h to remove the organic solvent. To remove the non-encapsulated drug, the suspension was filtered (1.2 μm), washed using centrifugation (15,000 rpm, 45 min) and suspended in water.

II.1.2 Physico-chemical characterization of PTX PLGA-NPs

The average particle size and polydispersity index of the PTX PLGA-NPs were measured by dynamic light scattering and zeta (ζ) potential measurements performed by laser Doppler velocimetry using a Zetasizer NanoZS (Malvern Instruments, UK) (n=3).

II.1.3 Quantitative determinations of the PTX in PTX PLGA-NPs

PTX was quantified by high-performance liquid chromatography (HPLC) using a Shimadzu Prominence system (Shimadzu, Japan). The separation was conducted using a BDS Hypersil C18 (Thermo Scientific, USA) (100×4.6 mm; particle size 3 μm) column with a mobile phase comprising acetonitrile (VWR Chemicals, France) and water at a ratio of 45:55 (v/v). The detection wavelength was set to 227 nm, and the flow rate was maintained at 1.2 mL/min. Under these conditions, the retention time of PTX was approximately 6.5 min. A calibration curve was obtained by diluting PTX in acetonitrile at concentrations between 1 and 100 μg/mL (correlation coefficient of R^2=0.9993). The limit of quantification was 0.84 μg/mL, and the limit of detection was 0.28 μg/mL. The total quantity of PTX loaded in the PTX PLGA-NPs was evaluated by the dissolution of an amount of nanoparticles in acetonitrile (dilution ratio 1:100) and quantification by HPLC. The encapsulation efficiency and drug loading of PTX in the PLGA-NPs were quantified as described [27].

II.1.4 Preparation of PTX PLGA-NPs-loaded hydrogel

PTX PLGA-NPs were diluted in water to reach 3.5 mg/mL of PTX and mixed with PEG-DMA (average Mw=550 g/mol) (Sigma-Aldrich, USA) at a 75:25 v/v ratio. Next, 0.5% of Lucirin-TPO® (BASF) was added as the photoinitiator. Then, the pre-gel solution was irradiated at 750 mW/cm² for 15 s with a blue light (Lumencor, USA). The hydrogel formation was re-optimized with different concentrations of PEG-DMA and photoinitiator (Supplementary data, Figure S1). Unloaded and blank PLGA-NPs-loaded PEG-DMA hydrogels were also prepared as controls by adding water or blank PLGA-NPs instead of the PTX PLGA-NPs in the pre-gel solution. The stability of PTX under blue light exposure as well as that of PTX in the PTX PLGA-NPs-loaded PEG-DMA hydrogel was assessed by HPLC by measuring the recovery of the total amount of PTX, the PTX peak integrity and retention time (Supplementary data, Figure S2).

II.2 PTX RELEASE FROM PTX PLGA-NPS/PEG-DMA HYDROGEL

The *in vitro* release of PTX from the PTX PLGA-NPs/PEG-DMA hydrogel was performed over one week. Two hundred microliters of gel were placed at the bottom of a 50 mL tube and covered with 5 mL of PBS (pH 7.35). The samples were incubated at 37 °C and, at fixed time intervals, all the release buffer was collected and replaced with 5 mL of fresh medium. Samples were frozen at -80 ºC and then lyophilized. The release samples containing free PTX and PTX PLGA-NPs were diluted in acetonitrile to break the PLGA nanoparticle structure and solubilize PTX. The supernatant was analyzed by HPLC (see section 2.1.3) (n=3).

II.3 *IN VITRO* EFFICACY STUDIES OF PTX PLGA-NPS

II.3.1 Cell cultures

U87 MG GBM cells (ATCC, USA) were cultivated in Eagle's Minimum Essential Medium (EMEM, ATCC, USA) with 10% fetal bovine serum (FBS, Gibco, USA) and a 1% penicillin/streptomycin mixture (Gibco, USA). Cells were cultured in 75 cm^2 culture flasks (Corning® T-75, Sigma-Aldrich, USA) and incubated at 37 °C and 5% CO_2.

II.3.2 Cytotoxicity studies

The PTX PLGA-NPs cytotoxicity on U87 MG cells was assessed by the MTT (thiazolyl blue tetrazolium bromide, Sigma-Aldrich, USA) assay [14]. Briefly, 96-well plates were coated with 0.1

mg/mL poly (D) lysine (MP Biomedicals, USA) and cells were seeded at 5×10^3 cells/well. After 24 h, different concentrations of PTX PLGA-NPs (1 ng/ml to 10 μg/ml) were added and incubated for 48 h. Cells without treatment and cells treated with Triton X-100 1% (Sigma-Aldrich, USA) served as controls (100% and 0% viability, respectively). After 48 h of incubation, cells were washed and incubated with MTT solution (0.5 mg/mL). Formazan crystals were then solubilized in DMSO (Merck, USA), and spectrophotometric readings were performed at 560 nm using a MultiSkan EX plate reader (Thermo Scientific, USA) (n=6).

The PTX PLGA-NPs cytotoxicity on U87 MG cells was also evaluated by a clonogenic assay adapted from Franken *et* al. [29]. Briefly, 1×10^5 U87 MG cells/well were seeded in a 12-well plate and incubated for 24 h. The next day, different concentrations of PTX PLGA-NPs (0.0032 to 1 μg/mL) were added and incubated for 48 h with the cells. Then, U87 MG cells were detached and 1000 cells/well were seeded in six-well plates in EMEM complete media for 12 days. The medium was then discarded and the clones were fixed by adding 50% ethanol, 5% acetic acid and 0.5% crystal violet for 30 min at room temperature. Then, the cells were washed twice with water and air-dried. The clones were counted manually and the number of clones was compared to untreated cells (n=3).

II.4 *IN VIVO* STUDIES

All experiments were performed following the Belgian national regulations guidelines in accordance with EU Directive 2010/63/EU and were approved by the ethical committee for animal care of the Université catholique de Louvain medicine faculty (2014/UCL/MD/004). The animals had free access to water and food. Animal body weight was monitored daily throughout the experiments.

II.4.1 In vivo tolerability assays of hydrogel in healthy mouse brain

Seven-week-old female NMRI mice (Janvier, France) were randomly divided into 3 groups: *(i)* resection alone, *(ii)* resection + irradiation, and *(iii)* resection + photopolymerized PEG-DMA hydrogel. The resection was performed as previously described [30]. Five microliters of unloaded PEG-DMA hydrogel were injected into the resection cavity and polymerized as described in part 2.1.4. The cranial window was then covered with Neuro-Patch® (Aesculap, USA) previously soaked with fibrin glue (Baxter Innovations, Austria). Mice were then sutured and monitored the behavior for 2 or 4 months. At the end of the experiment, mice were sacrificed and their brains were extracted, fixed in 10% formalin solution (Merck, USA) overnight, washed with PBS and incubated

in 30% sucrose for 2 days at 4 °C. The brains were then embedded in OCT (Tissue-Tek, USA) and sectioned at 18 μm using a Leica CM 1950 cryostat (Leica, Germany).

Microglial activation was evaluated by Iba-1 immunostaining as described [12]. Slides were scanned using a SCN400 Leica slide scanner, and image analysis was performed on selected zone with Digital Image Hub (Leica, Germany). Apoptosis was evaluated with the Fluorometric TUNEL System kit® (Promega, USA) according to the manufacturer's instructions. Slides were examined under an inverted fluorescence microscope (Evos, USA) with 350 nm (blue, DAPI) and 450–500 nm (green, TUNEL) excitation filters. The stainings were performed on 3 animals (n=3).

II.4.2 Orthotopic U87 MG human GBM tumor resection model

Six-week-old female NMRI nude mice (Janvier, France) were anesthetized and positioned in a stereotactic frame. As previously described [30], a five microliters Hamilton syringe fitted with a 26 G needle was used to inject two to three microliters of complete culture medium containing 3×10^4 U87 MG glioma cells into the right frontal lobe. The injection coordinates were 0.5 mm anterior, 2.1 mm lateral from the bregma and 2.5 mm deep from the outer border of the cranium.

The presence, volume and location of the tumors were determined by magnetic resonance imaging (MRI) using the 11.7 T Bruker Biospec MRI system (Bruker) for all mice on day 11 or 12 post-tumor cell implantation. The tumor volume was assessed using the rapid acquisition with relaxation enhancement (RARE) sequence (TR=2500 ms; effective echo time (TE_{eff})=30 ms; RARE factor=8; FOV=2×2 cm; matrix 256×256; twenty-five contiguous slices of 0.3 mm, NA=4).

On day 13 post-tumor injection, tumor resection was performed based on a biopsy-punch resection model [30]. A 2 mm Ø biopsy punch (Kai Medical, Germany) was then inserted 3 mm deep and twisted for 15 s to cut the tumor site. Once withdrawn, the tumor and brain tissues were aspirated using a diaphragm vacuum pump. Five microliters of hydrogel was photopolymerized into the resection cavity before sealing the cranial window with a 4 mm×4 mm square piece of Neuro-Patch® (Aesculap, Germany) impregnated with a reconstituted fibrin glue (Baxter Innovations, Austria).

II.4.3 In vivo anti-tumor efficacy of PTX PLGA-NPs-loaded hydrogel on the U87 MG GBM model after tumor resection

The *in vivo* anti-tumor efficacy of PTX PLGA-NPs-loaded hydrogel was conducted post-tumor injection by administration of the treatment in the resection cavity as follows: Group 1: untreated

group (*n*=7), Group 2: resection and untreated group (*n*=8), Group 3: PTX PLGA-NPs-treated group (*n*=8), Group 4: blank PLGA-NPs-loaded PEG-DMA hydrogel *in situ* photopolymerized treated group (*n*=8) and Group 5: PTX PLGA-NPs-loaded PEG-DMA hydrogel *in situ* photopolymerized treated group (*n*=9). The dose of PTX administered was 0.525 mg/kg. The delivered dose of drug without the PEG-DMA gel was the same as that within the PEG-DMA hydrogel. The mice were sacrificed when they presented a 20% body weight loss or 10% body weight loss associated with clinical signs of distress (paralysis, arched back, apathy).

II.5 STATISTICAL ANALYSIS

The results are expressed as the mean ± SD or SEM of at least three replicates. Statistical analysis was performed using GraphPad Prism and Excel software based on $*p < 0.05$, $**p < 0.01$ and $***p < 0.001$ for significant differences. In these experiments, *n* is the number of replicates for each experiment. For Figure 5, log-rank test was performed to demonstrate statistical differences between groups using the software GraphPad Prism.

III. RESULTS AND DISCUSSION

III.1 PHYSICO-CHEMICAL CHARACTERIZATION OF PTX PLGA-NPS

The PTX PLGA-NPs formulation was prepared using a modified emulsion-diffusion technique. The blank PLGA-NPs and PTX PLGA-NPs were characterized in terms of their physico-chemical properties and encapsulation capacities. As shown in Table 1, the size of both the blank PLGA-NPs and PTX PLGA-NPs was approximately 190 nm, and the polydispersity indices showed a narrow size distribution (0.07 and 0.13, respectively). The zeta potential values were negative for the two formulations (approximately -17 mV). The presence of PTX in the formulation did not influence the size or zeta potential of the nanoparticles. The PTX encapsulation efficacy and drug loading, assessed after breaking the PLGA nanoparticle structure in acetonitrile, were approximately 53% and 4%, respectively. The physico-chemical parameters are consistent with those previously described for the encapsulation of PTX [24, 28, 31].

III.2 PTX RELEASE FROM PTX PLGA-NPS-LOADED PEG-DMA HYDROGEL

The hydrogel system was developed to fill the cavity after the surgical resection of the tumor to act as a PTX drug depot and kill the residual infiltrating GBM cells. Thus, we evaluated the *in vitro* release profile of PTX. The *in vitro* release kinetics of PTX PLGA-NPs from the PEG-DMA hydrogel was evaluated after incubation at 37 °C in PBS pH=7.35. An initial burst release of 10.9±2.3% was observed in the first 8 h, followed by a sustained release of the drug over 1 week (28.9±3.7%) (Figure 2). Over 90 % of the drug was recovered when the total amount of released PTX was sum up with the quantity of PTX that remained in the hydrogel. Comparing to the release of TMZ free drug (45% burst release and 65% sustained release over 1 week) in PEG-DMA hydrogel, the small burst and continuous PTX release may be attributed to the diffusion of PTX localized in the PLGA core of the nanoparticles [22]. After resection, as most tumor cells were removed, the PTX initial burst release may kill the closer tumor cells, while the continued release could kill the remaining infiltrative cells [7].

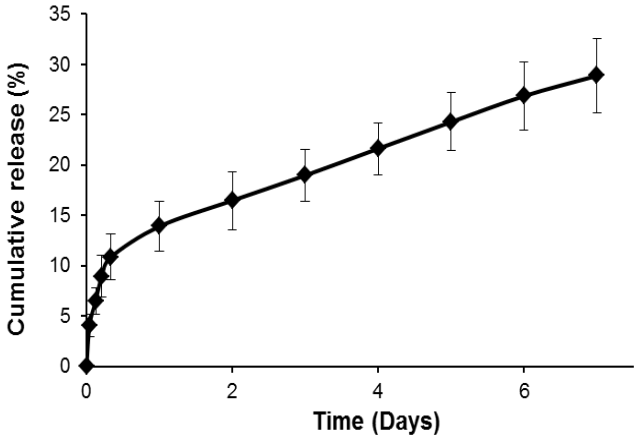

Figure 2: *In vitro* cumulative release of PTX from PTX PLGA-NPs/PEG-DMA hydrogels. Release was performed at 37 °C in PBS (pH=7.4). The amount of PTX released was quantified by HPLC (mean ± SD; *n*=3).

III.3 *IN VITRO* CYTOTOXICITY OF PTX PLGA-NPS IN U87 MG GBM CELLS

To evaluate the cytotoxicity of PTX PLGA-NPs, an MTT assay was conducted on U87 MG GBM cells after 48 h of incubation with different concentrations of PTX (0.001 to 10 µg/mL). The results are illustrated in Figure 3A. PTX PLGA-NPs induced an obvious cytotoxic effect on U87 MG cells, demonstrating concentration-dependent inhibitory effects. The IC_{50} value of PTX PLGA-NPs was 0.010 µg/mL. To confirm this result, a modified clonogenicity study was conducted to evaluate the proliferative and reproductive ability of U87 MG cells after incubation with PTX PLGA-NPs for 48 h (Figure 3B). The numbers of clones were counted, and the resulting IC_{50} value (0.014 µg/mL) was close to that obtained in the MTT test. Some authors previously evaluated the cytotoxic effect of PTX on GBM cells, showing a similar sensitivity of U87 MG GBM cells to PTX (from 0.003 µg/mL to 4.5 µg/mL) [32-35]. No cytotoxic activity was observed for the drug-free nanoparticles at a polymer concentration below 2 mg/mL (data not shown).

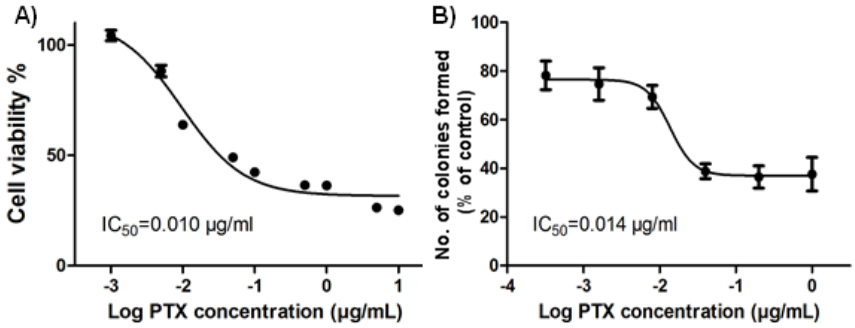

Figure 3: *In vitro* cytotoxicity study. U87 MG glioma cells were treated with PTX PLGA-NPs at different PTX concentrations. The cytotoxic effect of PTX PLGA-NPs was assessed by the MTT (A) and clonogenic assays (B). Mean ± SD, *n*=6 for MTT assay and *n*=3 for clonogenic assay.

III.4 *IN VIVO* TOLERABILITY OF PEG-DMA HYDROGEL IN HEATHY MOUSE BRAIN

The influence of the PEG-DMA on brain microglial activation and apoptosis was evaluated 2 and 4 months after implantation in healthy mice. After 2 and 4 months, none of the animals with brain resection with or without PEG-DMA hydrogel implantation showed behavioral changes or loss of body weight. Microglial activation was observed whatever the condition both after 2 and 4 months (Figure 4A), probably due to the surgery. No positive TUNEL signal was observed whatever the timing and the treatment (Figure 4B). We previously observed that after 1 week exposure to the same hydrogel, the brain resection itself induced microglial activation and some cell apoptosis at the cavity margin [12]. Our results show that there is also inflammation but no significant apoptosis resulting from surgical resection alone after 2 and 4 month. It has been previously shown that microglial activation followed by resection or biomaterial implantations into the brain can last much longer time [36, 37]. There is still Iba-1 staining at 4 months indicating that the microglia activation was not resolved. However, it remains controversial whether microglia activation is beneficial or detrimental. On one hand, microglial activation may be considered as a positive factor as it could remove cell debris and recover tissue integrity in the injured brain [38]. Other author even proposed the restoration of the microglial anti-tumor function as a treatment for GBM [39]. On the other hand, excessive activation may cause neuronal damage through the secretion of cytotoxic molecules [40]. However, irradiation and hydrogel implantation did not increase the extent of microglia activation. In conclusion, the *in situ* photopolymerization of PEG-DMA hydrogel is tolerated in healthy mice brains and is therefore suitable for local administration into the mouse brain.

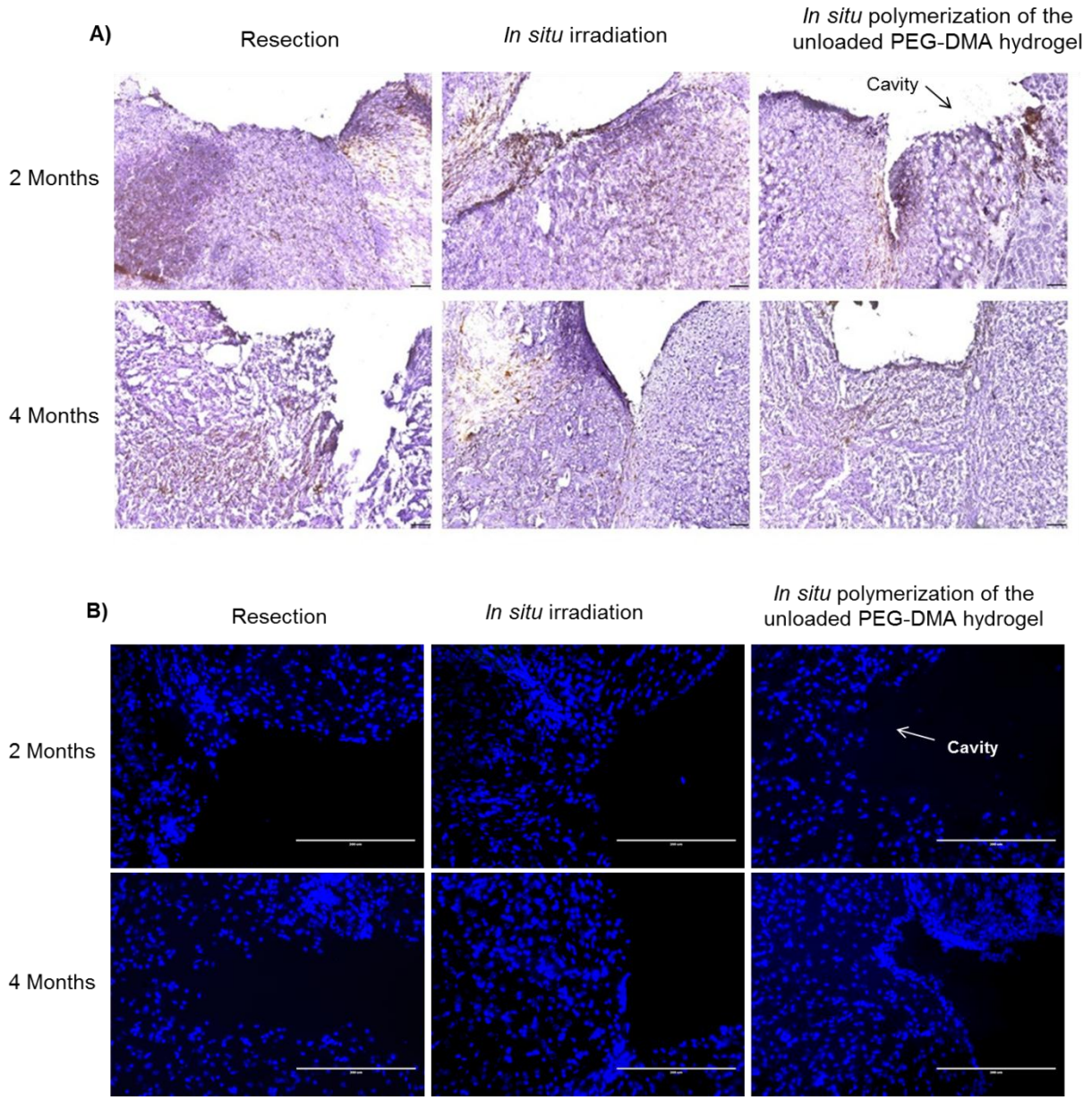

Figure 4: (A) Mid- and long-term effects of the *in situ* photopolymerization of unloaded PEG-DMA hydrogels on microglial activation (positive staining: brown cells). Mouse brain was extracted at 2 and 4 months post-surgery and counterstained with hematoxylin and Iba-1 immunostaining. The groups are the resection alone, *in situ* irradiation (400 nm, 750 mW/cm², 15 s) and *in situ* photopolymerization of the unloaded PEG-DMA hydrogel (n=3). Scale bar=100 µm

(B) Mid- and long-term effects of the *in situ* photopolymerization of unloaded PEG-DMA hydrogels on brain cell apoptosis. Mouse brain was extracted at 2 and 4 months post-surgery and evaluated with a TUNEL assay. The groups are resection alone, *in situ* irradiation (400 nm, 750 mW/cm², 15 s), and *in situ* photopolymerization of unloaded PEG-DMA hydrogel (n=3). Scale bar=200 µm

III.5 *IN VIVO* ANTI-TUMOR EFFICACY OF PTX PLGA-NPS-LOADED HYDROGEL ON THE U87 MG GBM MODEL AFTER TUMOR RESECTION

To evaluate the anti-tumor efficacy of the hydrogel and its capacity to slow down tumor recurrences in a clinically relevant model, the GBM was surgically resected on day 13 post-tumor inoculation, and the treatments were intra-operatively injected into the resection cavity (Figure 5A). The tumors were well-demarcated and visible by MRI imaging (Figure 5B). The hydrogel was visible and stayed in place during the entire course of the experiment (Figure 5B). The median survival times of mice with or without resection were significantly different (52 and 35 days, respectively; $p < 0.001$), demonstrating the effect of surgical resection (Figure 5C). Injection of PTX-NPs and blank NPs-loaded hydrogel in the resection cavity failed to significantly prolong the median survival time of mice compared to that of resected mice ($p > 0.05$). However, the survival time of the PTX PLGA-NPs hydrogel-treated mice was significantly enhanced ($p < 0.01$) compared to that of mice in the resection untreated group, and more than 50% of the mice were still alive 150 days after the injection of tumor cells. One mouse out of 5 surviving mice showed the sign of tumor recurrence on days 147 by MRI imaging (data not shown).

The improvement of animal survival was reported with the conventional enhanced delivery (CED) or local implantation of hydrogels [36, 41-45]. For example, when camptothecin was encapsulated in PLGA-NPs and delivered via CED in rats, 30% of the group treated with the system experienced long-term survival until 60 days, the median survival of which was significantly improved compared to the control [45]. More recently, in a similar experimental model, lauroyl-gemcitabine lipid nanocapsule-based hydrogel was delivered intra-surgically in the resection cavity in U87 MG-bearing mice, and a significantly prolonged medial survival of 62 days was observed compared to that of the untreated group (35.5 days) [36]. In comparison, our promising results (150 days long-term survivors) highlight the high potential of PTX-loaded PLGA-NPs/PEG-DMA hydrogel for local implantation after surgical resection to significantly improve the overall survival of mice bearing GBM.

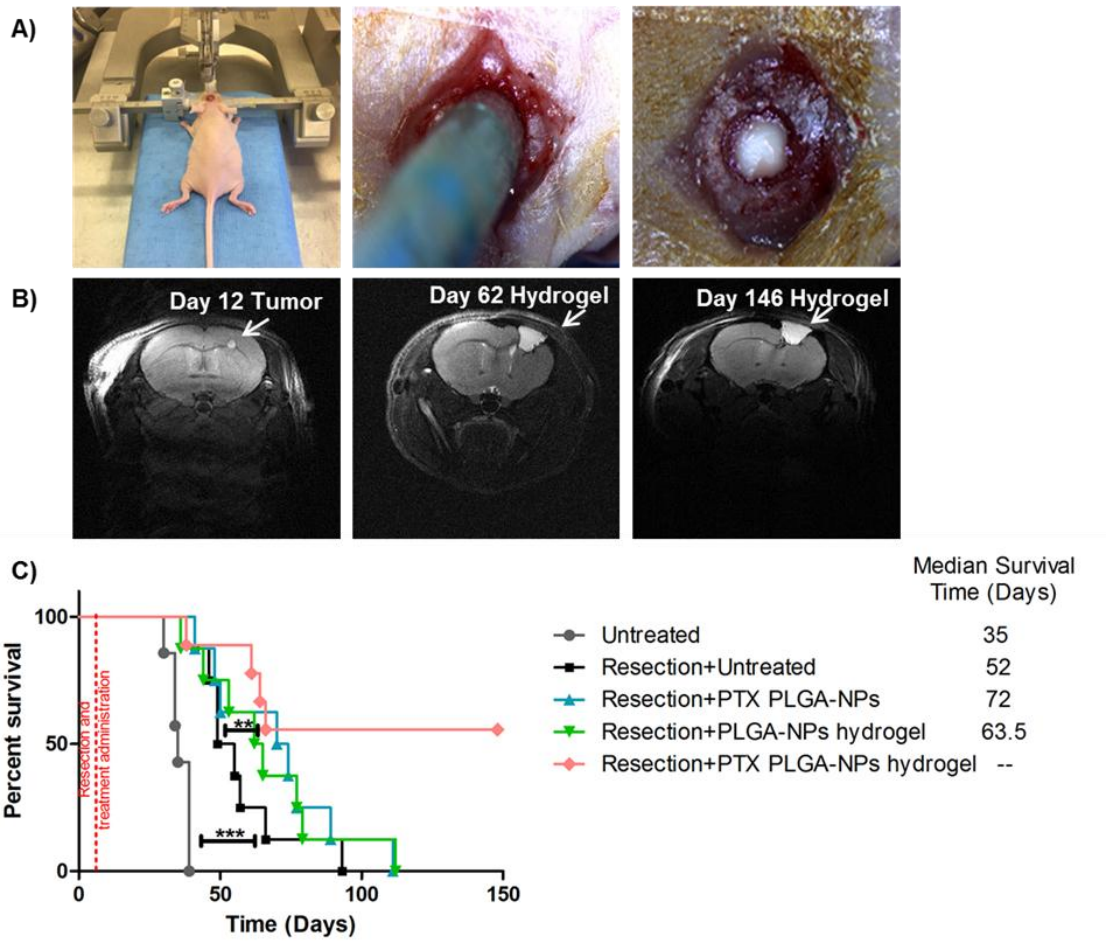

Figure 5: (A) Pictures of the tumor resection surgeries and treatment administration. Briefly, mice were fixed on a stereotactic frame for the tumor cell injections (left), biopsy punch resections of tumor tissue (middle) and *in situ* photopolymerization of PEG-DMA hydrogels with PTX PLGA-NPs (right). (B) Axial (T2-weighted) images of a mouse brain: brain tumor before resection (day 12, left), treatment with PTX PLGA-NPs/PEG-DMA hydrogel (day 62 post-tumor inoculation, middle; day 146 post-tumor inoculation, right). (C) Kaplan-Meier survival curves for mice after different treatments in the resection cavity. (n=7-9). ** $p < 0.01$, *** $p < 0.001$

IV.CONCLUSION

In conclusion, we designed and characterized an injectable photopolymerizable PEG-DMA hydrogel containing PTX-loaded PLGA-NPs that fits many requirements of a local drug delivery system for the treatment of GBM. We demonstrated the sustained release of PTX over one week. The *in vitro* cytotoxicity study confirmed U87 MG cells were sensitive to PTX. The *in vivo* tolerability studies showed that the implantation of hydrogel into the brains of healthy mice was well tolerated for 4 months. The *in vivo* anti-tumor efficacy studies performed on a clinically relevant tumor model (orthotopic U87 MG resection model on mice) showed that PTX-loaded PLGA NPs in PEG-DMA hydrogel significantly prolonged mouse survival, and 50% of the mice were alive at 5 months after tumor implantation. Future pre-clinical studies may take advantage of the potential therapeutic benefits of this system.

V. SUPPLEMENTARY MATERIAL

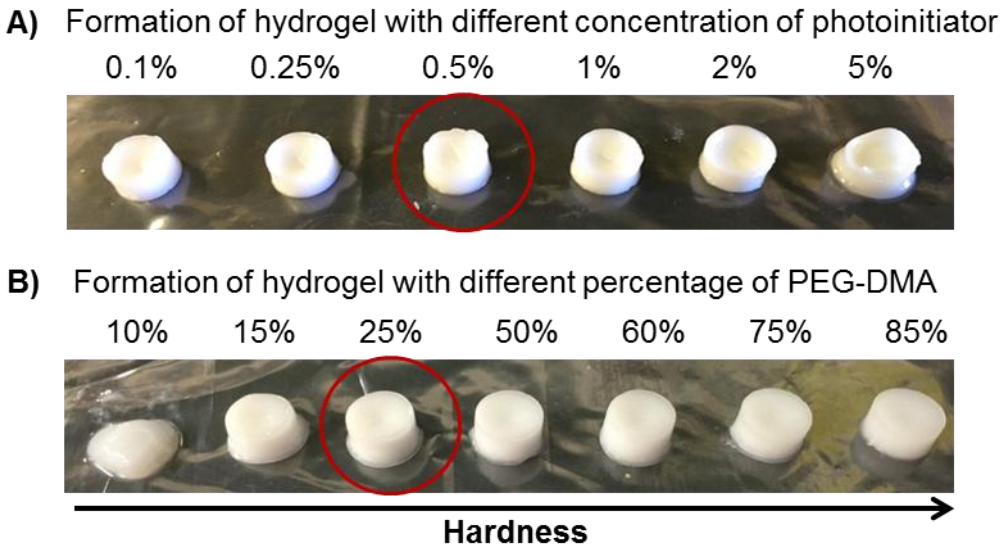

Figure S1: Formation of hydrogels with different concentrations of photoinitiator (A) and percentage of PEG-DMA (B) in the presence of PTX PLGA-NPs.

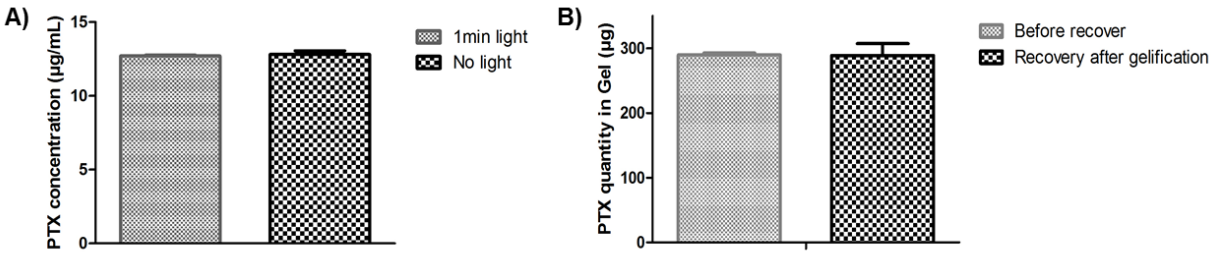

Figure S2: Evaluation of paclitaxel stability. The PTX stability was assessed after 1 min of blue light exposure (A) or photopolymerization (B). The PTX quantity was assessed by HPLC (mean ± SD; n=3), p>0.05.

VI. REFERENCES

1. Milano MT, Okunieff P, Donatello RS, Mohile NA, Sul J, Walter KA, et al. Patterns and timing of recurrence after temozolomide-based chemoradiation for glioblastoma. International Journal of Radiation Oncology• Biology• Physics. 2010; 78: 1147-55.
2. Davis ME. Glioblastoma: Overview of Disease and Treatment. Clinical journal of oncology nursing. 2016; 20: S2-S8.
3. Wilson TA, Karajannis MA, Harter DH. Glioblastoma multiforme: State of the art and future therapeutics. Surgical Neurology International. 2014; 5: 64.
4. Stupp R, Mason WP, van den Bent MJ, Weller M, Fisher B, Taphoorn MJB, et al. Radiotherapy plus concomitant and adjuvant temozolomide for glioblastoma. The New England journal of medicine. 2005; 352: 987-96.
5. Ostrom QT, Bauchet L, Davis FG, Deltour I, Fisher JL, Langer CE, et al. The epidemiology of glioma in adults: a "state of the science" review. Neuro-Oncology. 2014; 16: 896-913.
6. Stupp R, Hegi ME, Mason WP, van den Bent MJ, Taphoorn MJ, Janzer RC, et al. Effects of radiotherapy with concomitant and adjuvant temozolomide versus radiotherapy alone on survival in glioblastoma in a randomised phase III study: 5-year analysis of the EORTC-NCIC trial. The lancet oncology. 2009; 10: 459-66.
7. Bastiancich C, Danhier P, Préat V, Danhier F. Anticancer drug-loaded hydrogels as drug delivery systems for the local treatment of glioblastoma. Journal of Controlled Release. 2016; 243: 29-42.
8. Patel DM, Agarwal N, Tomei KL, Hansberry DR, Goldstein IM. Optimal timing of whole-brain radiation therapy following craniotomy for cerebral malignancies. World neurosurgery. 2015; 84: 412-9.
9. Bota DA, Desjardins A, Quinn JA, Affronti ML, Friedman HS. Interstitial chemotherapy with biodegradable BCNU (Gliadel(®)) wafers in the treatment of malignant gliomas. Therapeutics and Clinical Risk Management. 2007; 3: 707-15.
10. Perry J, Chambers A, Spithoff K, Laperriere N. Gliadel wafers in the treatment of malignant glioma: a systematic review. Current Oncology. 2007; 14: 189-94.
11. Engelhard HH. The role of interstitial BCNU chemotherapy in the treatment of malignant glioma. Surgical Neurology. 2000; 53: 458-64.
12. Fourniols T, Randolph LD, Staub A, Vanvarenberg K, Leprince JG, Préat V, et al. Temozolomide-loaded photopolymerizable PEG-DMA-based hydrogel for the treatment of glioblastoma. Journal of Controlled Release. 2015; 210: 95-104.
13. Kitange GJ, Carlson BL, Schroeder MA, Grogan PT, Lamont JD, Decker PA, et al. Induction of MGMT expression is associated with temozolomide resistance in glioblastoma xenografts. Neuro-Oncology. 2009; 11: 281-91.
14. Bastiancich C, Vanvarenberg K, Ucakar B, Pitorre M, Bastiat G, Lagarce F, et al. Lauroyl-gemcitabine-loaded lipid nanocapsule hydrogel for the treatment of glioblastoma. Journal of Controlled Release. 2016; 225: 283-93.
15. Vinchon-Petit S, Jarnet D, Michalak S, Lewis A, Benoit J-P, Menei P. Local implantation of doxorubicin drug eluting beads in rat glioma. International journal of pharmaceutics. 2010; 402: 184-9.
16. Qi N, Cai C, Zhang W, Niu Y, Yang J, Wang L, et al. Sustained delivery of cytarabine-loaded vesicular phospholipid gels for treatment of xenografted glioma. International journal of pharmaceutics. 2014; 472: 48-55.
17. Gupta ML, Bode CJ, Georg GI, Himes RH. Understanding tubulin–Taxol interactions: Mutations that impart Taxol binding to yeast tubulin. Proceedings of the National Academy of Sciences. 2003; 100: 6394-7.

18. Xin H, Chen L, Gu J, Ren X, Luo J, Chen Y, et al. Enhanced anti-glioblastoma efficacy by PTX-loaded PEGylated poly (ε-caprolactone) nanoparticles: in vitro and in vivo evaluation. International journal of pharmaceutics. 2010; 402: 238-47.
19. Zhan C, Gu B, Xie C, Li J, Liu Y, Lu W. Cyclic RGD conjugated poly (ethylene glycol)-co-poly (lactic acid) micelle enhances paclitaxel anti-glioblastoma effect. Journal of Controlled Release. 2010; 143: 136-42.
20. Shen Y, Pi Z, Yan F, Yeh C-K, Zeng X, Diao X, et al. Enhanced delivery of paclitaxel liposomes using focused ultrasound with microbubbles for treating nude mice bearing intracranial glioblastoma xenografts. International Journal of Nanomedicine; 2017. p. 5613-29.
21. Chang SM, Kuhn JG, Robins HI, Schold SC, Spence AM, Berger MS, et al. A phase II study of paclitaxel in patients with recurrent malignant glioma using different doses depending upon the concomitant use of anticonvulsants. Cancer. 2001; 91: 417-22.
22. Danhier F, Ansorena E, Silva JM, Coco R, Le Breton A, Préat V. PLGA-based nanoparticles: An overview of biomedical applications. Journal of Controlled Release. 2012; 161: 505-22.
23. Danhier F, Vroman B, Lecouturier N, Crokart N, Pourcelle V, Freichels H, et al. Targeting of tumor endothelium by RGD-grafted PLGA-nanoparticles loaded with Paclitaxel. Journal of Controlled Release. 2009; 140: 166-73.
24. Amoozgar Z, Wang L, Brandstoetter T, Wallis SS, Wilson EM, Goldberg MS. Dual-Layer Surface Coating of PLGA-Based Nanoparticles Provides Slow-Release Drug Delivery To Achieve Metronomic Therapy in a Paclitaxel-Resistant Murine Ovarian Cancer Model. Biomacromolecules. 2014; 15: 4187-94.
25. Luo T, Loira-Pastoriza C, Patil HP, Ucakar B, Muccioli GG, Bosquillon C, et al. PEGylation of paclitaxel largely improves its safety and anti-tumor efficacy following pulmonary delivery in a mouse model of lung carcinoma. Journal of Controlled Release. 2016; 239: 62-71.
26. Cui Y, Xu Q, Chow PK-H, Wang D, Wang C-H. Transferrin-conjugated magnetic silica PLGA nanoparticles loaded with doxorubicin and paclitaxel for brain glioma treatment. Biomaterials. 2013; 34: 8511-20.
27. Danhier F, Lecouturier N, Vroman B, Jérôme C, Marchand-Brynaert J, Feron O, et al. Paclitaxel-loaded PEGylated PLGA-based nanoparticles: In vitro and in vivo evaluation. Journal of Controlled Release. 2009; 133: 11-7.
28. Schleich N, Sibret P, Danhier P, Ucakar B, Laurent S, Muller RN, et al. Dual anticancer drug/superparamagnetic iron oxide-loaded PLGA-based nanoparticles for cancer therapy and magnetic resonance imaging. International Journal of Pharmaceutics. 2013; 447: 94-101.
29. Franken NA, Rodermond HM, Stap J, Haveman J, Van Bree C. Clonogenic assay of cells in vitro. Nature protocols. 2006; 1: 2315.
30. Bianco J, Bastiancich C, Joudiou N, Gallez B, Des Rieux A, Danhier F. Novel model of orthotopic U-87 MG glioblastoma resection in athymic nude mice. Journal of neuroscience methods. 2017; 284: 96-102.
31. Jin C, Bai L, Wu H, Song W, Guo G, Dou K. Cytotoxicity of Paclitaxel Incorporated in PLGA Nanoparticles on Hypoxic Human Tumor Cells. Pharmaceutical Research. 2009; 26: 1776-84.
32. Najlah M, Kadam A, Wan K-W, Ahmed W, Taylor KMG, Elhissi AMA. Novel paclitaxel formulations solubilized by parenteral nutrition nanoemulsions for application against glioma cell lines. International Journal of Pharmaceutics. 2016; 506: 102-9.
33. Xu Y, Shen M, Li Y, Sun Y, Teng Y, Wang Y, et al. The synergic antitumor effects of paclitaxel and temozolomide co-loaded in mPEG-PLGA nanoparticles on glioblastoma cells. Oncotarget. 2016; 7: 20890.
34. Maleki H, Dorkoosh F, Adabi M, Khosravani M, Arzani H, Kamali M. Methotrexate-loaded plga nanoparticles: Preparation, characterization and their cytotoxicity effect on human glioblastoma U87MG cells. International Journal of Medical Nano Research. 2017; 4: 020.

35. Ruan H, Chen X, Xie C, Li B, Ying M, Liu Y, et al. Stapled RGD Peptide Enables Glioma-Targeted Drug Delivery by Overcoming Multiple Barriers. ACS applied materials & interfaces. 2017; 9: 17745-56.
36. Bastiancich C, Bianco J, Vanvarenberg K, Ucakar B, Joudiou N, Gallez B, et al. Injectable nanomedicine hydrogel for local chemotherapy of glioblastoma after surgical resection. Journal of Controlled Release. 2017; 264: 45-54.
37. Bjugstad K, Lampe K, Kern D, Mahoney M. Biocompatibility of poly (ethylene glycol) - based hydrogels in the brain: An analysis of the glial response across space and time. Journal of Biomedical Materials Research Part A. 2010; 95: 79-91.
38. Zhang S, Wang Y, Xie H, Yu Q, Wu J, Wu Y, et al. Necroptosis and microglia activation after chronic ischemic brain injury in mice. European Journal of Inflammation. 2017; 15: 78-84.
39. Chiu T-L, Wang M-J, Su C-C. The treatment of glioblastoma multiforme through activation of microglia and TRAIL induced by rAAV2-mediated IL-12 in a syngeneic rat model. Journal of Biomedical Science. 2012; 19: 45.
40. Dheen T, Kaur C, Ling E-A. Microglial Activation and its Implications in the Brain Diseases; 2007.
41. Zhang R, Saito R, Mano Y, Sumiyoshi A, Kanamori M, Sonoda Y, et al. Convection-enhanced delivery of SN-38-loaded polymeric micelles (NK012) enables consistent distribution of SN-38 and is effective against rodent intracranial brain tumor models. Drug delivery. 2016; 23: 2780-6.
42. Chen T, Gong T, Zhao T, Liu X, Fu Y, Zhang Z, et al. Paclitaxel loaded phospholipid-based gel as a drug delivery system for local treatment of glioma. International Journal of Pharmaceutics. 2017; 528: 127-32.
43. Stephen ZR, Kievit FM, Veiseh O, Chiarelli PA, Fang C, Wang K, et al. Redox-responsive magnetic nanoparticle for targeted convection-enhanced delivery of O 6-benzylguanine to brain tumors. ACS nano. 2014; 8: 10383-95.
44. Tyler B, Fowers KD, Li KW, Recinos VR, Caplan JM, Hdeib A, et al. A thermal gel depot for local delivery of paclitaxel to treat experimental brain tumors in rats. Journal of neurosurgery. 2010; 113: 210-7.
45. Sawyer AJ, Saucier-Sawyer JK, Booth CJ, Liu J, Patel T, Piepmeier JM, et al. Convection-enhanced delivery of camptothecin-loaded polymer nanoparticles for treatment of intracranial tumors. Drug Delivery and Translational Research. 2011; 1: 34-42.

CHAPTER IV

CODELIVERY OF PACLITAXEL AND TEMOZOLOMIDE THROUGH A PHOTOPOLYMERIZABLE HYDROGEL PREVENTS GLIOBLASTOMA RECURRENCE AFTER SURGICAL RESECTION

Mengnan Zhao, Elia Bozzato, Nicolas Joudiou, Sina Ghiassinejad, Fabienne Danhier, Bernard Gallez, Véronique Préat

Adapted from Journal of Controlled Release, 2019; 309: 72-81

TABLE OF CONTENTS

ABSTRACT

A photopolymerizable hydrogel-based local drug delivery system was developed for the postsurgical treatment of glioblastoma. We aimed for a local drug combination therapy with paclitaxel (PTX) and temozolomide (TMZ) within a hydrogel to synergistically inhibit tumor growth. The *in vitro* cytotoxicity of TMZ was assessed in U87MG cells. We demonstrated the synergistic effect of PTX and TMZ on U87MG cells by clonogenic assay. Treatment with TMZ did not induce O6-methylguanine-DNA methyltransferase related drug resistance in tumor-bearing mice. PTX had sustained release for at least 1 month *in vivo* in healthy mice brains. The drug combination was tolerable and suppressed tumor growth more efficiently than the single drugs in the U87MG orthotopic tumor model. The PTX and TMZ codelivery hydrogel showed superior antitumor effects and can be considered a promising approach for the postsurgical treatment of GBM.

I. INTRODUCTION

Glioblastoma multiforme (GBM) is the most malignant and frequently occurring tumor in the central nervous system, accounting for 16% of all central nervous system neoplasms [1]. GBM is an uncurable disease; 70% of GBM patients will experience disease progression within 1 year of diagnosis [2], with a median overall survival of 14 to 20 months in recent clinical trials [3, 4]. Current gold standard treatments include massive safe surgical resection and subsequent radiotherapy with concurrent oral temozolomide (Temodar®, TMZ) followed by adjuvant chemotherapy with TMZ [5]. However, higher doses of TMZ were related to dose-limiting myelosuppression [6]. Due to the cellular and molecular heterogeneity of GBM, we were motivated to identify and characterize a combination agent inducing a synergistic effect with TMZ. Paclitaxel (PTX) is an efficient anticancer drug and has different mechanisms of action, non-overlapping toxicities and distinct mechanisms of resistance compared to TMZ [7]. We hypothesized that PTX could be a promising combination agent with TMZ.

Extensive and complete surgical resection of GBM is difficult, because GBM is often highly infiltrative. Additionally, the existence of the blood-brain barrier (BBB) prevents most oral and intravenous chemotherapeutic agents from reaching the tumor site [8]. GBM most commonly recurs within 2 cm of the resection border in the form of local continuous growth. Therefore, local brain treatment with antitumor chemotherapeutic agents can be administered after surgery to ensure the delivery of cytotoxic drugs to the remaining infiltrating tumor cells [9]. The only local delivery implant currently approved by the FDA is the Gliadel®, a carmustine-loaded polyanhydride copolymer wafer that has been shown to prolong the overall survival of patients to 16.4 months compared to 13.1 months for patients without wafers [10]. However, the cylinder-like structure of the wafer limits the close contact with the brain parenchyma and induces side effects, e.g., infection and inflammation [10-12]. Among all local delivery systems, hydrogels are highly desirable. Cytotoxic drugs loaded in a hydrogel can be administered into the tumor resection cavity and adhere to the brain parenchyma [13]. The hydrogel matrix would ensure the sustained release of the loaded drugs. The ideal hydrogel delivery system for GBM has to meet the following requirements: sterile, injectable, adhesive to the resection cavity and biocompatible [13]. Recently, we reported a novel photopolymerizable hydrogel extraordinarily formed of polyethylene glycol dimethacrylate (PEG-DMA) delivering PTX encapsulated in poly (lactic-co-glycolic acid) (PLGA) nanoparticles for the local administration of GBM treatment [14, 15]. This injectable hydrogel system was suitable for brain tumor postresection implantation and allowed sustained drug release. This system was well tolerated in the mouse brain, inhibited tumor recurrence and led to long-term survival in the aggressive U87MG mouse model. This system can also be loaded with TMZ [14].

To further improve GBM treatment, the aim of the present study was to investigate the antitumor efficacy of this photopolymerizable hydrogel system loaded with the combination of TMZ and PTX (Figure 1). The cytotoxicity, combination effect, drug resistance (O6-methylguanine-DNA methyltransferase, MGMT) after TMZ treatment, *in vivo* PTX diffusion, drug combination safety and antitumor efficacy in an orthotopic U87MG tumor resection model were investigated.

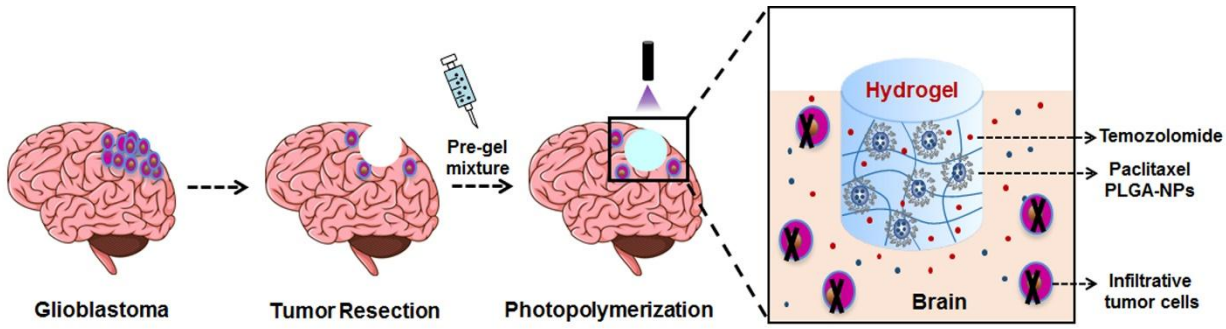

Figure 1: Codelivery of PTX and TMZ through a photopolymerizable hydrogel for the postresection treatment of GBM.

II. MATERIALS AND METHODS

II.1 HYDROGEL PREPARATION AND CHARACTERIZATION

II.1.1 Preparation of PTX PLGA-NPs and TMZ coloaded hydrogels (PTX PLGA-NPs/TMZ/PEG-DMA)

TMZ and L-histidine were purchased from Sigma-aldrich (USA). The same amounts of TMZ and L-histidine (w:w) were solubilized together in water to obtain a clear solution [16]. PTX PLGA-NPs were formulated using an emulsion-evaporation method as previously described [15]. The TMZ/L-histidine solution and the PTX PLGA-NPs were mixed together with a drug ratio of 2:1 (as illustrated in section 3.3). Then, 75% (v:v) drug mixture was added to 25% PEG-DMA (average Mn = 550 g/mol) (Sigma-Aldrich) with Lucirin TPO® (BASF, USA) as a photoinitiator [15]. Then, the injectable pregel mixture was photopolymerized under 400 nm light. Single drug-loaded PEG-DMA hydrogels were also prepared by adding single drug formulations to the pregel mixture. For *in vivo* PTX diffusion assays, 15 μg/mL Oregon Green™ 488-PTX (Thermo Fisher, USA) -loaded PLGA-NPs were prepared by the same emulsion-evaporation method.

II.1.2 Mechanical properties of the PEG-DMA hydrogel

Rheological measurements were carried out with a Kinexus Pro rheometer (Malvern Instruments, UK). A parallel plate geometry of 8 mm in diameter was selected, and a constant 1 mm gap was maintained between the two plates. Ninety microliters of pregel mixture was introduced between the two plates. The light source was placed under the lower plate made of transparent glass. Immediately after placement of the pregel mixture, the plate cartridge was closed and a small amplitude oscillatory strain was applied to the sample, at a frequency of 10 rad/s and the strain amplitude of 1 %, which was chosen in order to stay in the linear regime of deformation. The evolution of the storage modulus G' and loss modulus G" were investigated through time for a total time of 120 s, following a specific protocol: The first 10 s were used to determine the initial modulus. Then, lamp was turned on for 15 s, before turning it off for the remaining time of the experiment. Measurements were performed at 25 °C. The total crosslinking time of the hydrogel was defined as the time required to reach 95% of the maximum storage modulus following radical initiation. For swelling analysis, hydrogels after polymerization were incubated at 37 °C in phosphate-buffered solution (PBS, pH = 7.4). A line was drawn to show the initial volume of the pregel mixture. Gels were weighed before and after the 24 h immersion (n=3).

II.2 .*IN VITRO* CYTOTOXICITY STUDIES

II.2.1 Cell cultures

U87MG cell lines (ATTC, USA) were cultivated in Eagle's Minimum Essential Medium (EMEM) with 10% Fetal Bovine Serum (FBS) (Gibco, USA) and a 1% penicillin/streptomycin mixture (Gibco) (EMEM complete medium). Cells were cultured in 75 cm^2 culture flasks (Corning® T-75, Sigma-Aldrich) and incubated at 37 °C and 5% CO_2.

II.2.2 Clonogenic assay

The clonogenic assay for TMZ and combinations of TMZ and PTX on U87MG cells was adapted from Franken et al [17]. Briefly, 1×10^5 U87MG cells were seeded per well in a 12-well plate and incubated at 37 °C with 5% CO_2 for 24 h. Cells were then incubated with different treatments for 48 h. Next, the cells were detached from the plate, and 300 cells were seeded in a 6-well plate with EMEM complete medium. At day 12, the medium was discarded, and the clones were fixed and stained by adding 50% ethanol, 5% acetic acid and 0.5% crystal violet for 30 min at room temperature. Then, the clones were washed twice with water and air dried. The numbers of colonies were counted by an automatic colony counter pen and compared with the untreated cells ($n = 3$).

II.2.3 Evaluation of the combination effect by the coefficient of drug interaction (CDI)

The combination effect was evaluated by the CDI, which was calculated as follows: CDI = AB/ (A × B). AB is the numbers of colonies formed (% of control) of the combined effects of both drugs. A or B is the numbers of colonies formed (% of control) of each drug alone. [18]. The synergistic cytotoxicity was also confirmed by the CompuSyn software [19].

II.3 *IN VIVO MGMT* EXPRESSION AFTER TMZ TREATMENT

In this experiment, U-251 and T98G cell lines were used as negative and positive controls, respectively. Mice bearing recurrent U87MG tumors after resection or TMZ treatment were sacrificed, and the brains were harvested. Total RNA was extracted from U87MG cells and tumor tissues using Trizol (Invitrogen, USA) plus an RNA purification system (Thermo fisher). Reverse transcription PCR was performed with isolated and purified total RNA and synthesized to cDNA in a 20 μL reaction system using reverse transcriptase (Promega, USA) with oligo-dT primers

according to the manufacturer's instructions. cDNA was obtained to determine *MGMT* gene expression after amplification with the following primers: Fw 5'- GGA GGC ACC GCT GTA TTA AA -3' and Rv 5'- GCA GGT AGG AAA CAA AGC TAG A -3' [20]. Human-derived β-actin was the endogenous control. PCR was performed under classical conditions with the initial denaturation for 3 min at 94 °C; 30 total cycles of 1 min denaturation at 94 °C and annealing for 1 min at 55 °C, followed by extension for 1 min at 72 °C; and a final extension step of 7 min at 72 °C. Amplified products were separated by electrophoresis on a 1% agarose gel and visualized under UV illumination (n=3). *MGMT* levels against actin were determined by image J software.

II.4 *IN VIVO* STUDIES

All the experiments were performed following the Belgian national regulation guidelines in accordance with EU Directive 2010/63/EU and were approved by the ethical committee for animal care of the Université catholique de Louvain medicine faculty (2014/UCL/MD/004). Animals had free access to water and food, and the body weights were monitored daily throughout the experiments.

II.4.1 Orthotopic U87MG human GBM tumor resection model

Six-week-old NMRI female nude mice (Janvier, France) were anesthetized by intraperitoneal injection of ketamine/xylazine (100 and 13 mg/kg, respectively) and positioned on a stereotactic frame as previously described [21]. A five-microliter Hamilton syringe with a 26 G needle was used to inject up to 3 μL of complete culture medium containing 3×10^4 U87MG glioma cells into the right frontal lobe. The injection site was 0.5 mm anterior, 2.1 mm lateral from the bregma and 2.5 mm deep from the cranium. After 13 days, the cranium was opened again, and a 2 mm diameter biopsy punch (Kai Medical, Germany) was inserted 3 mm deep and twisted for 15 s to cut the tumor tissues. Then, the tumor tissues were aspirated using a diaphragm vacuum pump. Five microliters of hydrogel was photopolymerized into the resection cavity before closing the cranial window with a 4 mm × 4 mm Neuro-Patch® (Aesculap, Germany) saturated with a reconstituted fibrin glue (Baxter Innovations, Austria).

II.4.2 In vivo local PTX diffusion

Six-week-old healthy female Swiss mice (Janvier) were anesthetized and positioned in a stereotactic frame. Five microliters of hydrogel loaded with 15 μg/mL Oregon Green™ 488-PTX (Thermo Fisher) within PLGA-NPs was photopolymerized into the resection cavity before sealing the

cranial window with a 4 mm × 4 mm square piece of Neuro-Patch® impregnated with a reconstituted fibrin glue (Baxter Innovations). Animals were then sacrificed at 0 h, 24 h, 96 h, 10 days or 1 month after hydrogel injection. The brain was rapidly harvested and embedded in OCT on dry ice. Brains were cryosectioned using a Leica 1950 cryostat (Leica, Germany) into 40 µm thick slices and stained with DAPI (2 µg/mL, nuclear stain) (Thermo Fisher). Images were acquired on Zeiss LSM 710 and Zeiss BF/LF Axio Imager microscopes, and the analyses were processed in a ZEN 2.5 (Zeiss, Germany) system (*n*=3-6).

II.4.3 In vivo safety study of the drug combination

Six-week-old healthy female NMRI nude mice (Janvier) were anesthetized intraperitoneally. Normal brain resections were performed using the biopsy punch resection model as described in 2.4.1. The *in vivo* safety evaluation of the drug combination was conducted by injecting the treatment in the brain resection cavity as follows: resection group (*n*=5); resection and unloaded PEG-DMA hydrogel implanted group (*n*=5); resection, PTX PLGA-NPs and TMZ coloaded PEG-DMA hydrogel implanted group (*n*=5). The doses of PTX and TMZ administered were 0.3 mg/kg and 0.6 mg/kg, respectively. After 1 month, brains were cryosectioned using a Leica 1950 cryostat into 15 µm thick slices. Hematoxylin and eosin (H&E) and Iba-1 immunohistochemistry were performed as previously described [9, 15]. Slides were scanned using an SCN400 Leica slide scanner, and image analysis was performed on a selected zone with Digital Image Hub (Leica).

II.4.4 Immunostaining of tumor-bearing and tumor-resected brains

All the treatments were tested on the U87MG orthotopic model described in section 2.4.1. After tumor injection, the tumor-bearing brains (days 13 and 36) and the tumor-resected brains (day 13) were sectioned with a Leica CM 1950 cryostat into 15 µm thick slices and stored at -20 °C until use. The positive controls were the sections of brain with tumors on day 36. As described previously [14, 21], the day 13 tumor-bearing brains were evaluated by immunostaining with anti-human mitochondria antibody and anti-glial fibrillary acidic protein (GFAP) antibody (Thermo Fisher). After tumor resection, proliferative tumor cells were detected using an anti-Ki67 monoclonal antibody (Thermo Fisher). The nucleus was counterstained with hematoxylin. The brain digital images were acquired using an EVOS fluorescence microscope (Evos, USA) and Digital Image Hub (*n*=3).

II.4.5 In vivo antitumor efficacy of PTX PLGA-NPs/TMZ coloaded PEG-DMA hydrogels on the orthotopic U87MG tumor resection model

Tumor resection was performed using the biopsy punch resection model described in section 2.4.1. The *in vivo* antitumor efficacy of the drug combination was determined on day 13 post tumor injection by administration of the following treatments in the tumor resection cavity: untreated group (n=7); resection and untreated group (n=8); resection and PTX PLGA-NP-loaded PEG-DMA hydrogel treated group (n=6); resection and TMZ-loaded PEG-DMA hydrogel treated group (n=6); resection and PTX PLGA-NPs and TMZ coloaded PEG-DMA hydrogel treated group (n=9). The doses of PTX and TMZ were 0.3 mg/kg and 0.6 mg/kg, respectively. Mice were sacrificed when they presented a 20% body weight loss or 10% body weight loss associated with clinical signs of distress (paralysis, arched back, or apathy). The rest of the mice were sacrificed 110 days after tumor implantation. The size and location of the tumors were determined by T2-weighed magnetic resonance imaging (MRI) using an 11.7 T Bruker BioSpec MRI system (Bruker, Germany) for all mice 12 days post tumor cell implantation and before being sacrificed as previously described [15].

II.5 STATISTICAL ANALYSIS

All the *in vitro* experiments were performed at least three times with three replicates each time (N=3, n=3). The results are expressed as the mean ± standard deviation (SD) or the mean ± standard error (SEM). Statistical analysis was performed using GraphPad Prism for paired t-test and ANOVA. *In vivo* Kaplan–Meier survival analysis was performed using log-rank test. The significance was set to probabilities of * p <0.05, ** p < 0.01, and *** p < 0.001 when compared with controls.

III. RESULTS AND DISCUSSION

III.1 *IN VITRO* CHARACTERIZATION OF THE PEG-DMA HYDROGEL

The resulting PTX PLGA-NPs were 190 ± 4 nm in size. Twenty-five percent PEG-DMA (v:v) was chosen to ensure hydrogel formation with a higher drug amount (Figure S1). To investigate the crosslinking kinetics and rheological properties of the hydrogels, rheological time-sweep tests were performed. Figure 2 shows the evolution of the storage modulus (G') and loss modulus (G") over the time course of gel formation when irradiated with 400 nm light. It was observed that only 15 s of light exposure can initiate the fast curing process. The total crosslinking time of the hydrogel is 66 s for the gel with or without nanoparticles. The final storage modulus G' (elastic behavior) of PEG-DMA/PLGA-NPs and PEG-DMA/water (195.3 ± 58.2 kPa and 107.3 ± 16.9 kPa, respectively) was significantly higher than that of the loss modulus G" (viscous behavior) (1.25 ± 0.14 kPa and 0.58 ± 0.03 kPa, respectively) ($p < 0.05$). This result indicates that elasticity dominates in all samples, which is a typical behavior of solid-like materials. The storage modulus is directly related to the extent of crosslinking; the higher the degree of crosslinking, the greater the storage modulus. Although the storage modulus of hydrogel is higher than the brain storage modulus (0.6 to 22.1 kPa) [22], the tolerability studies conducted at 1 week, 2 months and 4 months indicated that the gel did not increase microglia activation and apoptosis compared to the lesion after resection [14, 15], suggesting that the mechanical properties are acceptable. To avoid an increase in intracranial pressure, gel swelling must be avoided. No significant change was observed in hydrogel mass ($p > 0.05$) or gel volume after 24 h, indicating that the unloaded or drug coloaded PEG-DMA hydrogels had a low swelling capacity and that the volume of the pregel mixture remained the same as the final solid hydrogel.

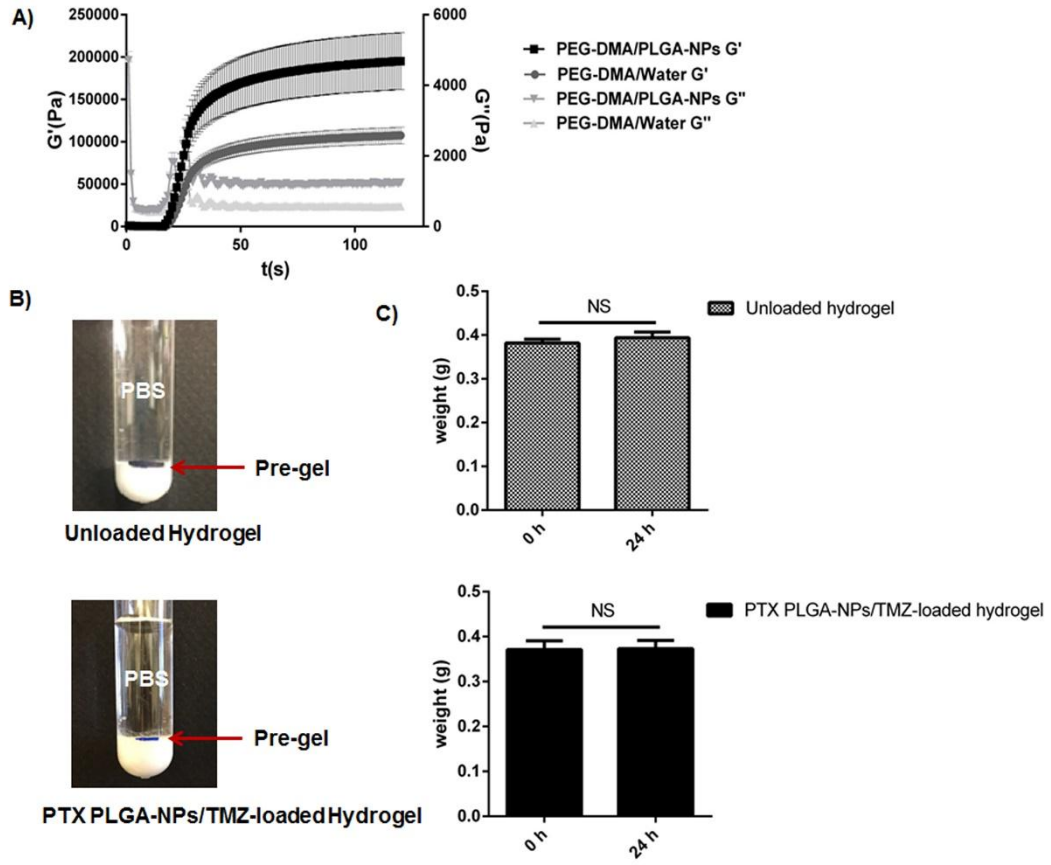

Figure 2: In vitro hydrogel characterizations. (A) Storage (G') and loss modulus (G") during photopolymerization were measured. Mean ± SEM, *n*=3. (B) After immersing in PBS for 24 h, the volume of unloaded or drug coloaded hydrogels remained same as compared with the pregel mixture. (C) The weights of hydrogel before and after immersing in PBS for 24 h were also measured. Mean ± SD, *n*=3.

III.2 *IN VITRO* CYTOTOXICITY OF TMZ ON U87MG CELLS

As the *in vitro* cytotoxicity effects of PTX were already performed in previous work [15], we focused only on the cytotoxicity of TMZ. The preliminary study was conducted with the MTT assay (Figure S2). An IC_{50} of TMZ (841 µg/mL) was obtained (Figure S2A). However, we found a dose-dependent interaction between TMZ and MTT (Figure S2B). Next, crystal violet was chosen because it is enzyme-independent and directly measures the DNA mass of adherent cells [23]. Crystal violet staining was performed after 48 h of incubation with TMZ. As shown in Figure S2C, the IC_{50} value of TMZ was 397 µg/mL. Some authors have previously evaluated the cytotoxic effects of TMZ on GBM cells, and the IC_{50} values varied between 1.4 µg/mL and 111 µg/mL [24-26]. However, the IC_{50} we obtained was higher than most of the reported values.

To find a better method to study TMZ cytotoxicity, a clonogenic assay was conducted. The resulting IC_{50} (2.4 µg/mL) dramatically decreased compared to that of crystal violet or MTT assays after incubation with lower TMZ concentrations (from 0.024 to 100 µg/mL in Figure 3A). This indicates that the sensitivity of U87MG cells to TMZ was more pronounced in the clonogenic

survival assay. For the following experiment, a clonogenic assay was chosen to investigate the combination effects of the two drugs.

III.3 *IN VITRO* COMBINATION EFFECTS OF PTX AND TMZ ON U87MG CELLS

Combination therapy with anti-cancer drugs can act synergistically, additionally or antagonistically against tumor cell growth depending on the ratios of the drugs that composing the combination [27]. Thus, to investigate the combination effects of PTX and TMZ at different ratios, cells were treated with different drug concentrations selected based on the IC_{50} values. In Figure 3B, the PTX and TMZ combination group showed significantly higher cytotoxicity than TMZ alone. Although not all combinations showed significant differences compared with PTX alone, there were fewer colonies formed after the treatment by drug combination than by PTX alone. A CDI <1, = 1 or >1 indicates that the drug combination has a synergistic, additive or antagonistic effect [18]. From Figure 3C, the combination of PTX and TMZ at all concentrations tested showed that PTX and TMZ had additive or synergistic effects. To confirm these results, the combination effect was also evaluated with the software CompuSyn [19]. The CI value obtained was comparable with the CDI value calculated above (data not shown). Due to the limited solubility of TMZ, the highest TMZ concentration was 4 mg/mL. To load as much PTX as possible while maintaining a synergistic effect, we chose a concentration ratio of 1:2 (PTX to TMZ) for the *in vivo* study.

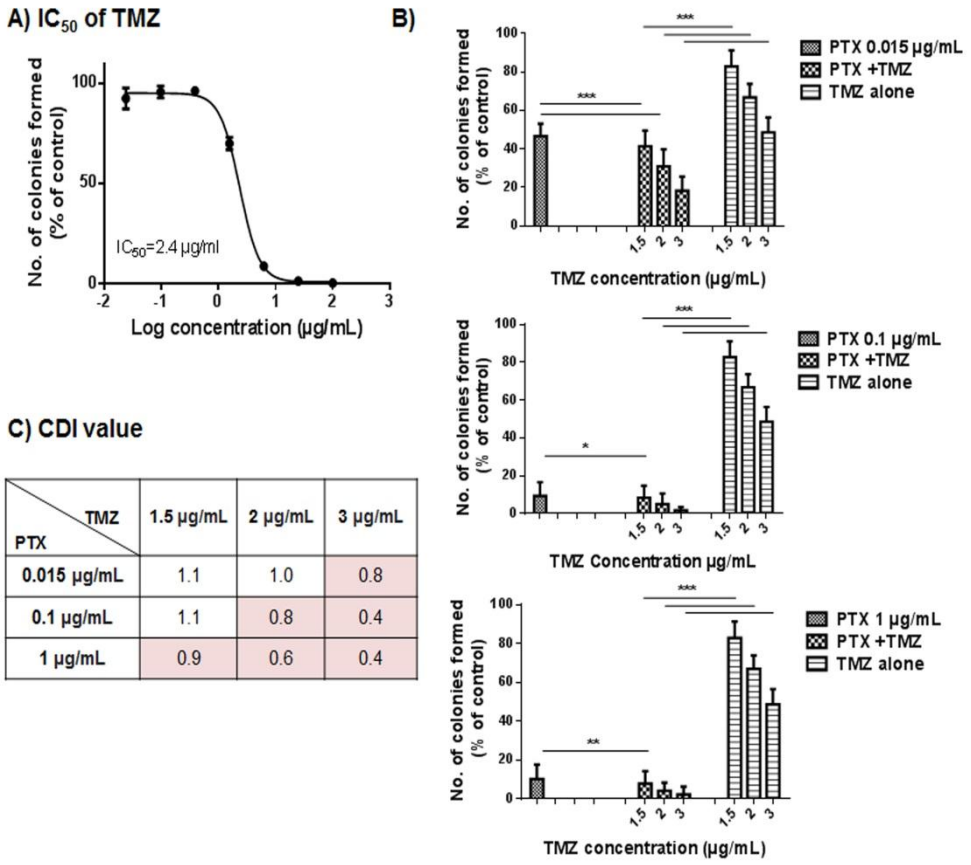

C) CDI value

PTX \ TMZ	1.5 µg/mL	2 µg/mL	3 µg/mL
0.015 µg/mL	1.1	1.0	0.8
0.1 µg/mL	1.1	0.8	0.4
1 µg/mL	0.9	0.6	0.4

Figure 3: The cytotoxic effect of TMZ (A) and the combination effect of PTX in PLGA-NPs and TMZ (B) were assessed by clonogenic assay. U87MG glioma cells were treated for 48 h with TMZ at different concentrations. Mean ± SEM, n=3, *$p < 0.05$, **$p < 0.01$, ***$p < 0.001$. Data are presented as the numbers of colony formation (untreated cells assumed as 100%). The CDI value was calculated to present the combination effect (C).

III.4 *IN VIVO MGMT* EXPRESSION AFTER TMZ TREATMENT

The critical lethal lesion O6-alkylguanines induced by TMZ is neutralized in GBM by the DNA repair protein MGMT [28]. Thus, *MGMT* mRNA expression was investigated to determine whether TMZ resistance occurred after exposition of the tumors to TMZ. The expression of *MGMT* gene varies depending on different cell lines [29, 30]. As shown in Figure 4, U-251 and U87MG are TMZ-sensitive cell lines, as almost no *MGMT* expression were detected, while T98G is a TMZ-resistant cell line. The semi-quantitative analysis using Image J software demonstrated that the *in vivo* treatment with the TMZ-loaded hydrogel did not up-regulate the *MGMT* mRNA expression as compared with the untreated resected tumors. Some research has indicated that the promoter region for the *MGMT* gene in U87MG cells is methylated; thus, *MGMT* expression is silenced [31]. This finding could explain why treatment with TMZ did not increase *MGMT* expression. It has been reported that the establishment of the U87 TMZ-resistant glioma cell lines required exposure to gradually increasing concentrations of TMZ in culture media for 6 months [32]. However, under our experimental conditions, most of the TMZ was released within 1 week,

and the drug release rate gradually decreased [14], suggesting that local treatment with the TMZ hydrogel would not induce drug resistance.

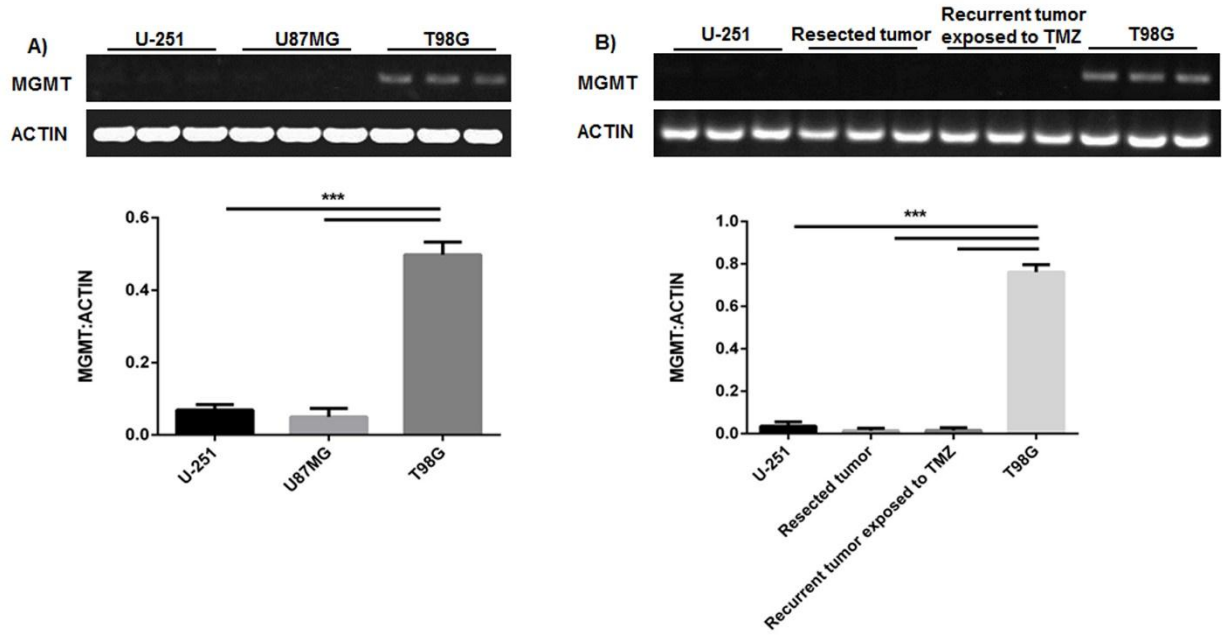

Figure 4: *MGMT* gene expression in U87MG cells (A), resected tumor without treatments in 3 mice brains and recurrent tumor exposed to TMZ in 3 mice brains (B) were investigated by RT-PCR. U-251 and T98G cell lines were the negative and positive controls, respectively. Each *MGMT* levels against actin were determined by image J software. Mean ± SD, n=3, ***$p < 0.001$.

III.5 *IN VIVO* LOCAL PTX DIFFUSION

To assess *in vivo* PTX diffusion from the hydrogel to the surrounding brain tissue, we administered an Oregon Green™ 488 conjugated PTX PLGA-NP-loaded PEG-DMA hydrogel into the mouse brain. As shown in Figure 5A and B, no visible green fluorescence was found within the surrounding brain tissue at 0 h and 24 h, indicating that PTX did not diffuse through the resection border. Oregon Green™ 488 PTX was observed both within and outside the hydrogel at 96 h and 10 days post administration (Figure 5C and D). In Figure 5E, the Oregon Green™ 488-conjugated PTX signal remained outside the hydrogel after 1 month. The drug diffusion was not uniform at every gel-brain border. A strong burst release of PTX adsorbing to the surface of NPs must be avoided because it reduces the sustained release. In our case, PTX slowly diffused through the hydrogel; thus, in contrast to *in vitro* studies that showed that after an initial burst release, 30% PTX was slowly released in a sustained manner over 1 week [15], almost no burst release was found 24 h post hydrogel injection. The sustained drug release lasts for at least 1 month, making this hydrogel a potential drug delivery system to fill in the 1 month wound-healing gap in the GBM standard treatment strategy [13].

The *in vivo* brain distribution of FITC-labeled PLGA-NPs within the hydrogel (Figure S3) showed that the NPs were entrapped inside the hydrogel after 24 h and did not diffuse away. This result occurred because the NPs are noncovalently immobilized in hydrogel. To support this hypothesis, the mesh size (nm) was calculated from the molecular weight between two crosslinking points and the swelling experiment [33]. The mesh size in our hydrogel is approximately 10 nm. This could explain why the PLGA nanoparticles (190 nm size) were not able to diffuse out of the hydrogel. Thus the *in vitro* release profile of the NPs was not studied.

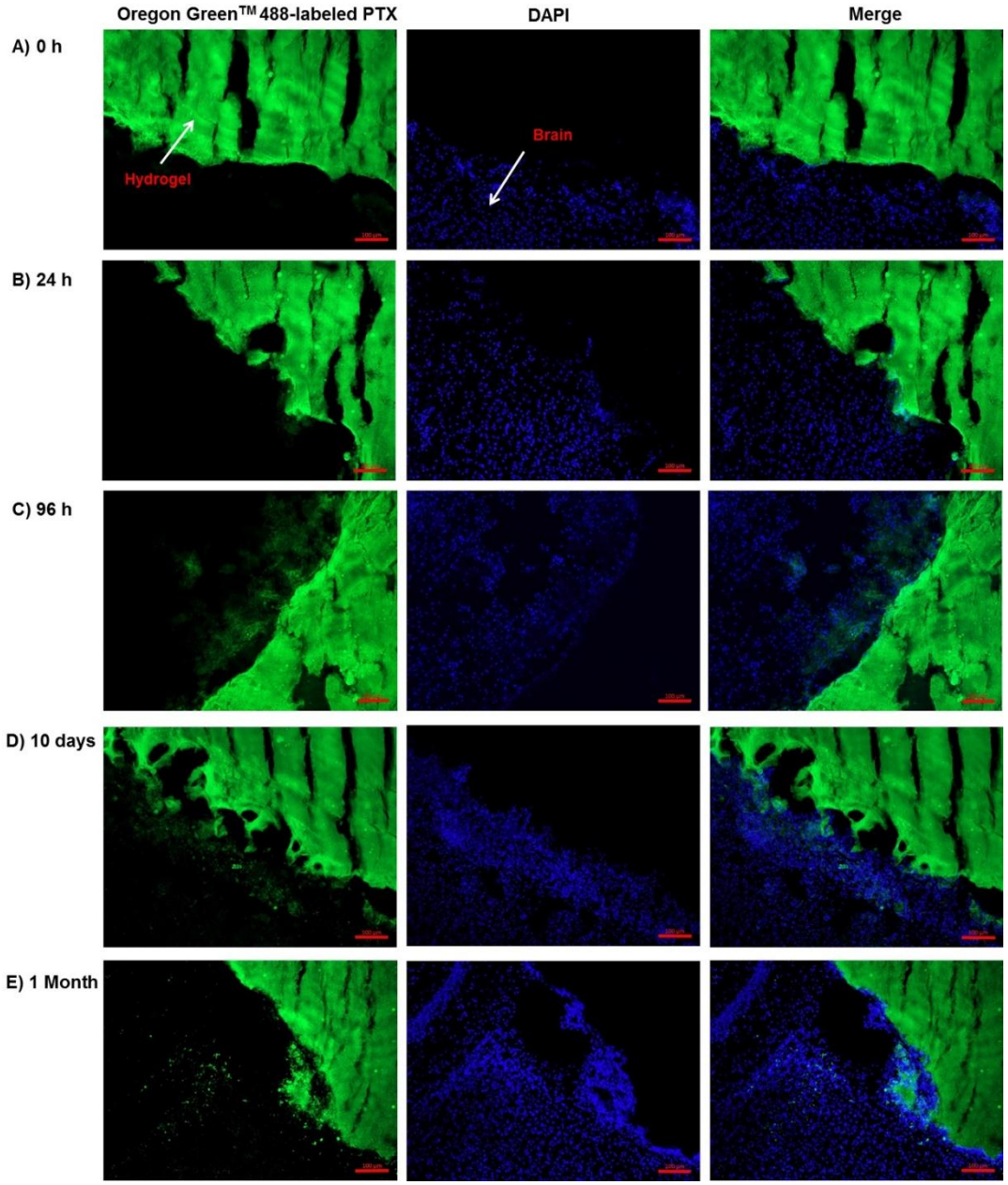

Figure 5: *In vivo* local PTX diffusion was conducted with Oregon Green™ 488-labeled PTX (green) PEG-DMA hydrogels containing PLGA-NPs in healthy mouse brains. The nuclei were stained with DAPI (blue). Scale bar = 100 μm (*n*=3-6).

III.6 *IN VIVO* SAFETY STUDY OF THE DRUG COMBINATION

The potential toxicity of the PTX PLGA-NPs/TMZ/PEG-DMA hydrogel was evaluated after 1 month of exposure via local administration to the healthy mouse brain at doses of 0.3 mg/kg and 0.6 mg/kg for PTX and TMZ, respectively. As shown in Figure S4, there was no significant difference in body weight and water and food consumption witnessed in the PTX PLGA-NPs/TMZ/PEG-DMA hydrogel group compared to the unloaded hydrogel or resection groups during this experiment. As shown in Figure 6, microglial activation was observed in all groups and could generate reactive oxygen species and release signals to recruit peripheral immune cells. Biopsy punch resection can cause positive staining of the microglia activation marker Iba-1 [15]. The hydrogel alone and the drug coloaded hydrogel did not increase the extent of microglial activation compared to the resected group. No inflammation was observed from the H&E staining of brain sections. In conclusion, hydrogels loaded with PTX and TMZ at doses of 0.3 mg/kg and 0.6 mg/kg, respectively, were tolerable for local administration in mouse brains.

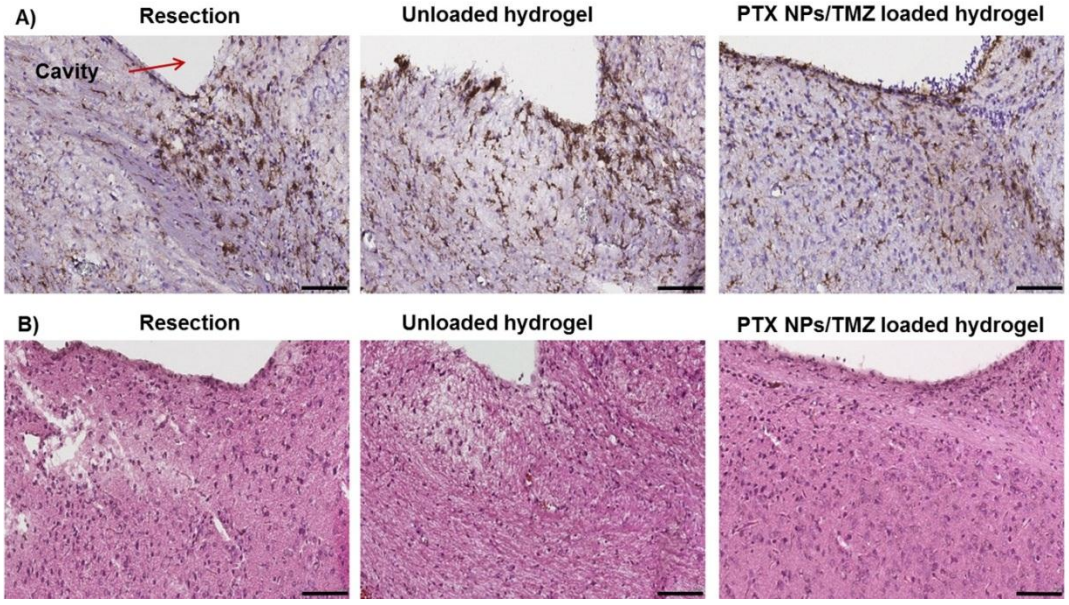

Figure 6: *In vivo* safety study of drug combination: evaluation of microglia activation by Iba1 staining (brown) (A) and brain structure by H&E staining (B) in the brain tissue 1 month after treatment with different groups (resection, resection + unloaded hydrogel and resection + PTX NPs/TMZ coloaded hydrogel). The doses of PTX and TMZ were 0.3 mg/kg and 0.6 mg/kg, respectively. Scale bar = 100 μm (n=3).

III.7 *IN VIVO* ANTITUMOR EFFICACY OF PTX PLGA-NPS/TMZ COLOADED PEG-DMA HYDROGELS ON AN ORTHOTOPIC U87MG TUMOR RESECTION MODEL.

Immunostaining with an anti-human mitochondria antibody to detect human U87MG and an anti-GFAP antibody to detect brain tissue were performed on day 13 in tumor-bearing mouse brains. An anti-Ki67 antibody was employed to detect proliferating tumor cells just after tumor resection. A day 36 tumor was the positive control. As shown in Figure 7A, the growth of human U87MG tumor cells could be identified by an anti-human mitochondria antibody (green). At the tumor-brain border, the tumor cells and brain tissues (red) were intertwined, and some tumor cells infiltrated into the brain parenchyma. Ki67-positive tumor cells (brown) were found in the main tumor mass of the day 36 tumor (Figure 7B) and in the resection border of the day 13 tumor (Figure 7C). Some infiltrative tumor cells were found far from the resection cavity after the removal of the tumor (Figure 7D). These infiltrative tumor cells are likely to induce tumor recurrence after biopsy punch resection. After implantation of the hydrogel for > 3 months, some cells can be observed at the interface between the hydrogel and the cavity border but none inside the hydrogel (Figure 7E).

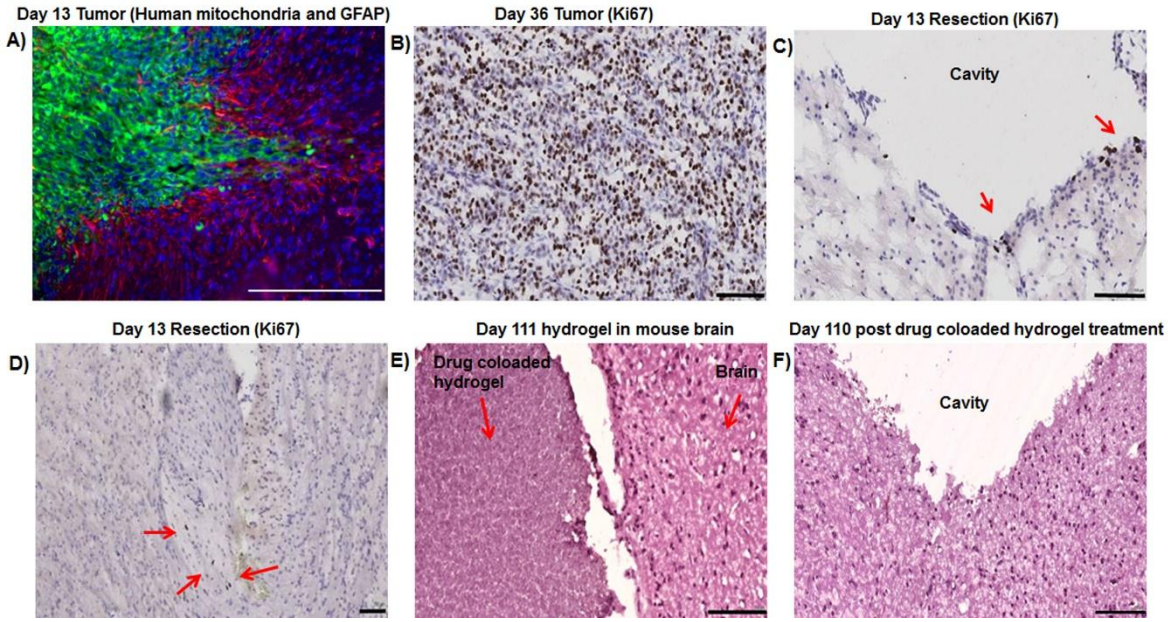

Figure 7: (A) Anti-GFAP (red) with anti-human mitochondria staining (green) shows normal brain parenchyma and the day 13 tumor mass. Scale bar = 200 µm. (B-D) Anti-Ki67 staining (brown) with hematoxylin (blue) counterstaining shows the tumor cells in a day 36 recurrent tumor mass without resection (B) and day 13 tumor resection cavities in 2 different mice brains (C and D). *n*=3. (E-F) H&E staining of 2 mice brains shows no infiltrative cells inside the drug coloaded hydrogel (E) and no tumor recurrence after treatment with drug coloaded hydrogel (F) on day 111 and 110 post tumor inoculation. Scale bar = 100 µm.

To evaluate the antitumor efficacy of the PTX PLGA-NPs/TMZ coloaded hydrogel and its capacity to reduce tumor recurrence, treatments were intraoperatively injected into the resection cavity. As shown in Figure 8A, we checked that all mice developed a tumor that was

well-demarcated and visible by MRI imaging on day 12 post tumor cell injection. The hydrogel remained in place during the entire course of the experiment (Figure 8B). The ester groups in PEG-DMA are susceptible to be degradable slowly *in vivo* [34, 35]. The PLGA is also degradable via hydrolysis over months [36]. As no inflammation or cell death was observed (Fig 7E and F), the remaining of the hydrogel in the cavity for >3 months was not an issue.

As shown in Figure 8C and 8D, injection of single drug treatment with PTX PLGA-NPs or TMZ-loaded hydrogels in the resection cavity significantly prolonged the median survival time of mice compared to that of the resected mice ($p < 0.05$ and $p < 0.01$, respectively). The combination treatment showed significantly higher survival compared to the other groups ($p < 0.001$), with an undefined median survival. Only 2 out of 9 mice had tumor recurrence within 110 days after injection of the tumor cells. The rest of the mice showed no sign of tumor recurrence by MRI imaging (Figure S5) and H&E staining of the brain tissues (e.g. Figure 7F). Among the 7 surviving mice, 2 brains showed edema around the resection cavity, which did not influence the behavior of the mice. These data suggest that the PTX and TMZ could diffuse from the hydrogel to avoid most of the recurrences.

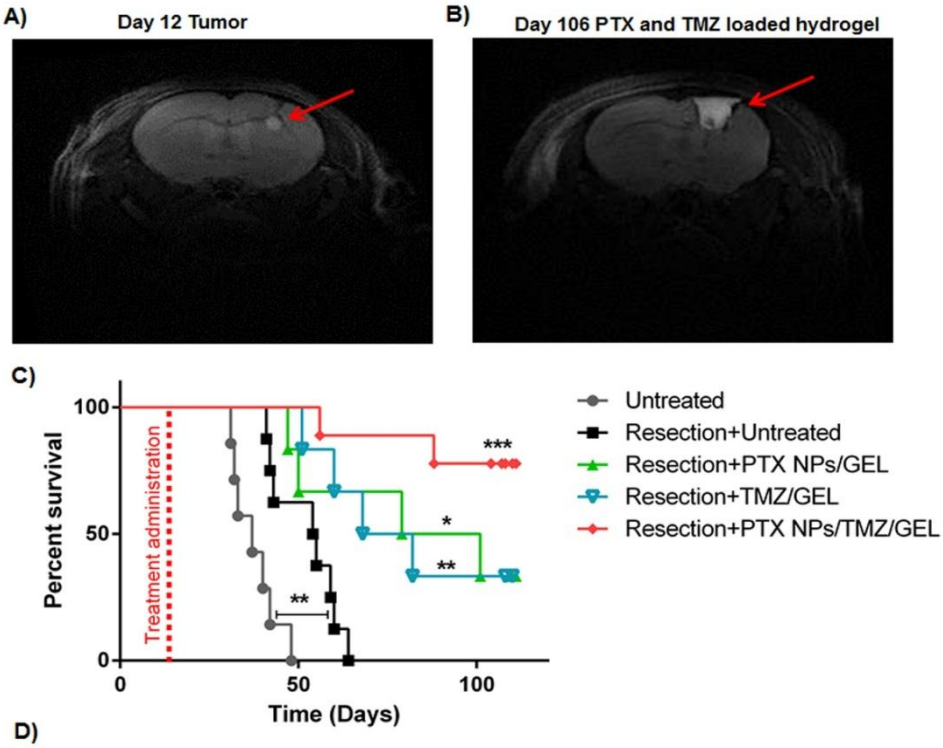

D)

Treatment	*n*	Median survival (days)	Log-rank test
Untreated	7	37	
Resection + untreated	8	54.5	** (*vs* untreated)
Resection + PTX NPs/Hydrogel	6	90	* (*vs* Resection + untreated)
Resection + TMZ/Hydrogel	6	75	** (*vs* Resection + untreated)
Resection + PTX NPs/TMZ/Hydrogel	9	Undefined	*** (*vs* Resection + untreated)

Figure 8: Axial (T2-weighted) images of a mouse brain: tumor before resection (day 12 post U87MG tumor inoculation) (A) and the same brain treated with drug coloaded PEG-DMA hydrogel on day 106 post tumor inoculation (B). Kaplan-Meier survival curves (C) and median survival (D) for animals treated with different therapies in the resection cavity. n=6-9, *$p < 0.05$, **$p < 0.01$, ***$p < 0.001$.

It is well-known that the combination of chemotherapeutic drugs with different mechanisms of action may contribute to better antitumor effects. Here, PTX and TMZ have different mechanisms of action, resistance and established efficacy in glioma cells [37-39]; thus, the expected survival enhancement was observed in our results. In addition, clinical trials have demonstrated that the combination of PTX or docetaxel with TMZ has a synergistic effect in metastatic melanoma [40-42], making this combination a reasonable option for GBM treatment. The synergistic effect of PTX and TMZ on GBM cell lines has been investigated *in vitro* [38, 39, 43], but barely studied in the form of a local combination therapy in orthotopic models. Robert Clark equations were used to calculate *in vivo* synergism based on the median survival [44]. However, as the median survival of combination treatment was undefined due to the long-term survivors, we were not able to measure

the *in vivo* synergism with our current data. In one study, the PEG-dipalmitoylphosphatidyle-thanoiamine calcium phosphate nanoparticle-based injectable thermo-responsive hydrogel was developed to sustain the local delivery of PTX and TMZ for only 3 days [45]. Although this thermo-responsive hydrogel induced significant therapeutic efficacy, all of the treatment groups had tumor recurrences and no animal survived for long-term. Our findings indicate that the combination group showed most significantly survival benefits in the U87MG tumor resection model and highlight the local combination option of PTX and TMZ as a promising strategy for GBM therapy.

IV. CONCLUSIONS

In conclusion, to address the unmet medical need for the treatment of recurrent GBM after surgery, we developed a local combination treatment strategy with PTX and TMZ based on the photopolymerizable PEG-DMA hydrogel. We demonstrated the synergistic effect of PTX and TMZ on U87MG cells by clonogenic assay. We also confirmed that TMZ treatment did not up-regulate MGMT expression in U87MG tumor-bearing mice. PTX release was sustained *in vivo* and diffused from the hydrogel to the surrounding brain tissue for at least 1 month. The local combination of PTX with TMZ was safe, effective and synergistic in the treatment of the U87MG orthotopic model. Although combination therapy protocols are becoming an integrated part of cancer treatment, rational and efficient combination therapy to improve the treatment of GBM remains limiting. We showed that a rational combination of drugs and their postsurgical delivery in the resection cavity of GBM led to long-term survivors in mice. Future preclinical studies may take advantage of the potential benefits of this local combination treatment strategy. Clinical studies may also take PTX and TMZ into consideration as potential drug combination options.

V. SUPPLEMENTARY MATERIALS

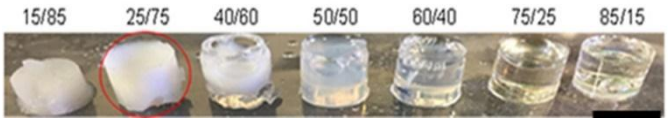

Figure S1: Formation of hydrogels with different ratios of PEG-DMA: TMZ (v:v). Scale bar=0.65 cm.

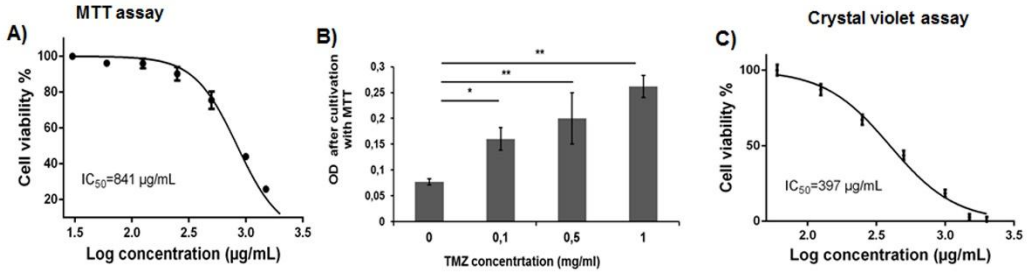

Figure S2: *In vitro* cytotoxicity study by MTT (A) and crystal violet assay (C). U87MG glioma cells were treated for 48 h with increasing TMZ concentrations and IC_{50} were determined as described previously [9, 15]. Data are presented as the percent cell survival (untreated cells assumed as 100%). Mean ± SEM, n=6. (B) The interaction of MTT with TMZ was also investigated. Mean ± SD, n=6. *$p < 0.05$, **$p < 0.01$.

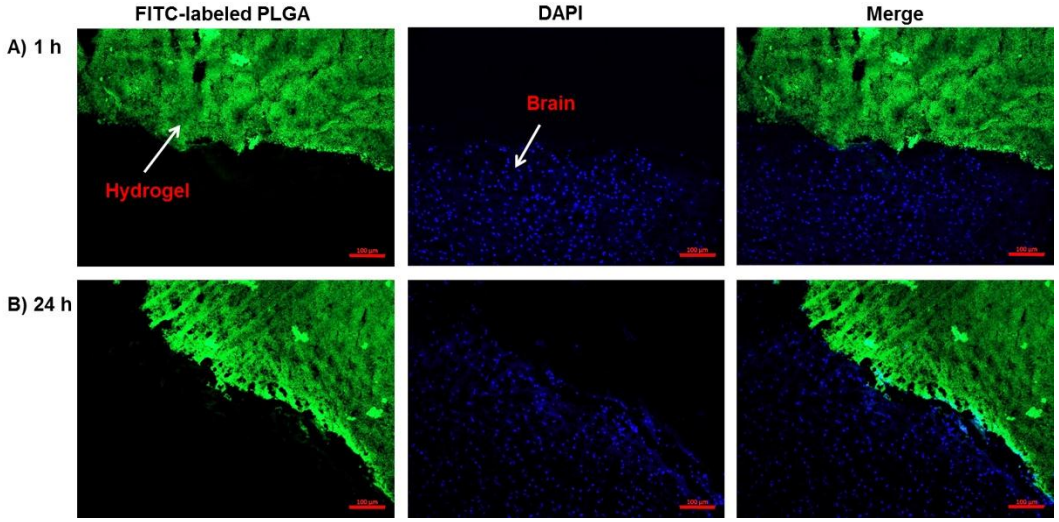

Figure S3: In vivo local PLGA-NP distribution was conducted with FITC-labeled PLGA (green) in PEG-DMA hydrogel in healthy mice brains. The nuclei were stained with DAPI (blue). Scale bar = 100 µm (n=3).

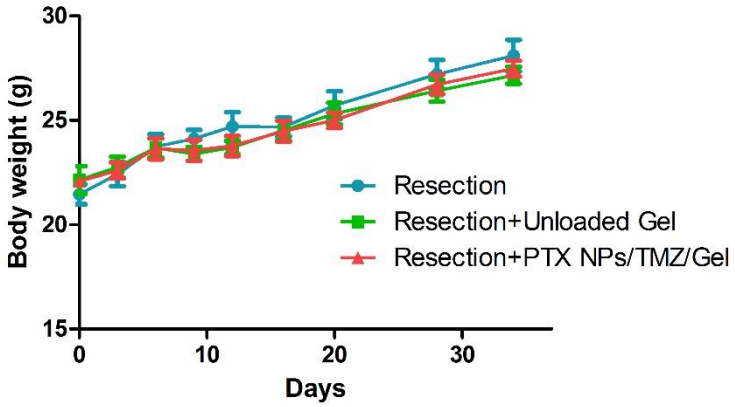

Figure S4: *In vivo* safety study of combination treatment: body weight of healthy mice after resection, resection + unloaded hydrogel and resection + drug combination coloaded hydrogel Mean ± SEM, n=5.

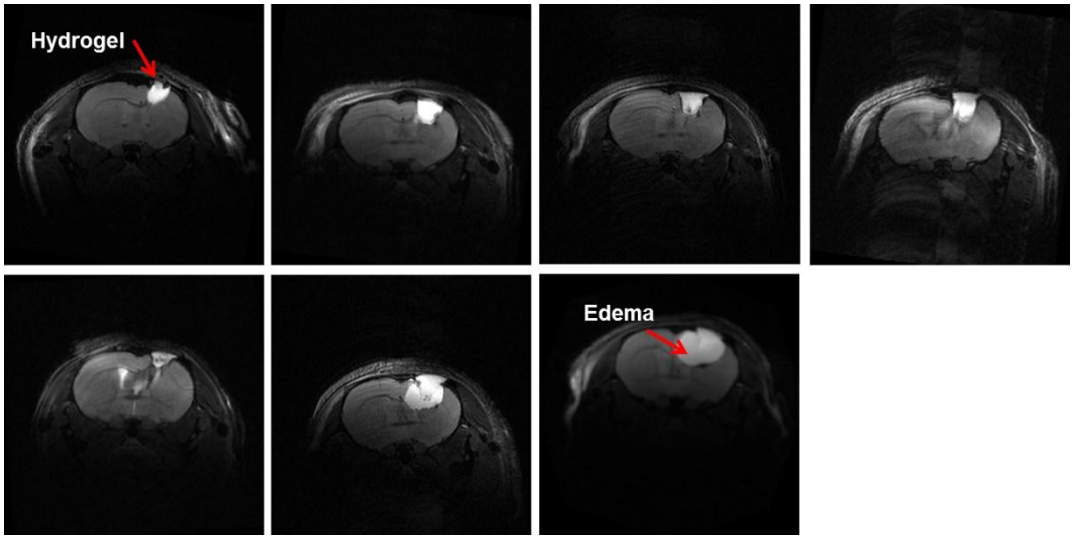

Figure S5: Axial (T2-weighted) images of 7 surviving mice brains treated with PTX PLGA-NPs/TMZ coloaded PEG-DMA hydrogel (day 105-110 post U87MG tumor inoculation). No signs of a tumor were observed.

VI. REFERENCES

1. Davis ME. Glioblastoma: overview of disease and treatment. Clinical Journal of Oncology Nursing. 2016; 20: S2.
2. Stupp R, Mason WP, van den Bent MJ, Weller M, Fisher B, Taphoorn MJB, et al. Radiotherapy plus concomitant and adjuvant temozolomide for glioblastoma. New England Journal of Medicine. 2005; 352: 987-96.
3. Ashby LS, Smith KA, Stea B. Gliadel wafer implantation combined with standard radiotherapy and concurrent followed by adjuvant temozolomide for treatment of newly diagnosed high-grade glioma: a systematic literature review. World Journal of Surgical Oncology. 2016; 14: 225.
4. Stupp R, Taillibert S, Kanner AA, Kesari S, Steinberg DM, Toms SA, et al. Maintenance therapy with tumor-treating fields plus temozolomide vs temozolomide alone for glioblastoma: a randomized clinical trial. JAMA. 2015; 314: 2535-43.
5. Stupp R, Hegi ME, Mason WP, van den Bent MJ, Taphoorn MJ, Janzer RC, et al. Effects of radiotherapy with concomitant and adjuvant temozolomide versus radiotherapy alone on survival in glioblastoma in a randomised phase III study: 5-year analysis of the EORTC-NCIC trial. The Lancet Oncology. 2009; 10: 459-66.
6. Newlands ES, Blackledge GRP, Slack JA, Rustin GJ, Smith DB, Stuart NS, et al. Phase I trial of temozolomide (CCRG 81045: M&B 39831: NSC 362856). British journal of cancer. 1992; 65: 287-91.
7. Azzabi A, Hughes AN, Calvert PM, Plummer ER, Todd R, Griffin MJ, et al. Phase I study of temozolomide plus paclitaxel in patients with advanced malignant melanoma and associated in vitro investigations. British journal of cancer. 2005; 92: 1006-12.
8. Ganipineni LP, Danhier F, Preat V. Drug delivery challenges and future of chemotherapeutic nanomedicine for glioblastoma treatment. Journal of Controlled Release. 2018; 281: 42-57.
9. Bastiancich C, Bianco J, Vanvarenberg K, Ucakar B, Joudiou N, Gallez B, et al. Injectable nanomedicine hydrogel for local chemotherapy of glioblastoma after surgical resection. Journal of Controlled Release. 2017; 264: 45-54.
10. Chakroun RW, Zhang P, Lin R, Schiapparelli P, Quinones-Hinojosa A, Cui H. Nanotherapeutic systems for local treatment of brain tumors. Wiley Interdiscip Rev Nanomed Nanobiotechnol. 2018; 10: e1479.
11. Mu F, Lucas JT, Watts JM, Johnson AJ, Bourland JD, Laxton AW, et al. Tumor resection with carmustine wafer placement as salvage therapy after local failure of radiosurgery for brain metastasis. Journal of Clinical Neuroscience. 2015; 22: 561-5.
12. Lin SH, Kleinberg LR. Carmustine wafers: localized delivery of chemotherapeutic agents in CNS malignancies. Expert Review of Anticancer Therapy. 2008; 8: 343-59.
13. Bastiancich C, Danhier P, Préat V, Danhier F. Anticancer drug-loaded hydrogels as drug delivery systems for the local treatment of glioblastoma. Journal of Controlled Release. 2016; 243: 29-42.
14. Fourniols T, Randolph LD, Staub A, Vanvarenberg K, Leprince JG, Préat V, et al. Temozolomide-loaded photopolymerizable PEG-DMA-based hydrogel for the treatment of glioblastoma. Journal of Controlled Release. 2015; 210: 95-104.
15. Zhao M, Danhier F, Bastiancich C, Joudiou N, Ganipineni LP, Tsakiris N, et al. Post-resection treatment of glioblastoma with an injectable nanomedicine-loaded photopolymerizable hydrogel induces long-term survival. International Journal of Pharmaceutics. 2018; 548: 522-9.
16. Wauthoz N, Deleuze P, Hecq J, Roland I, Saussez S, Adanja I, et al. In vivo assessment of temozolomide local delivery for lung cancer inhalation therapy. European Journal of Pharmaceutical Sciences. 2010; 39: 402-11.

17. Franken NA, Rodermond HM, Stap J, Haveman J, Van Bree C. Clonogenic assay of cells in vitro. Nature protocols. 2006; 1: 2315.
18. Zhao Y, Gao J-L, Ji J-W, Gao M, Yin Q-S, Qiu Q-L, et al. Cytotoxicity enhancement in MDA-MB-231 cells by the combination treatment of tetrahydropalmatine and berberine derived from Corydalis yanhusuo W. T. Wang. Journal of Intercultural Ethnopharmacology. 2014; 3: 68-72.
19. Chou T-C. Drug combination studies and their synergy quantification using the Chou-Talalay method. Cancer Research. 2010: 0008-5472. CAN-09-1947.
20. Clark PA, Gaal JT, Strebe JK, Pasch CA, Deming DA, Kuo JS, et al. The effects of tumor treating fields and temozolomide in MGMT expressing and non-expressing patient-derived glioblastoma cells. Journal of Clinical Neuroscience. 2017; 36: 120-4.
21. Bianco J, Bastiancich C, Joudiou N, Gallez B, des Rieux A, Danhier F. Novel model of orthotopic U-87 MG glioblastoma resection in athymic nude mice. Journal of Neuroscience Methods. 2017; 284: 96-102.
22. Donnelly B, Medige J. Shear properties of human brain tissue. Journal of Biomechanical Engineering. 1997; 119: 423-32.
23. Śliwka L, Wiktorska K, Suchocki P, Milczarek M, Mielczarek S, Lubelska K, et al. The comparison of MTT and CVS assays for the assessment of anticancer agent interactions. PloS one. 2016; 11: e0155772.
24. Banelli B, Daga A, Forlani A, Allemanni G, Marubbi D, Pistillo MP, et al. Small molecules targeting histone demethylase genes (KDMs) inhibit growth of temozolomide-resistant glioblastoma cells. Oncotarget. 2017; 8: 34896-910.
25. Hermisson M, Klumpp A, Wick W, Wischhusen J, Nagel G, Roos W, et al. O6 - methylguanine DNA methyltransferase and p53 status predict temozolomide sensitivity in human malignant glioma cells. Journal of Neurochemistry. 2006; 96: 766-76.
26. Ryu CH, Yoon WS, Park KY, Kim SM, Lim JY, Woo JS, et al. Valproic acid downregulates the expression of MGMT and sensitizes temozolomide-resistant glioma cells. BioMed Research International. 2012; 2012.
27. Mayer LD, Harasym TO, Tardi PG, Harasym NL, Shew CR, Johnstone SA, et al. Ratiometric dosing of anticancer drug combinations: controlling drug ratios after systemic administration regulates therapeutic activity in tumor-bearing mice. Molecular Cancer Therapeutics. 2006; 5: 1854-63.
28. Weller M, Stupp R, Reifenberger G, Brandes AA, Van Den Bent MJ, Wick W, et al. MGMT promoter methylation in malignant gliomas: ready for personalized medicine? Nature Reviews: Neurology. 2010; 6: 39.
29. Choi EJ, Cho BJ, Lee DJ, Hwang YH, Chun SH, Kim HH, et al. Enhanced cytotoxic effect of radiation and temozolomide in malignant glioma cells: targeting PI3K-AKT-mTOR signaling, HSP90 and histone deacetylases. BMC Cancer. 2014; 14: 17.
30. Lan F, Yang Y, Han J, Wu Q, Yu H, Yue X. Sulforaphane reverses chemo-resistance to temozolomide in glioblastoma cells by NF-κB-dependent pathway downregulating MGMT expression. International Journal of Oncology. 2016; 48: 559-68.
31. Gao Y, Chen X, Liu H. Up-regulation of miR-370-3p restores glioblastoma multiforme sensitivity to temozolomide by influencing MGMT expression. Scientific reports. 2016; 6: 32972.
32. Zhu D, Tu M, Zeng B, Cai L, Zheng W, Su Z, et al. Up-regulation of miR-497 confers resistance to temozolomide in human glioma cells by targeting mTOR/Bcl-2. Cancer medicine. 2017; 6: 452-62.
33. Hwang JW, Noh SM, Kim B, Jung HW. Gelation and crosslinking characteristics of photopolymerized poly (ethylene glycol) hydrogels. Journal of Applied Polymer Science. 2015; 132.

34. Tan H, Marra KG. Injectable, biodegradable hydrogels for tissue engineering applications. Materials. 2010; 3: 1746-67.
35. Nicodemus GD, Bryant SJ. Cell encapsulation in biodegradable hydrogels for tissue engineering applications. Tissue Engineering Part B: Reviews. 2008; 14: 149-65.
36. Makadia HK, Siegel SJ. Poly lactic-co-glycolic acid (PLGA) as biodegradable controlled drug delivery carrier. Polymers. 2011; 3: 1377-97.
37. Vellimana AK, Recinos VR, Hwang L, Fowers KD, Li KW, Zhang Y, et al. Combination of paclitaxel thermal gel depot with temozolomide and radiotherapy significantly prolongs survival in an experimental rodent glioma model. Journal of Neuro-Oncology. 2013; 111: 229-36.
38. Ni S, Fan X, Wang J, Qi H, Li X. Biodegradable implants efficiently deliver combination of paclitaxel and temozolomide to glioma C6 cancer cells in vitro. Annals of Biomedical Engineering. 2014; 42: 214-21.
39. Xu Y, Shen M, Sun Y, Gao P, Duan Y. Nano composite thermo-sensitive gel for paclitaxel and temozolomide co-delivery to glioblastoma cells. Journal of Nanoscience and Nanotechnology. 2016; 16: 12288-98.
40. Yoon C, Papadopoulos NE, Camacho LH, McIntyre S, Alvarado GC, Bedikian AY, et al. The clinical efficacy of combination of docetaxel and temozolomide in previously treated patients with stage IV melanoma. Melanoma research. 2010; 20: 43-7.
41. Azzabi A, Hughes A, Calvert P, Plummer E, Todd R, Griffin M, et al. Phase I study of temozolomide plus paclitaxel in patients with advanced malignant melanoma and associated in vitro investigations. British Journal of Cancer. 2005; 92: 1006.
42. Bafaloukos D, Gogas H, Georgoulias V, Briassoulis E, Fountzilas G, Samantas E, et al. Temozolomide in combination with docetaxel in patients with advanced melanoma: a phase II study of the Hellenic Cooperative Oncology Group. Journal of Clinical Oncology. 2002; 20: 420-5.
43. Xu Y, Shen M, Li Y, Sun Y, Teng Y, Wang Y, et al. The synergic antitumor effects of paclitaxel and temozolomide co-loaded in mPEG-PLGA nanoparticles on glioblastoma cells. Oncotarget. 2016; 7: 20890-901.
44. Van Woensel M, Mathivet T, Wauthoz N, Rosière R, Garg AD, Agostinis P, et al. Sensitization of glioblastoma tumor micro-environment to chemo-and immunotherapy by Galectin-1 intranasal knock-down strategy. Scientific reports. 2017; 7: 1217.
45. Ding L, Wang Q, Shen M, Sun Y, Zhang X, Huang C, et al. Thermoresponsive nanocomposite gel for local drug delivery to suppress the growth of glioma by inducing autophagy. Autophagy. 2017; 13: 1176-90.

CHAPTER V
COMBINATION OF PACLITAXEL PHOTOPOLYMERIZABLE HYDROGEL AND ORAL TEMOZOLOMIDE FOR THE TREATMENT OF GLIOBLASTOMA

Mengnan Zhao, Elia Bozzato, Nicolas Joudiou, Yining Xu, Fabienne Danhier, Bernard Gallez, Véronique Préat

TABLE OF CONTENTS

ABSTRACT

To mimic the current standard of care, we investigated the combination effect of paclitaxel (PTX)-loaded PEG-DMA hydrogel in combination with oral delivery of temzolomide (TMZ). *In vivo* safety study was conducted with on healthy nude mice brains. *In vivo* efficacy study showed that as compared with single drug treatment, more long-term survivors were obtained after combination treatment, illustrating the potential advantages of this combination treatment strategy.

I. INTRODUCTION

Current gold standard treatments of glioblastoma (GBM) patients include massive safe surgical resection followed by radiotherapy and concurrent temozolomide (TMZ), with 6 maintenance cycles of oral TMZ administration. Postoperative radiotherapy begins several weeks after surgical removal of the tumor. This gap is due to the fact that radiotherapy may induce problematic wound healing. Poor wound healing may lead to chronic ulceration, pain, secondary infection and psychological distress [1]. During this time, the residual infiltrative tumor cells are free of treatments and keep proliferating. The local delivery of paclitaxel (PTX)-loaded PEG-DMA hydrogel containing PLGA nanoparticles (PLGA-NPs), that sustain PTX release for at least 1 month, is highly promising to fill this gap.

TMZ is able to cross the blood brain barriers and undergo spontaneous conversion to its active form MTIC under physiological conditions without the requirement for enzymatic conversion. The approved conventional schedule of TMZ delivery for GBM treatment is a daily dose of 150 to 200 mg per square meter of body-surface area for 5 days of every 28-day cycle [2].

To mimic the current standard of care, the oral TMZ dose for mice was converted from the dose for patients from 1 cycle of oral TMZ using equivalent surface area dosage conversion factor and km factor. The *in vivo* safety study of combination treatments was conducted in mice brains. The *in vivo* antitumor efficacy of PTX-loaded PEG-DMA hydrogel in combination with oral TMZ was investigated in U87MG orthotopic tumor resection mice model.

II. MATERIALS AND METHODS

II.1 PREPARATION OF PTX LOADED HYDROGELS

PTX PLGA-NPs were formulated using an emulsion-evaporation method as previously described [3]. 75% (v:v) PTX PLGA-NPs were added to 25% PEG-DMA (average Mn = 550 g/mol) (Sigma-Aldrich) with Lucirin TPO® (BASF, USA) as a photoinitiator [3]. Then, the injectable pregel mixture was photopolymerized under 400 nm light. Single drug-loaded PEG-DMA hydrogels were also prepared by adding single drug formulations to the pregel mixture.

II.2 *IN VIVO* STUDIES

All the experiments were performed following the Belgian national regulation guidelines in accordance with EU Directive 2010/63/EU and were approved by the ethical committee for animal care of the Université catholique de Louvain medicine faculty (2014/UCL/MD/004). Animals had free access to water and food, and the body weights were monitored daily throughout the experiments.

II.2.1 Orthotopic U87MG human GBM tumor resection model

Six-week-old NMRI female nude mice (Janvier, France) were anesthetized by intraperitoneal injection of ketamine/xylazine (100 and 13 mg/kg, respectively) and positioned on a stereotactic frame as previously described [4]. A five-microliter Hamilton syringe with a 26 G needle was used to inject up to 3 μL of complete culture medium containing 3×10^4 U87MG glioma cells into the right frontal lobe. The injection site was 0.5 mm anterior, 2.1 mm lateral from the bregma and 2.5 mm deep from the cranium. After 13 days, the cranium was opened again, and a 2 mm diameter biopsy punch (Kai Medical, Germany) was inserted 3 mm deep and twisted for 15 s to cut the tumor tissues. Then, the tumor tissues were aspirated using a diaphragm vacuum pump. Five microliters of hydrogel was photopolymerized into the resection cavity before closing the cranial window with a 4 mm × 4 mm Neuro-Patch® (Aesculap, Germany) saturated with a reconstituted fibrin glue (Baxter Innovations, Austria).

II.2.2 In vivo safety study of the combination treatment

Six-week-old healthy female NMRI nude mice (Janvier) were anesthetized intraperitoneally. Normal brain resections (without tumor implantation) were performed using the biopsy punch resection model as described in II.2.1. The unloaded and PTX PLGA-NP-loaded PEG-DMA hydrogel was polymerized as described in Chapter IV. DMSO was used to re-suspend TMZ with a concentration of 100 mg/mL. The stock solution was sonicated with 10% amplitude for 5s and diluted in sterilized water at 10 mg/mL [5].

Due to the incision suture, the oral TMZ (60 mg/kg/day) was given at day 5-9 post hydrogel implantation (n=5). The current dose was calculated from 1 cycle of the standard treatment for patients: the oral TMZ administration is given 6 maintenance cycles with 150-200 mg/m^2/day for 5 days of a 28 days/cycle. The Km factor of 37 for adult human was used to convert the mg/m^2 dose to the mg/kg dose, resulting in 5.4 mg/kg/day for human. Then to convert this dose in human to that in mice, the equivalent surface area dosage conversion factors (12 from human to mouse) was used [6, 7], resulting in 64.8 mg/kg/day for mice. Thus TMZ was administered at 60 mg/kg/day.

The *in vivo* safety evaluation of the drug combination was conducted as follows: resection group (n=5); resection and unloaded PEG-DMA hydrogel group (n=5); resection, PTX PLGA-NP-loaded PEG-DMA hydrogel and oral TMZ group (n=5). From the previous *in vivo* efficacy study on PTX loaded-PEG-DMA hydrogel with the maximum PTX dose of 0.525 mg/kg, more than 50% of mice survived for at least 150 days (Chapter III). In order to see the possible combination benefits, PTX was administered at 0.3 mg/kg. One month after the treatments, mice were sacrificed and brains were cryosectioned into 15 µm thick slices. Hematoxylin and eosin (H&E) and Iba-1 immunohistochemistry were performed as previously described [3, 8].

II.2.3 In vivo antitumor efficacy of the combination treatment

Tumor resection was performed using the U87MG biopsy punch resection model described in section II.2.1. To prepare a TMZ solution without DMSO, same amounts of TMZ and L-histidine (w:w) were mixed to obtain a 4 mg/mL solution (maximum TMZ solubility by adding histidine) [9]. The *in vivo* antitumor efficacy study was conducted by administration of the following treatments: untreated group (n=7); resection and untreated group (n=8); resection and PTX PLGA-NP-loaded PEG-DMA hydrogel treated group (n=6); resection and oral TMZ treated group (n=8); resection and PTX PLGA-NP-loaded PEG-DMA hydrogel and oral TMZ treated group (n=7). In order to see the advantages of the combination treatments, PTX was administered with a reduced dose of 0.3 mg/kg [3]. Due to the high dose-related toxicity in *in vivo* safety study (discussed in 3.1), TMZ was given at 20 mg/kg/day from day 10 to 14 post hydrogel implantation.

The choice of the timing corresponds to the beginning of the exponential growth of U87MG tumors [10].

II.3 STATISTICAL ANALYSIS

The results are expressed as the mean ± standard error (SEM). Statistical analysis was performed using GraphPad Prism for ANOVA. *In vivo* Kaplan–Meier survival analysis was performed with GraphPad Prism by log-rank test. The significance was set to probabilities of * p <0.05, ** p < 0.01, and *** p < 0.001 when compared with controls.

III. RESULTS AND DISCUSSION

III.1 *IN VIVO* SAFETY STUDY OF THE COMBINATION TREATMENT

As shown in Figure 1, mice treated with PTX PLGA-NPs/hydrogel and oral TMZ showed significant weight loss as compared to the resection and unloaded gel treated group. The dramatic weight loss happened during the five days of oral TMZ administration. The maximum tolerated dose (MTD) for a mouse is usually defined as the dose that produces 15% - 20% weight loss [11]. After gavage, we observed the weight loss of mice ranging from 7% to 11% with behavior changes. In recent studies, different doses of TMZ were administered orally or intraperitoneally to mice. For example, in a mouse brain metastatic cell model, 60 mg/kg/day TMZ (in 10% DMSO) was given orally for 5 consecutive days [5]. TMZ (80 mg/kg/day) in 10% DMSO was injected intraperitoneally for 2 consecutive days in subcutaneous, IDH1 mutant tumor-bearing mice [12]. In an intracranial GBM9 mouse tumor model, 20 mg/kg/day TMZ in PEG300 was administered by gavage with 12 doses for every other day over a 24-day period [13]. As 60 mg/kg/day of TMZ in 10% DMSO with 5 consecutive days' gavage led to a significant body weight loss in our experiment, 20 mg/kg/day of TMZ was chosen for *in vivo* efficacy study. The dose of 20 mg/kg/day was chosen because it was demonstrated to be effective on U87MG orthotopic tumor model and TMZ could be solubilized in water with the dissolution agent L-histidine without adding DMSO [9, 10].

As illustrated, microglial activations were observed in all groups. The positive Iba-1 staining was slightly increased compared to the resection and unloaded hydrogel treated group. It was shown that chemotherapy induced peripheral inflammation may trigger microglial activation and associated neuroinflammation [14]. The elevated microglia activation might be due to the oral TMZ treatment. No inflammation was observed from the H&E staining of brain sections.

In conclusion, as the significant weight loss during TMZ gavage, we reduced the amount of oral TMZ for the next *in vivo* efficacy study.

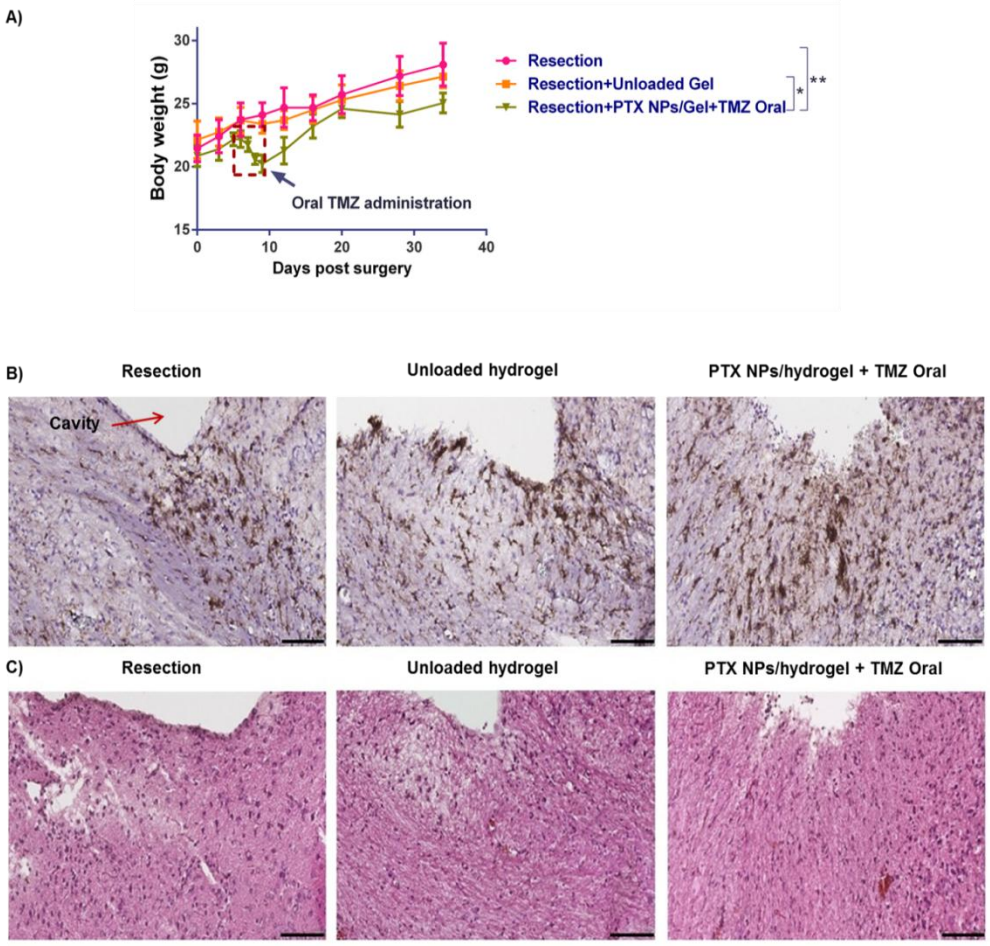

Figure 1: *In vivo* safety study of combination therapy on healthy mice brains: (A) body weights of mice; (B) evaluation of microglia activation by Iba-1 staining (brown) and brain structures by H&E staining (C) 1 month after different treatments. The local PTX and oral TMZ were given at 0.3 mg/kg and 60 mg/kg/day for 5 days, respectively. Scale bar = 100 μm (n=5), * p <0.05, ** p < 0.01.

III.2 *IN VIVO* ANTITUMOR EFFICACY OF THE COMBINATION TREATMENT

Although the survival enhancement was not significant compared to single drug treatment, combination treatment group still demonstrated survival benefits (Figure 2A and B). Only 2 mice out of 7 had tumor recurrence within 110 days after injection of the tumor cells with an undefined median survival. During the oral TMZ administration, mice weights decreased for the first day, remained stable for the following 4 days and increased to similar level as compared with other treatment groups (Figure 2C). After gavage, the average weights loss was 3%.

Treatment with oral TMZ or PTX PLGA-NP-loaded hydrogels resulted in significant survival enhancements as compared with the resected mice (p < 0.001 and p < 0.05 respectively) with the median survival time of 106 and 90 days respectively. By MRI imaging, some mice showed edema after single drug alone or combination treatments, which did not influence the behavior of the mice (Data not shown). As compared with 20 mg/kg/day of oral TMZ for 5 days, the much lower

dose of local TMZ treatment (0.6 mg/kg, Chapter IV) in parallel showed similar therapeutic efficacy with no significant difference, which demonstrates the advantages of local drug delivery against GBM.

In a recent study, a much more significant benefits was reported with intracranial injection of a PTX hydrogel combined with oral TMZ for the treatment of intracranial 9L implanted mice [15]. However, due to the different experimental conditions (animal model, tumor size, tumor resection), our result was not as good as reported. In our condition, most of the tumor cells were already resected, only few residual infiltrative tumor cells were left. Thus it is much easier to treat the residual tumor cells than the whole tumor. Anyway, combination with local PTX and oral TMZ could still be a promising strategy for the treatment of GBM and is worth to be evaluated in different *in vivo* conditions.

A)

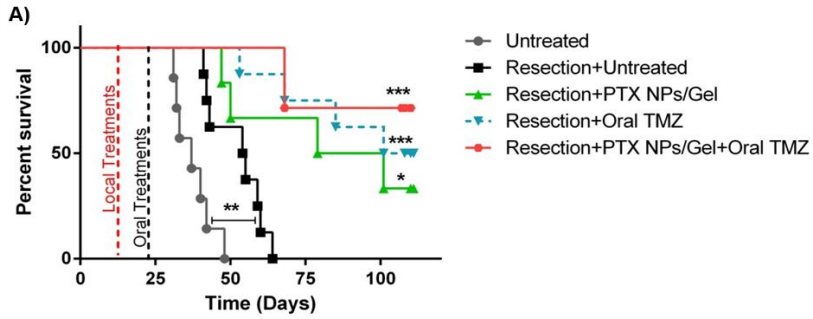

B)

Treatment	*n*	Median survival (days)	Log-rank test	Long-term surviving mice
Untreated	7	37		0
Resection + untreated	8	54.5	** (*vs* untreated)	0
Resection + PTX NPs/Hydrogel	6	90	* (*vs* Resection + untreated)	2
Resection + Oral TMZ	8	106	*** (*vs* Resection + untreated)	4
Resection + PTX NPs/Hydrogel + Oral TMZ	7	Undefined	*** (*vs* Resection + untreated)	5

C)

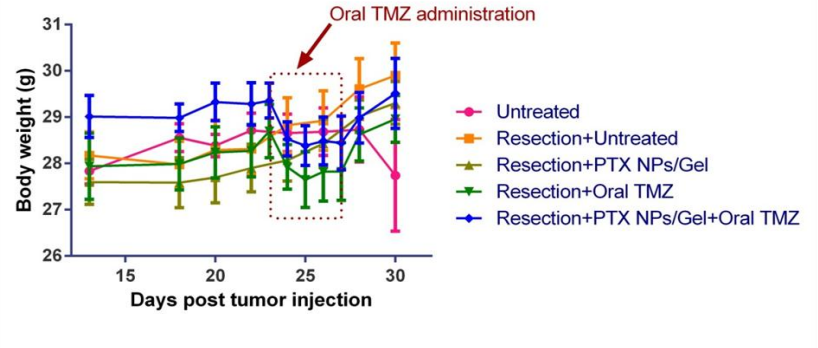

Figure 2: The Kaplan-Meier survival curves (A), median survival (B) and weights (C) of U87MG orthotopic tumor-bearing mice treated with different therapies. The doses of local PTX and oral TMZ were 0.3 mg/kg and 20 mg/kg/day for 5 days (n=6-8 for survival); *$p < 0.05$, ** $p < 0.01$, ***$p < 0.001$.

IV.CONCLUSIONS

In conclusion, we evaluated the therapeutic efficacy of the combination treatment strategy with local PTX PLGA-NP-loaded PEG-DMA hydrogel injected in the resection cavity and oral TMZ administration to mimic the standard of care for GBM patients. We demonstrated the oral TMZ dosing of 60 mg/kg/day for 5 consecutive days caused a significant body weight decrease in mice. The combination of local PTX with oral TMZ (20 mg/kg/day for 5 consecutive days) failed to have statistical difference with single treatment alone but did show a survival benefit in the treatment of the U87MG orthotopic tumor-bearing mice. Future studies may still consider of the potential advantages of this combination treatment strategy.

V. REFERENCES

1. Dormand EL, Banwell PE, Goodacre TE. Radiotherapy and wound healing. International Wound Journal. 2005; 2: 112-27.
2. Friedman HS, Kerby T, Calvert H. Temozolomide and treatment of malignant glioma. Clinical Cancer Research. 2000; 6: 2585-97.
3. Zhao M, Danhier F, Bastiancich C, Joudiou N, Ganipineni LP, Tsakiris N, et al. Post-resection treatment of glioblastoma with an injectable nanomedicine-loaded photopolymerizable hydrogel induces long-term survival. International Journal of Pharmaceutics. 2018; 548: 522-9.
4. Bianco J, Bastiancich C, Joudiou N, Gallez B, des Rieux A, Danhier F. Novel model of orthotopic U-87 MG glioblastoma resection in athymic nude mice. Journal of Neuroscience Methods. 2017; 284: 96-102.
5. Martínez-Aranda A, Hernández V, Picón C, Modolell I, Sierra A. Development of a preclinical therapeutic model of human brain metastasis with chemoradiotherapy. International journal of molecular sciences. 2013; 14: 8306-27.
6. Freireich EJ, Gehan E, Rall D, Schmidt L, Skipper H. Quantitative comparison of toxicity of anticancer agents in mouse, rat, hamster, dog, monkey, and man. Cancer chemotherapy reports. 1966; 50: 219.
7. Robinson CG, Palomo JM, Rahmathulla G, McGraw M, Donze J, Liu L, et al. Effect of alternative temozolomide schedules on glioblastoma O(6)-methylguanine-DNA methyltransferase activity and survival. British journal of cancer. 2010; 103: 498-504.
8. Bastiancich C, Bianco J, Vanvarenberg K, Ucakar B, Joudiou N, Gallez B, et al. Injectable nanomedicine hydrogel for local chemotherapy of glioblastoma after surgical resection. Journal of Controlled Release. 2017; 264: 45-54.
9. Wauthoz N, Deleuze P, Hecq J, Roland I, Saussez S, Adanja I, et al. In vivo assessment of temozolomide local delivery for lung cancer inhalation therapy. European Journal of Pharmaceutical Sciences. 2010; 39: 402-11.
10. Danhier F, Messaoudi K, Lemaire L, Benoit J-P, Lagarce F. Combined anti-Galectin-1 and anti-EGFR siRNA-loaded chitosan-lipid nanocapsules decrease temozolomide resistance in glioblastoma: In vivo evaluation. International journal of pharmaceutics. 2015; 481: 154-61.
11. Aston WJ, Hope DE, Nowak AK, Robinson BW, Lake RA, Lesterhuis WJ. A systematic investigation of the maximum tolerated dose of cytotoxic chemotherapy with and without supportive care in mice. BMC Cancer. 2017; 17: 684-.
12. Koncar RF, Chu Z, Romick-Rosendale LE, Wells SI, Chan TA, Qi X, et al. PLK1 inhibition enhances temozolomide efficacy in IDH1 mutant gliomas. Oncotarget. 2017; 8: 15827-37.
13. Gil Del Alcazar CR, Todorova PK, Habib AA, Mukherjee B, Burma S. Augmented HR Repair Mediates Acquired Temozolomide Resistance in Glioblastoma. Molecular cancer research : MCR. 2016; 14: 928-40.
14. Santos JC, Pyter LM. Neuroimmunology of Behavioral Comorbidities Associated With Cancer and Cancer Treatments. Frontiers in Immunology. 2018; 9.
15. Vellimana AK, Recinos VR, Hwang L, Fowers KD, Li KW, Zhang Y, et al. Combination of paclitaxel thermal gel depot with temozolomide and radiotherapy significantly prolongs survival in an experimental rodent glioma model. Journal of Neuro-Oncology. 2013; 111: 229-36.

CHAPTER VI
DISCUSSION AND PERSPECTIVES

TABLE OF CONTENTS

I. MAJOR FINDINGS

We hypothesized that local drug delivery with a hydrogel in tumor resection cavity may contribute to sustained drug release and delivery of multiple chemotherapeutic drugs with synergistic effect. Firstly, a photopolymerizable hydrogel loaded with paclitaxel PLGA nanoparticles (PTX PLGA-NPs) was developed and the antitumor efficiency in U87MG orthotopic mouse model was investigated (Chapter III). Then the combination effect of PTX PLGA-NPs and temozolomide (TMZ) was evaluated. The drug coloaded hydrogel achieved superior antitumor efficacy in mouse model (Chapter IV). We have also demonstrated the beneficial therapeutic efficacy of the combination treatments with PTX PLGA-NP-loaded hydrogel and the oral administration of TMZ (Chapter V).

The major finds of the research work are:

Hydrogel formation:

- We prepared PTX PLGA-NPs using emulsion-evaporation method. The hydrogel was formed by photo-crosslinkable reaction of PEG-DMA in the presence of photoinitiator under 400 nm light. The final storage modulus G' of PEG-DMA/PLGA-NPs (195 ± 58 kPa) was significantly higher than that of the loss modulus G" (1.25 ± 0.14 kPa), which is a typical behavior of solid-like materials. The unloaded and drug-coloaded hydrogel showed no swelling capacity.

Drug release:

- The *in vitro* release kinetics of PTX from the PEG-DMA hydrogel containing PLGA-NPs were characterized by 10% burst release during the first 8 hours, followed by 30% sustained release during one week. *In vivo* PTX diffusion study using Oregon Green™ 488 PTX PLGA-NP-loaded hydrogel demonstrated a sustained drug release for at least 1 month.

In vitro cytotoxicity:

- Similar IC_{50} values of PTX PLGA-NPs were obtained by MTT assay and clonogenic assay (0.010 μg/mL and 0.014 μg/mL respectively) in U87MG cells. However, dramatic variations of TMZ IC_{50} value were observed by MTT, crystal violet and clonogenic assay (841 μg/mL, 397 μg/mL and 2.4 μg/mL respectively). We observed dose-dependent interference between TMZ and MTT assay.
- Clonogenic assay could determine cell reproductive death after treatment with cytotoxic agents, thus are used to evaluate the drug combination effect. The combination of PTX NPs and TMZ showed additive or synergistic effects. Due to the limited solubility of TMZ,

to load as much PTX as possible while maintaining a synergistic effect, we chose a drug concentration ratio of 1:2 (PTX to TMZ) for *in vivo* studies.

TMZ resistance:

- *MGMT* mRNA expression was investigated to determine whether TMZ resistance occurred. *MGMT* expression was undetectable both in *vitro* in U87MG cells and *in vivo* in resected tumors, and was not up-regulated in recurrent tumor after treatment with TMZ-loaded hydrogel, suggesting that local treatment with TMZ hydrogel did not induce MGMT-related drug resistance.

Safety study:

- The unloaded PEG-DMA hydrogel was well tolerated in healthy mouse brains for 2 and 4 months. Hydrogels coloaded with PTX and TMZ (0.3 mg/kg and 0.6 mg/kg, respectively) were tolerable for local administration in mice brains for 1 month. To mimic the current standard of care, mice were treated with PTX-loaded hydrogel in combination with oral TMZ (60mg/kg/day for 5 days). However, we observed a significant weight loss and behavior changes. Thus, a reduced oral dose of 20 mg/kg/day TMZ for 5 days was chosen for *in vivo* efficacy study.

Efficacy study:

- The post-surgical administration of PTX PLGA-NP-loaded hydrogel (0.525 mg/kg PTX) in the resection cavity significantly delayed the tumor recurrences in orthotopic U87MG tumor resection model. Five out of nine mice survived for 150 days after tumor inoculation. The PTX PLGA-NPs and TMZ co-loaded hydrogel (0.3 mg/kg and 0.6 mg/kg, respectively) treated mice showed the most significant survival benefits compared to single drug treatment group. Seven out of nine mice showed long-term survival and no signs of tumor recurrence were observed for at least 110 days. The combination treatment with PTX PLGA-NP-loaded hydrogel and oral TMZ also resulted in survival enhancements, but no statistical improvements were observed compared to the oral TMZ treatment group alone.

II. DISCUSSION

II.1 ANTITUMOR EFFICACY OF COMBINATION THERAPY

In Chapter VI, we hypothesized that local combination treatment with photopolymerizable hydrogel coloaded with PTX and TMZ could have beneficial antitumor effect. Although the survival benefits of the combination treatment were not significant compared to the single drug treatment (p = 0.07 for either PTX or TMZ based on log-rank test), the drug combination treatment group demonstrated improved long-term survival of mice, more significancy ($p < 0.001$) over control group and undefined median survival. The antitumor efficacy of the drug combination led to a survival rate of 78% for approximate 4 months. Higher efficacy can be obtained by increasing the dose. However, due to the limited solubility and drug loading capacity of TMZ and PTX, respectively, even with maximum dose of single drug, limited efficacy is observed. For example, the maximum dose of TMZ is 0.6 mg/kg, which resulted in 33% of long-term surviving mice (Chapter IV). In addition, with maximum local dose of PTX (0.525 mg/kg), only 55% of mice demonstrated long-term survival (Chapter III). Nevertheless, a much higher survival could be gained by using drug combination. In clinical combination chemotherapy, a single drug is usually administered at its maximum tolerated dose (MTD) with limited therapeutic efficacy. With combination therapy, higher survival is observed with drugs used at doses lower than MTD. We demonstrated the *in vitro* synergistic effect of PTX and TMZ. However, the *in vivo* synergism could not be demonstrated. The *in vivo* synergism was reported to be calculated by Robert Clark Equations based on the median survival [1]. Nevertheless, as the median survival of combination treatment was undefined, we were not able to measure the synergism with our current data.

Intra-cavity depot drug delivery system for the treatment of GBM has been studied extensively. Recently, the local delivery of a lauroyl-gemcitabine lipid nanocapsule-based hydrogel in the tumor resection cavity of GBM significantly increased the survival time compared to the controls in orthotopic U87MG mouse model and 9L rat model [2, 3]. The hydrogel was covered and sealed by a Neuro-Patch and was still present in the resection cavity 1 week after implantation in rat brain. As compared with PEG-DMA containing PLGA-NPs, the direct release of lauroyl-gemcitabine from the hydrogel led to more burst effect. In addition, the potential dislocation of the Neuro-Patch may lead to leakage of the soft LNC hydrogels, but not the solid PEG-DMA hydrogel. More recently, a PLGA-PEG paste combining temozolomide and etoposide were developed to treat surgically resected high-grade glioma. *In vitro* release study showed the releases of etoposide and temozolomide were sustained for up to 22 and 7 days respectively. *In vivo* studies revealed a

significant overall survival benefit in post-surgery 9L orthotopic gliosarcomas after combined treatment with PLGA-PEG/temozolomide/etoposide paste and radiotherapy. Long-term survivors were observed in over half the animals with histological confirmation of disease-free brain. However, more than 90% of etoposide was released in 10 days *in vitro*; the *in vivo* drug diffusion was not studied [4]. Since radio- and chemotherapy will affect the wound healing process, GBM patients generally start the radio- and chemotherapy regimen approximately 4 weeks after the surgical resection of tumor [5]. Despite promising therapeutic efficacy demonstrated in preclinical studies, intra-cavity depot drug delivery system containing a wide range of antitumor compounds which could sustain drug release over 4 weeks *in vivo* and reach the residual infiltrative tumor cells is still required to fulfill the medical need.

II.2 RELEASE PROFILE OF PTX

A photopolymerizable PEG-DMA hydrogel that sustainably release 70% of TMZ for one week *in vitro* was developed by our group [6]. Thus, we were motivated to develop PEG-DMA hydrogel containing PLGA-NPs loaded with PTX, to fill the surgical resection cavity and further sustain the release of PTX for at least 1 month.

PTX PLGA-NP-loaded PEG-DMA hydrogel could be administered by directly injecting the pre-gel mixture in the tumor resection cavity and photopolymerized *in situ*. This hydrogel was able to sustainably release 30% of PTX for at least one week *in vitro* (Chapter III). *In vivo* drug release was performed with Oregon Green™ 488 PTX PLGA-NPs loaded hydrogel. The hydrogel was able to sustainably release PTX for at least one month (Chapter IV). The Oregon Green™ 488 PTX differs from PTX in many aspects, such as molecular weight, solubility in different solvents. Despite the differences, Oregon Green™ 488 was still used for this study because it was not possible to perform the study with autoradiography due to low resolution. Furthermore, time-of-flight secondary ion mass spectrometry (TOF-SIMS) is a technique based on the fact that ions with the same energy but different masses travel with different velocities. However, due to the low sensitivity of PTX, this method is not appropriate to evaluate PTX brain diffusion. Therefore, Oregon Green™ 488 PTX was selected to study *in vivo* drug release as it is detectable under confocal microscope.

II.3 INDUCTION OF CHEMORESISTANCE

It has been reported that the establishment of the U87 TMZ-resistant glioma cell lines required exposure to gradually increasing concentrations of TMZ in culture medium for 6 months [7].

However, under our experimental conditions, most of the TMZ was released within one week, and the drug release rate gradually decreased [8]. The stepwise increasing concentrations of PTX (100-300 nM) for a period of 9 months was also demonstrated to induce stable drug-resistance in U87 cell lines [9]. Similarly with TMZ, in our case, after the burst release, the tumor cells would expose to the gradually released small amount of PTX and would not progressively build up the tolerance towards the increasing dose of PTX. However, since the efficacy of PTX is often inhibited by the ATP-binding cassette multidrug efflux transporter: p-glycoprotein [10], the evaluation of p-glycoprotein expression, will be able to answer this question.

II.4 *IN VITRO* CYTOTOXICITY STUDIES

We found a dramatic discrepancy between TMZ IC_{50} value when using MTT, crystal violet and clonogenic assay (841 μg/mL, 397 μg/mL and 2.4 μg/mL respectively). MTT assay is probably the most widely used method for studying the cytotoxic effect. It assesses cell metabolic activity depending on NAD (P) H-dependent cellular oxidoreductase enzymes. These enzymes are capable of reducing the tetrazolium dye MTT 3-(4, 5-dimethylthiazol-2-yl)-2, 5-diphenyltetrazolium bromide to insoluble formazan, which has a purple color. However, we found a dose-dependent interference between TMZ and MTT.

Crystal violet is an enzyme-independent and directly measures the DNA mass in adherent cells [11]. However, U87MG cells are not able to tightly adhere to the surface of 96-well cell cultivation plate. The washing steps in this method may influence the accuracy of the final result.

The clonogenic assay is based on the ability of a single cell to grow into a colony. It has more advantages compared to the other two methods: (i) it is enzyme independent; (ii) the colonies can be counted directly; (iii) the experiments were not conducted in 96-well plate and (iv) fewer washing step; (v) Clonogenic assay could determine cell reproductive death after treatment with cytotoxic agents, while both MTT and crystal violet are only suitable for the examination of the impact of chemotherapeutics on cell survival and growth inhibition.

III. PERPECTIVES

This PhD thesis provides solid bases to consider the TMZ and PTX combination treatment as a promising strategy against GBM. However, to exploit the full potential of this system and, to avoid GBM recurrences and improve survival, several issues need to be investigated.

III.1 THE *IN VIVO* MOUSE MODEL

In order to predict the clinical outcome of abovementioned novel therapeutic strategy, an ideal mouse glioma model is needed. The model should be orthotopic and highly reproducible with predictable growth, and bear a genetic similarity to human glioma, show cellular heterogeneity and angiogenic-like growth [12]. In comparison with the treatment of entire tumor, the orthotopic tumor resection mouse model could better mimic the surgery scenario in clinics. U87MG is a human primary GBM cell line that commonly used in brain cancer research. It was selected for tumor implantation and resection due to the invasive growth, good reproducibility and disease progression. Furthermore, the cell line also forms well-demarcated tumor mass visible by MRI images, making it possible to monitor the tumor growth and recurrence after the treatments [13].
A vast number of reports showed the therapeutic efficacy of novel treatment modalities in various animal models, yet these tumor models failed to reflect the biological properties of the tumors, display the same pharmacokinetics and reflect the cellular heterogeneity as in human tumors [14]. In this project, we attempted to mimic the human GBM and performed the *in vivo* efficacy study based on one of the most widely studied U87MG glioma cell line. Nonetheless, the limitations of this tumor model developed by U87MG cell line were inevitable. For example, gene expression and phenotypic shifts, clonal selection, and genetic alterations happened during the adaptation of the tumor cells to monolayer cultures. There are 512 homozygously mutated genes in U87MG glioma cell line ordered from ATCC, including 154 by single nucleotide variations, 178 by small (< 21 bp) insertions and deletions, 145 by large microdeletions, and 35 by interchromosomal translocations [15]. In addition, orthotopic U87 tumor is generally with a disrupted BBB and a lack of diffusely infiltrative growth, leading to an inadequate phenotype for diffusive glioma [13]. Furthermore, the xenographic U87MG tumor model is developed in immunocompromised mice. However, chemotherapy may lead to the changes in host immunity and the tumor microenvironment, which are important factors affecting the therapeutic effect. For example, modulation of TMZ dose affects T-cell response to immune checkpoint inhibition [16]. Whether PTX may cause the toxicity to the immune system or enhance the antitumor potential of immune system depends on the dose

of PTX as well [17]. Nevertheless, the effect of chemotherapeutic drugs on the immune system and the consequence to malignant tumor cells cannot be verified in immunocompromised mouse models. Despite the problems above, there are several factors associated with the *in vivo* therapeutic efficacy of a drug delivery system, such as the brain distribution of drug from the administration site, the invasiveness and infiltration abilities of tumor cells, the resection timing of major tumor mass and so on. Therefore it is imperative to understand that despite our hydrogel drug delivery system significantly enhanced the survival of U87MG tumor-bearing mice, it might show different antitumor efficacy in a model that grows in a more invasive and infiltrative way.

Patient derived GBM cells display the biology, genetics and gene expression profiles of the corresponding human GBM. However, its inability to fully restate the genetic heterogeneity and phenotype of spontaneously occurring human brain tumors in a foreign microenvironment is still a major limitation of transgenic models [18]. Canine spontaneous brain tumors are a valuable model system to evaluate the clinical translation of different brain tumor therapeutic strategies due to many reasons. The prevalence of malignant gliomas among dogs is comparable to that in humans. The gross pathological, microscopic and immune-histochemical features are similar between human and canine spontaneous brain tumors. The immunologic features associated with human and canine brain tumors also share similarities, such as the tumor infiltration of macrophages or T cells and programmed death 1 (PD-1) immunoinhibitory mechanisms [19]. The features discussed above are less frequently observed or sometimes absent in rodent human brain tumor xenograft models. Thus, canine spontaneous brain tumors could be considered as a clinical relevant tumor model for investigations of novel drug delivery systems.

III.2 PREPARATION OF HYDROGEL FOR CLINICAL USE

Current PEG-DMA hydrogel could fit the mouse brain tumor resection cavity with the size of 9.4 mm^3, while brain tumors in patients can be much bigger (median volume of 13.8–54.4 cm^3)[20]. The diameter of the PEG-DMA hydrogel can be determined by lighting area. While the depth of hydrogel ranged only within 2-3 cm, which is due to the formation of white hydrogel blocking the penetration depth of 400 nm light. To solve this problem, we previously developed a gel spray with FORANE gas and different concentrations of glycerin in order to make it sprayable and attachable to the wall of the tumor resection cavity. Interestingly, after a few hours, a hydrogel with the foam-like structure was generated (Figure 1). This foam-like hydrogel will provide a supportive structure and prevent hydrogel collapse. This foam has high potential to fill the resection cavity itself or support the hydrogel layer attaching to the resection cavity border. However, we could not obtain a stable spray because of the self-gelling even without exposure to

the 400 nm light. Inspired by this interesting finding, the future perspective would be to formulate stable hydrogel foam (or mousse), which could fit a much bigger tumor resection cavity.

Total volume of Gel (ml)	Glycerine (%)	H2O (ml)	PEG-DMA (ml)
100	10%	65	25
100	15%	60	25
100	20%	55	25

Figure 1: The composition and picture of the spray and the foam-like hydrogel.

III.3 CONSIDERATIONS IN HYDROGEL MANUFACTURING

The current PEG-DMA hydrogel is composed of PEG-DMA polymer, PLGA-NPs and the anticancer drugs. PEG-DMA is commercially available (GMP) and can be sterilized through filtration by 0.22 μm filter, which should facilitate a future potential clinical translation.

In this context, the manufacture of nanoparticles under GMP conditions will be mainly discussed. At small scale in lab, it is easy to achieve reproducibility; while at the industrial scale, the successful manufacturing is more complicated. The manufacturing reproducibility can be affected by different factors, such as environmental conditions (pH, temperature), materials (raw materials, ratio between the different components, solvents) and formulation operations (e.g. sonication, centrifugation, solvent evaporation, lyophilization, sterilization). All of these factors are required to be optimized and controlled. Then, appropriate analytical methods have to be developed and validated to assess product quality. Some of the characterization methods include dynamic light scattering, zeta potential, scanning electron microscopy and transmission electron microscopy are frequently used [2].

Due to the aggregation propensity of nanoparticles in suspension, which may significantly degrades their performances, lyophilization is often introduced in the manufacturing for long term storage [21]. A lyoprotectant such as trehalose may prevent structural changes and contribute to the preservation of the surface properties during lyophilization.

Then, the sterility of nanoparticle delivery system is a major concern for their application in clinic [22]. The nanoparticles can be impacted by different sterilization method, depending on the

components, characterizations and method of preparation. Filtration and autoclave are the most commonly used sterilization techniques for nanoparticles. However, due to the size issue, PLGA nanoparticles cannot be filtered through 0.22 μm. Autoclave is not recommended because it might affect the stability of the encapsulated drug. It was reported that using γ radiation to sterilize PLGA nanoparticles for intraocular administration, and the drug release rate behaved similarly before and after the sterilization process [23]. All of these treatments should be reproducible and preserve the key attributes of the nanoparticles, including under storage conditions.

After sterilization, PEG-DMA can be stored in a syringe. Nanoparticles can be stored in a vial, lyophilized and sterilized. Before using, nanoparticles are re-suspended in certain volume of sterilized water and filled to the syringe containing PEG-DMA. The pre-gels could then be mixed upside down and injected to the resection cavity for photopolymerization.

III.4 TO EXPLOIT DIFFERENT COMBINATION POSSIBILITIES

We demonstrated the current hydrogel coloaded with two anticancer drugs resulted in superior antitumor effect compared to single drug-loaded hydrogels. The drug combination strategy could potentially resolve other remaining challenges in GBM treatment as well.

Glioma stem cells (GSC) harbor self-renewal, differentiation and propagation ability [24], which are more resistant to radio and chemotherapy than non GSC tumor cells, leading to the population of glioma stem cells remain alive after the initial treatment and reinitiate tumor recurrences [25]. Thus, the co-administration of anti-neoplastic drug and anti-GCSs drug (e.g. salinomycin) could be a beneficial combination treatment strategy for GBM.

O6-methylguanine DNA methyltransferase (MGMT) repairs the major cytotoxic methylation caused by TMZ and re-build the structural integrity of DNA bases [26]. The combination treatment with TMZ and efficient drugs that exhibits MGMT inhibition function could also be a research direction. Developing TMZ resistant cell lines or using the cell lines with high *MGMT* gene expression level (e.g. T98G) may contribute to the investigation of combination effect.

As the main multidrug resistance mechanisms, P-gycoprotein (P-gp) presents another challenge. P-gp is an energy dependent drug efflux pump that comprised of 1,280 amino acids encoded by the human *MDR1* gene, which inhibits chemotherapeutic drugs to reach brain tumor cells effectively [27]. Combination therapy with efflux transporters inhibitor could be an attractive strategy to boost drug administration into cancer cells. For example, β-asarone in combination with TMZ decreased the expression of *P-gp* and *MDR1*, and promoted TMZ entering into U251 glioma cells [28].

Chemotherapy and immunotherapy have been widely validated independently for the treatment of cancer in many publications. Chemotherapy has historically been considered to induce cancer cell

death by direct cytotoxicity or cell cycle arrest in an immunogenically silent manner [29]. Due to the immunosuppressive effects of chemotherapy, combination treatment with chemotherapy and immunotherapy is controversial. Indeed, systemic chemotherapy might suppress the bone marrow and consequently impact the amount and activation state of immune cells [30]. However, it was shown that paclitaxel following intraperitoneal injection boosted tumor vaccine-mediated T cell responses when given at lympho-depletion doses one day prior to vaccination [31]. More recently, local chemotherapy with carmustine (BCNU) or TMZ was able to potentiate anti-PD-1 mediated antitumor immune response in GL261 tumor bearing mice. The potential mechanism might be the increased antigen presentation, which is caused by dead tumor cells after chemotherapy. This was supported by the increased percentage of dendritic cells presenting in the local chemotherapy treated groups, allowing for greater antigen presentation and further clonal activation of tumor-specific T cell responses [32]. Moreover, it was shown that cancer cells may undergo bona fide immunogenic cell death (ICD) after exposure to some chemotherapeutics that are currently used in clinic, including oxaliplatin, doxorubicin, bortezomib, paclitaxel and mitoxantrone [33-35]. This process generates specific changes in cell surface structures and releases soluble mediators (e.g. ATP, calreticulin, high mobility group box 1, and chemokine ligand 10), allowing dendritic cells to recognize the dying cell and initiate an anti-tumor immune response to clear tumor cells. Inspired by those pioneering studies, immunotherapy (e.g. immune checkpoint inhibitors) in combination with the optimized dosing of paclitaxel could be a promising direction to fight GBM.

Table 1: Summary of the future perspectives of this PhD work.

Issues	Future perspectives
U87MG mouse model: **Less infiltrative** **Immunocompromised mice**	Model with invasive cell lines (e.g. GL261 cells, patient derived tumor cells); Syngeneic models (e.g. CNS-1, GL261, RG2); Canine spontaneously brain tumor model
The sterility of this local drug delivery system	PEG-DMA: 0.22 μm filter; PLGA-NPs: γ radiation
The much bigger tumor resection cavity in patients	Polymerize layer by layer; Foam-like hydrogel; Foam that support hydrogel layer attaching to the resection cavity border
Other challenges in GBM treatment: **GSCs** **MGMT** **MDR** **Immunosuppression of chemotherapy**	Exploit different drug combinations to overcome those barriers; Combination of optimized dosing of chemotherapy and immunotherapy

IV. REFERENCES

1. Van Woensel M, Mathivet T, Wauthoz N, Rosière R, Garg AD, Agostinis P, et al. Sensitization of glioblastoma tumor micro-environment to chemo-and immunotherapy by Galectin-1 intranasal knock-down strategy. Scientific reports. 2017; 7: 1217.
2. Ragelle H, Danhier F, Préat V, Langer R, Anderson DG. Nanoparticle-based drug delivery systems: a commercial and regulatory outlook as the field matures. Expert Opinion on Drug Delivery. 2017; 14: 851-64.
3. Bastiancich C, Lemaire L, Bianco J, Franconi F, Danhier F, Préat V, et al. Evaluation of lauroyl-gemcitabine-loaded hydrogel efficacy in glioblastoma rat models. Nanomedicine. 2018; 13: 1999-2013.
4. Smith SJ, Tyler B, Gould TW, Veal GJ, Gorelick NL, Rowlinson J, et al. Overall survival in malignant glioma is significantly prolonged by neurosurgical delivery of etoposide and temozolomide from a thermo-responsive biodegradable paste. Clinical Cancer Research. 2019: clincanres. 3850.2018.
5. Patel DM, Agarwal N, Tomei KL, Hansberry DR, Goldstein IM. Optimal timing of whole-brain radiation therapy following craniotomy for cerebral malignancies. World neurosurgery. 2015; 84: 412-9.
6. Fourniols T, Randolph LD, Staub A, Vanvarenberg K, Leprince JG, Préat V, et al. Temozolomide-loaded photopolymerizable PEG-DMA-based hydrogel for the treatment of glioblastoma. Journal of Controlled Release. 2015; 210: 95-104.
7. Zhu D, Tu M, Zeng B, Cai L, Zheng W, Su Z, et al. Up-regulation of miR-497 confers resistance to temozolomide in human glioma cells by targeting mTOR/Bcl-2. Cancer medicine. 2017; 6: 452-62.
8. Fourniols T, Randolph LD, Staub A, Vanvarenberg K, Leprince JG, Préat V, et al. Temozolomide-loaded photopolymerizable PEG-DMA-based hydrogel for the treatment of glioblastoma. Journal of Controlled Release. 2015; 210: 95-104.
9. Podolski-Renić A, Anđelković T, Banković J, Tanić N, Ruždijić S, Pešić M. The role of paclitaxel in the development and treatment of multidrug resistant cancer cell lines. Biomedicine & Pharmacotherapy. 2011; 65: 345-53.
10. Mimeault M, Hauke R, Batra SK. Recent advances on the molecular mechanisms involved in the drug resistance of cancer cells and novel targeting therapies. Clinical Pharmacology and Therapeutics. 2008; 83: 673-91.
11. Śliwka L, Wiktorska K, Suchocki P, Milczarek M, Mielczarek S, Lubelska K, et al. The comparison of MTT and CVS assays for the assessment of anticancer agent interactions. PloS one. 2016; 11: e0155772.
12. Stylli SS, Luwor RB, Ware TM, Tan F, Kaye AH. Mouse models of glioma. Journal of Clinical Neuroscience. 2015; 22: 619-26.
13. Jacobs VL, Valdes PA, Hickey WF, De Leo JA. Current review of in vivo GBM rodent models: emphasis on the CNS-1 tumour model. ASN neuro. 2011; 3: e00063-e.
14. Huszthy PC, Daphu I, Niclou SP, Stieber D, Nigro JM, Sakariassen PØ, et al. In vivo models of primary brain tumors: pitfalls and perspectives. Neuro-Oncology. 2012; 14: 979-93.
15. Clark MJ, Homer N, O'Connor BD, Chen Z, Eskin A, Lee H, et al. U87MG decoded: the genomic sequence of a cytogenetically aberrant human cancer cell line. PLoS genetics. 2010; 6: e1000832.
16. Karachi A, Yang C, Dastmalchi F, J Sayour E, Huang J, Azari H, et al. Modulation of temozolomide dose differentially affects T-cell response to immune checkpoint inhibition. Neuro-Oncology. 2019.
17. Shurin GV, Tourkova IL, Shurin MR. Low-dose chemotherapeutic agents regulate small Rho GTPase activity in dendritic cells. Journal of immunotherapy (Hagerstown, Md : 1997). 2008; 31: 491-9.

18. Simeonova I, Huillard E. In vivo models of brain tumors: roles of genetically engineered mouse models in understanding tumor biology and use in preclinical studies. Cellular and molecular life sciences. 2014; 71: 4007-26.
19. Arami H, Patel CB, Madsen SJ, Dickinson PJ, Davis RM, Zeng Y, et al. Nanomedicine for Spontaneous Brain Tumors: A Companion Clinical Trial. ACS nano. 2019.
20. Chaichana KL, Cabrera-Aldana EE, Jusue-Torres I, Wijesekera O, Olivi A, Rahman M, et al. When gross total resection of a glioblastoma is possible, how much resection should be achieved? World neurosurgery. 2014; 82: e257-e65.
21. Bazile D. Nanotechnologies in drug delivery-an industrial perspective. Journal of Drug Delivery Science and Technology. 2014; 24: 12-21.
22. Vetten MA, Yah CS, Singh T, Gulumian M. Challenges facing sterilization and depyrogenation of nanoparticles: effects on structural stability and biomedical applications. Nanomedicine: Nanotechnology, Biology and Medicine. 2014; 10: 1391-9.
23. Herrero-Vanrell R, Ramirez L. Biodegradable PLGA microspheres loaded with ganciclovir for intraocular administration. Encapsulation technique, in vitro release profiles, and sterilization process. Pharmaceutical research. 2000; 17: 1323-8.
24. Safa AR, Saadatzadeh MR, Cohen-Gadol AA, Pollok KE, Bijangi-Vishehsaraei K. Glioblastoma stem cells (GSCs) epigenetic plasticity and interconversion between differentiated non-GSCs and GSCs. Genes & Diseases. 2015; 2: 152-63.
25. Haar CP, Hebbar P, Wallace GC, Das A, Vandergrift WA, Smith JA, et al. Drug resistance in glioblastoma: a mini review. Neurochemical Research. 2012; 37: 1192-200.
26. Fan CH, Liu WL, Cao H, Wen C, Chen L, Jiang G. O6-methylguanine DNA methyltransferase as a promising target for the treatment of temozolomide-resistant gliomas. Cell Death & Disease. 2013; 4: e876.
27. Li Y, Yuan H, Yang K, Xu W, Tang W, Li X. The structure and functions of P-glycoprotein. Current Medicinal Chemistry. 2010; 17: 786-800.
28. Wang N, Zhang Q, Ning B, Luo L, Fang Y. beta-Asarone promotes Temozolomide's entry into glioma cells and decreases the expression of P-glycoprotein and MDR1. Biomedicine & Pharmacotherapy. 2017; 90: 368-74.
29. Gebremeskel S, Johnston B. Concepts and mechanisms underlying chemotherapy induced immunogenic cell death: impact on clinical studies and considerations for combined therapies. Oncotarget. 2015; 6: 41600-19.
30. Lombardi G, Rumiato E, Bertorelle R, Saggioro D, Farina P, Della Puppa A, et al. Clinical and Genetic Factors Associated With Severe Hematological Toxicity in Glioblastoma Patients During Radiation Plus Temozolomide Treatment: A Prospective Study. Journal of Clinical Oncology. 2015; 38: 514-9.
31. Machiels J-PH, Reilly RT, Emens LA, Ercolini AM, Lei RY, Weintraub D, et al. Cyclophosphamide, doxorubicin, and paclitaxel enhance the antitumor immune response of granulocyte/macrophage-colony stimulating factor-secreting whole-cell vaccines in HER-2/neu tolerized mice. Cancer research. 2001; 61: 3689-97.
32. Mathios D, Kim JE, Mangraviti A, Phallen J, Park C-K, Jackson CM, et al. Anti-PD-1 antitumor immunity is enhanced by local and abrogated by systemic chemotherapy in GBM. Science translational medicine. 2016; 8: 370ra180-370ra180.
33. Casares N, Pequignot MO, Tesniere A, Ghiringhelli F, Roux S, Chaput N, et al. Caspase-dependent immunogenicity of doxorubicin-induced tumor cell death. The Journal of Experimental Medicine. 2005; 202: 1691-701.
34. Galluzzi L, Buque A, Kepp O, Zitvogel L, Kroemer G. Immunogenic cell death in cancer and infectious disease. Nature Reviews Immunology. 2017; 17: 97-111.
35. Janicka M, Gubernator J. Use of nanotechnology for improved pharmacokinetics and activity of immunogenic cell death inducers used in cancer chemotherapy. Expert Opinion on Drug Delivery. 2017; 14: 1059-75.